

Copyright

by

Hsin I Hsu

2011

The Thesis Committee for Hsin I Hsu
Certifies that this is the approved version of the following thesis:

**A Modern Representation of the Flow of Electromagnetic Power and
Energy Using the Poynting's Vector and a Generalized Poynting's
Theorem**

APPROVED BY
SUPERVISING COMMITTEE:

Supervisor:

Mircea Driga, Supervisor

Mack W. Grady

**A Modern Representation of the Flow of Electromagnetic Power and
Energy Using the Poynting's Vector and a Generalized Poynting's
Theorem**

by

Hsin I Hsu, B.S.

Thesis

Presented to the Faculty of the Graduate School of
The University of Texas at Austin
in Partial Fulfillment
of the Requirements
for the Degree of

Master of Science in Engineering

The University of Texas at Austin
May 2011

Dedication

To the best parents, sister and brother in the world. Thank you for your infinite love and support and more and more. To my friends, no matter you are far away from me in Taiwan or close to me in the state. Thank you for everything.

Acknowledgements

Thank you, Dr. Driga. For all your help and guidance from the very first day I came to UT Austin until the day I leave UT Austin. Thank you, Dr. Grady. For being my reader and for your approval. This thesis would not have been possible without the support from these two fantastic professors.

Thank to everyone who has encouraged me to pursue Master's degree in the state and everyone who made it happen. I cherish this opportunity and the experience I've gotten during my graduate student life.

April 20, 2011

Abstract

A Modern Representation of the Flow of Electromagnetic Power and Energy Using the Poynting's Vector and a Generalized Poynting's Theorem

Hsin I Hsu, MSE

The University of Texas at Austin, 2011

Supervisor: Mircea Driga

A comprehensive and rigorous description of instantaneous balance of electromagnetic power defined as the derivative of energy with respect to time is offered by the Poynting's theorem. Such theorem is expressed as the sum of a series of volume integrals representing the volume densities of densities of different components of electromagnetic power and the power flow through the general surface surrounding the entire domain in which the Poynting's vector expresses the instantaneous power leaving the domain (the positive normal is the outward normal to the enclosing surface).

The original feature of the present approach is the introduction in the electromagnetic power balance and conservation of the electromechanical energy conversion by the use of the flux derivatives of the fields \vec{D} and \vec{B} . For the moving

points (rotors) involved in electromechanical energy conversion, the surface of integration is driven together with them and ε and μ remain substantially constant – (a point in movement maintains its properties as $\frac{d_s \mu}{dt} = \frac{\partial \mu}{\partial t} + \bar{u} \nabla \mu$).

$$\text{Then } \frac{\partial \vec{D}}{\partial t} \rightarrow \frac{\partial f \vec{D}}{\partial t}$$

$$\text{and } \frac{\partial \vec{B}}{\partial t} \rightarrow \frac{\partial f \vec{B}}{\partial t}$$

Then the balance of energy (and power) can be written at each infinitesimal time interval for the electromagnetic energy in which case the elementary mechanical work is produced by mechanical forces of electromagnetic origin. The thermal energy accounts for the Joule (and hysteresis) losses in the system. A treatment of the flow of electromagnetic energy is given for a complete of illustrative relationship in time and frequency domain.

Table of Contents

List of Tables	xii
List of Figures	xiii
Chapter: 1 Introduction	1
1.1 Localization of electromagnetic energy in space	1
1.2 Maxwell's equations	2
1.3 Flux derivative.....	4
1.4 The Larmor formula.....	5
Chapter 2: Poynting's Theorem.....	8
2.1 Poynting's theorem	8
2.2 Poynting's vector.....	11
2.2.1 Definition.....	11
2.2.2 Time-average Poynting's vector.....	12
Chapter 3: Coaxial Waveguide (two-conductor).....	14
3.1 TEM mode.....	14
3.2 TM mode	16
3.3 TE mode	27
3.4 First 16 modes	32
Chapter 4: Rectangular Waveguide (one-conductor)	35
4.1 TE mode	35
4.2 TM mode	41
4.3 First 18 modes	46
Chapter 5: Circular Waveguide (one-conductor)	50
5.1 TE mode	50
5.2 TM mode	54
5.3 First 30 modes	59
5.4 Mixed modes	64
Chapter 6: Several Examples Illustrating the Energy Flow Using the Poynting's Vector	67
6.1 Single conductor carrying a current	67

6.2 Poynting's vector illustrating the propagation of energy along a transmission line connecting a battery to a load	69
6.3 Simple circuit (battery plus two resistors).....	71
6.4 Leaky coaxial cable.....	73
Chapter 7: Examples illustrating the Poynting's vector transmission of energy in time-varying cases.....	75
7.1 Time Harmonic Plane Wave	75
7.1.1 Introduction	75
7.1.2 Fields and the Poynting's vector	75
7.1.3 Example	77
7.2 Two plane waves traveling in opposite directions	78
7.3 Poynting's vector in a resonator	81
7.3.1 Introduction	81
7.3.2 Electromagnetic field in a resonator.....	82
7.4 Poynting's vector flow of energy in a lossy material	84
7.4.1 Introduction	84
7.4.2 Example	85
7.5 Poynting's vector flow of energy in a good conductor	86
7.5.1 Introduction	86
7.5.2 Example	88
7.6 Poynting's vector in a transmission line.....	90
7.6.1 Introduction	90
7.6.2 Example	91
7.7 Traveling in two conductors system.....	93
7.7.1 Parallel Planes (TEM mode)	93
7.7.2 Parallel Planes (TM mode).....	94
7.7.3 Parallel Planes (TE mode).....	96
Chapter 8: Other Applications.....	99
8.1 RLC circuit.....	99
8.2 A solenoidal coil.....	100
8.3 Poynting's vector around a Hertzian dipole	102

8.4 Half-wave Antenna	106
Chapter 9: Conclusion	109
Bibliography	110
Vita	111

List of Tables

Table 1: Generalized Forms of Maxwell's equations	3
Table 2: x_{nl} for TM_{nl} mode of coaxial waveguide ($b/a = 1.8$)	17
Table 3: x'_{nl} for TE_{nl} mode of coaxial waveguide ($b/a = 1.8$)	27
Table 4: p'_{nl} for TE_{nl} mode of a circular waveguide ($a=3$ cm).....	51
Table 5: p_{nl} for TM_{nl} mode of a circular waveguide ($a=3$ cm)	55

List of Figures

Figure 1: The 3D pattern of Poynting vector field that.....	7
Figure 2: Illustration of the Poynting theorem	11
Figure 3: Coaxial waveguide	14
Figure 4: Fields distribution in a coaxial waveguide	15
Figure 5: The TEM mode of Poynting vector for a coaxial waveguide	16
Figure 6: The first four orders of the Bessel's function of the first kind	20
Figure 7: The first four orders of the Bessel's function of the second kind.....	20
Figure 8: The derivative of the first four orders of the Bessel's function of.....	21
Figure 9: The derivative of the first four orders of the Bessel's	22
Figure 10: TM_{01} mode of Poynting's vector along the radius.....	23
Figure 11: TM_{01} mode of Poynting vector for a coaxial waveguide.....	24
Figure 12: TM_{11} mode of Poynting vector for a coaxial waveguide.....	25
Figure 13: TM_{21} mode of Poynting vector for a coaxial waveguide.....	26
Figure 14: TE_{11} mode of Poynting vector for a coaxial waveguide.....	29
Figure 15: TE_{21} mode of Poynting vector for a coaxial waveguide.....	30
Figure 16: TE_{31} mode of Poynting vector for a coaxial waveguide.....	31
Figure 17: A rectangular waveguide with width a, height b and	35
Figure 18: The electromagnetic field configuration of TE_{10} mode	37
Figure 19: The electromagnetic field configuration in the z-y plane	37
Figure 20: The electromagnetic field configuration in the x-z plane	38
Figure 21: TE_{10} mode of Poynting vector for a rectangular waveguide	39
Figure 22: TE_{11} mode of Poynting vector for a rectangular waveguide	40
Figure 23: TE_{21} mode of Poynting vector for a rectangular waveguide	41

Figure 24: The electromagnetic field configuration of the TM_{11} mode	42
Figure 25: The electromagnetic field configuration in the z-y plane.....	43
Figure 26: TM_{11} mode of Poynting vector for a rectangular waveguide	44
Figure 27: TM_{21} mode of Poynting vector for a rectangular waveguide	45
Figure 28: TM_{22} mode of Poynting vector for a rectangular waveguide	46
Figure 29: TE_{01} mode of Poynting vector for a rectangular waveguide	52
Figure 30: TE_{11} mode of Poynting vector for a rectangular waveguide	53
Figure 31: TE_{21} mode of Poynting vector for a rectangular waveguide	54
Figure 32: TM_{01} mode of Poynting vector for a rectangular waveguide	56
Figure 33: TM_{11} mode of Poynting vector for a rectangular waveguide	57
Figure 34: TM_{21} mode of Poynting vector for a rectangular waveguide	58
Figure 35: The power density when TE_{01} and TE_{10} modes.....	65
Figure 36: The power density when TE_{11} and TM_{01} modes.....	66
Figure 37: The Poynting's vector $P = E \times H$ near a single conductor	67
Figure 38: Poynting vector flow from a battery to a load.....	70
Figure 39: A simple circuit with a battery and two resistors.....	71
Figure 40: The contour plot of the electric potential for a simple	72
Figure 41: The magnitude of Poynting vector	72
Figure 42: A coaxial cable with applied voltage V	73
Figure 43: The power density inside a leaky coaxial cable along the axial.....	74
Figure 44: The electromagnetic fields and the magnitude	76
Figure 45: The energy density at $t = 0, T/8$, and $T/4$	80
Figure 46: The direction of energy flow at $t = T/8$	81
Figure 47: The electromagnetic fields in a resonator system.....	82
Figure 48: The enegry density at $t = 0, l\mu\epsilon/4, l\mu\epsilon/2, 3l\mu\epsilon/4$	83

Figure 49: Power density loss when wave enters copper from free space.....	88
Figure 50: Electromagnetic fields in a transmission line.....	90
Figure 51: The side view of a transmission line	91
Figure 52: The power flow contour plot of a transmission line.....	92
Figure 53: Parrallel plane waveguide	93
Figure 54: TEM mode in parallel plane waveguide.....	94
Figure 55: The first three TM and TE modes of time-average Poynting vector.....	97
Figure 56: A series RLC circuit	99
Figure 57: The magnetic field inside a solenoid	101
Figure 58: The induced electric field inside a solenoid	101
Figure 59: The power density inside a solenoid	102
Figure 60: A Hertzian dipole.....	103
Figure 61: The 3-D power pattern of a Hertzian dipole.....	105
Figure 62: A half-wave antenna	107

Chapter: 1 Introduction

1.1 Localization of electromagnetic energy in space

The fundamental fact leading to the justification of the electromagnetic flow of energy expressed by Poynting's vector and Poynting's theorem is the localization of electromagnetic energy in space. For electric energy density:

$$W_E = \frac{1}{2} \vec{D} \cdot \vec{E} = \frac{1}{2} \epsilon E^2 = \frac{1}{2} \frac{D^2}{\epsilon} \quad (J/m^3) \quad (1.1)$$

where E = intensity of the electric field (V/m),

D = displacement vector (C/m^2),

and ϵ = electric permittivity (F/m).

For magnetic energy density:

$$W_m = \frac{1}{2} \vec{B} \cdot \vec{H} = \frac{1}{2} \mu H^2 = \frac{1}{2} \frac{B^2}{\mu} \quad (J/m^3) \quad (1.2)$$

where H = intensity of the magnetic field (A/m),

B = magnetic flux density (Tesla)

and μ = magnetic permeability (H/m).

We consider the rigorously correct expression which is the integral representation of the electric and magnetic energy over the volume of entire space,

$$W_{EM} = \iiint_V \frac{\vec{D} \cdot \vec{E}}{2} dv + \iiint_V \frac{\vec{B} \cdot \vec{H}}{2} dv \quad (1.3)$$

Proceeding from the notion of the localization of electromagnetic energy in space we arrive to the conclusion that the electromagnetic energy flows from the volume V surrounded by the surface S , its amount being $\oint P_n dS$ units of energy/second (J/sec). This statement is called Poynting's theorem and the vector P is called Poynting's vector.

The Maxwell's equations system, which will be considered in the following is uniquely and unambiguously determined by the fields system (the electromagnetic

field at each point in space and each moment in time is uniquely and unambiguously determined if the initial values of the vectors \vec{E} and \vec{H} are given for all points of space.) An observation must be made that the uniqueness theorem is not determined for the infinite space since only a finite region of space is available for our observation and probing. Only limiting the observation to a finite space confers a direct physical meaning to the uniqueness theorem to which the addition of boundary conditions or its boundary conditions permits unambiguous solutions of Maxwell's equations.

If it is considered that the flux of energy is equal to $\vec{P} + \nabla \times \vec{b}$ (where $\vec{P} = \vec{E} \times \vec{H}$) and \vec{b} is an arbitrary vector, then, after the integration over any closed surface the total energy flux through this surface remains equal to $\oint P_n dS$.

The uniqueness theorem is proven in classical manuals of electromagnetic field theory, such as Stratton. When considering the entire infinite space by setting the values of the field vectors on the boundary surface S , and as condition at infinity, HR^2 and ER^2 remain finite when $R \rightarrow \infty$; then the integral of Poynting's vector over an infinitely remote surface becomes zero which lead us to believe that the uniqueness of the solutions of the field equation also results from such condition.

For a constant field the condition expresses the fact that if all the charges and currents producing a field are in a definite region of space V , then the intensity of the field at infinity must decrease not slower than the reciprocal of the R^2 . Such conditions, used for a constant field cannot be applied to a varying field (the conditions are sufficient but not necessary for the vanishing of the flux of Poynting's vector through an infinitely remote surface.)

1.2 Maxwell's equations

The four Maxwell's equations are listed in Table 1.

Table 1: Generalized Forms of Maxwell's equations

Point Form	Integral Form	Remarks
$\nabla \cdot \vec{D} = \rho_v$	$\oint_s \vec{D} \cdot d\vec{S} = \int_{vol} \rho_v dv$	Gauss's law
$\nabla \cdot \vec{B} = 0$	$\oint_s \vec{B} \cdot d\vec{S} = 0$	Gauss's law for magnetic fields
$\nabla \times \vec{E} = -\frac{\partial \vec{B}}{\partial t}$	$\oint_s \vec{E} \cdot d\vec{l} = - \int_s \frac{\partial \vec{B}}{\partial t} \cdot d\vec{S}$	Faraday's law
$\nabla \times \vec{H} = \vec{J} + \frac{\partial \vec{D}}{\partial t}$	$\oint_s \vec{H} \cdot d\vec{l} = \int_s \vec{J} + \frac{\partial \vec{D}}{\partial t} \cdot d\vec{S}$	Ampere's circuit law

The Lorentz force equation:

$$\vec{F} = q(\vec{E} + \vec{u} \times \vec{B}) \quad (1.4)$$

It is associated with Maxwell's equations. The equation of continuity:

$$\nabla \cdot \vec{J} = -\frac{\partial \rho_v}{\partial t} \quad (1.5)$$

It is also implicit in Maxwell's equations. The concepts of linearity, isotropy, and homogeneity of a material medium still apply for time-varying fields; in a linear, homogeneous, and isotropic medium characterized by σ , ϵ , and μ , the constitutive relations hold of time-varying fields:

$$\vec{D} = \epsilon \vec{E} = \epsilon_0 \vec{E} + \vec{P} \quad (1.6)$$

$$\vec{B} = \mu \vec{H} = \mu_0 (\vec{H} + \vec{M}) \quad (1.7)$$

$$\vec{J} = \sigma \vec{E} + \rho_v \vec{u} \quad (1.8)$$

Therefore, the boundary conditions remain valid for time-varying fields:

$$E_{1t} - E_{2t} = 0 \quad \text{or} \quad (\vec{E}_1 - \vec{E}_2) \times \hat{n} = 0 \quad (1.9)$$

$$H_{1t} - H_{2t} = K \quad \text{or} \quad (\vec{H}_1 - \vec{H}_2) \times \hat{n} = \vec{K} \quad (1.10)$$

$$D_{1n} - D_{2n} = \rho_s \quad \text{or} \quad (\vec{D}_1 - \vec{D}_2) \cdot \hat{n} = \rho_s \quad (1.11)$$

$$B_{1n} - B_{2n} = 0 \quad \text{or} \quad (\vec{B}_1 - \vec{B}_2) \cdot \hat{n} = 0 \quad (1.12)$$

where \hat{n} is the unit normal vector to the boundary.

However, for a perfect conductor ($\sigma \cong \infty$) in a time-varying field,

$$\vec{E} = 0, \quad \vec{H} = 0, \quad \vec{J} = 0 \quad (1.13)$$

Thus,

$$\vec{B}_n = 0, \quad \vec{E}_t = 0 \quad (1.14)$$

For a perfect dielectric ($\sigma \cong 0$), equations (1.9) to (1.12) hold except that $\vec{K} = 0$. Though equations (1.4) to (1.14) are not Maxwell's equations, they are associated with them.

1.3 Flux derivative

From Ampere's law, we know that a magnetic field is proportional to electrical current sources. However, if the control volume or surface is not fixed, we cannot place the time differentiation in front of the integral. From Table 1, we have Ampere's law:

$$\nabla \times \vec{H} = \vec{J} - \frac{\partial \vec{D}}{\partial t} \quad (1.15)$$

In order to apply a more general formula to a moving surface, we assign \vec{u} to be a differentiable velocity field (the rate of the change of current position and reference position), not necessarily to be the velocity of any actual material. Subtract each side of the equation (1.15) with $\nabla \times (\vec{u} \times \vec{D})$, we get

$$\nabla \times \vec{H} - \nabla \times (\vec{u} \times \vec{D}) = -\frac{\partial \vec{D}}{\partial t} + \vec{J} - \nabla \times (\vec{u} \times \vec{D}) \quad (1.16)$$

Next, we add and subtract $\vec{u} \nabla \cdot \vec{D}$ on the right-hand side,

$$\begin{aligned} \nabla \times (\vec{H} - \vec{u} \times \vec{D}) &= -\frac{\partial \vec{D}}{\partial t} + \vec{J} - \nabla \times (\vec{u} \times \vec{D}) + \vec{u} \nabla \cdot \vec{D} - \vec{u} \nabla \cdot \vec{D} \\ &= (\vec{J} - \vec{u} \nabla \cdot \vec{D}) + \left(\frac{\partial \vec{D}}{\partial t} + \nabla \times (\vec{u} \times \vec{D}) + \vec{u} \nabla \cdot \vec{D} \right) \\ &= (\vec{J} - \vec{u} \rho_v) + \left(\frac{\partial \vec{D}}{\partial t} + \nabla \times (\vec{u} \times \vec{D}) + \vec{u} \rho_v \right) \end{aligned} \quad (1.17)$$

And then, we assign the magnetomotive intensity, \mathcal{H} :

$$\mathcal{H} = \vec{H} - \vec{u} \times \vec{D} \quad (1.18)$$

and the conduction current density, \mathcal{J} :

$$\mathcal{J} = (\vec{J} - \vec{u}\rho_v) \quad (1.19)$$

Therefore, equation (1.17) can be rewritten as the following:

$$\nabla \times \mathcal{H} = \mathcal{J} + \left(\frac{\partial \vec{D}}{\partial t} + \nabla \times (\vec{u} \times \vec{D}) + \vec{u}\rho_v \right) \quad (1.20)$$

Now, we compare equation (1.20) with (1.15),

$$\nabla \times \mathcal{H} = \mathcal{J} + \left(\frac{\partial \vec{D}}{\partial t} + \nabla \times (\vec{u} \times \vec{D}) + \vec{u}\rho_v \right) \quad (1.20)$$

$$\nabla \times \vec{H} = \vec{J} - \frac{\partial \vec{D}}{\partial t} \quad (1.15)$$

We then define the flux derivative of the field \vec{D} :

$$\frac{d_f \vec{D}}{dt} = \frac{\partial \vec{D}}{\partial t} + \nabla \times (\vec{u} \times \vec{D}) + \vec{u}\rho_v \quad (1.21)$$

Do the same thing to Faraday's law, and we have the flux derivative of the field \vec{B} :

$$\frac{d_f \vec{B}}{dt} = \frac{\partial \vec{B}}{\partial t} + \nabla \times (\vec{B} \times \vec{u}) \quad (1.22)$$

1.4 The Larmor formula

The Larmor formula gives the rate of energy of radiation from an accelerating or decelerating charge and found the power radiated in terms of the charge and acceleration.

By using Liénard-Wiechert formulae, we can find the potentials for moving charges, either accelerating or uniformly moving. The electric and magnetic fields then are derived from the potentials by utilizing the vector potential, \vec{A} , and the scalar potential, Φ :

$$\vec{E} = -\nabla\Phi - \frac{\partial \vec{A}}{\partial t} \quad (1.23)$$

and

$$\vec{B} = \nabla \times \vec{A} \quad (1.24)$$

For a moving charge which is at rest at the origin at time $t=0$, and the velocity of the charge is small relative to the speed of light, the generated electric field and magnetic field are

$$E_\theta \approx \frac{e}{4\pi\epsilon_0 c^2} \frac{\sin \theta}{r} \dot{u} \quad (1.25)$$

and

$$B_\phi \approx \frac{e}{4\pi\epsilon_0 c^3} \frac{\sin \theta}{r} \dot{u} \quad (1.26)$$

where u is the velocity of the charge, c is the speed of light and \dot{u} is the acceleration of the charge. r is the distance from the charge to a specific point in which we are interested. The radial Poynting's flux (which will be discussed more in Chapter 2) during the pulse of electric field in the θ direction changes from 0 to E_θ and back to 0 is

$$P_r = E_\theta \times H_\phi = E_\theta \times \frac{B_\phi}{\mu_0} = \frac{e^2}{16\pi^2\epsilon_0 c^3} \frac{\sin^2 \theta}{r^2} \dot{u}^2 \quad (1.27)$$

From equation (1.27) we know that the Poynting's vector has a dipolar form, as shown in Figure 1. Note that the energy loss is symmetric, which means that the radiating charge only loses power, there is no momentum lost.

We can integrate equation (1.27) to obtain the instantaneous power radiated by the charge

$$P = \frac{e^2}{6\pi\epsilon_0 c^3} \dot{u}^2 \quad (1.28)$$

Equation (1.28) indicated that the power that is radiated by an accelerating charge is proportional to the square of acceleration. However, remember that this formula breaks down for velocities that are close to the speed of light due to relativistic effects.

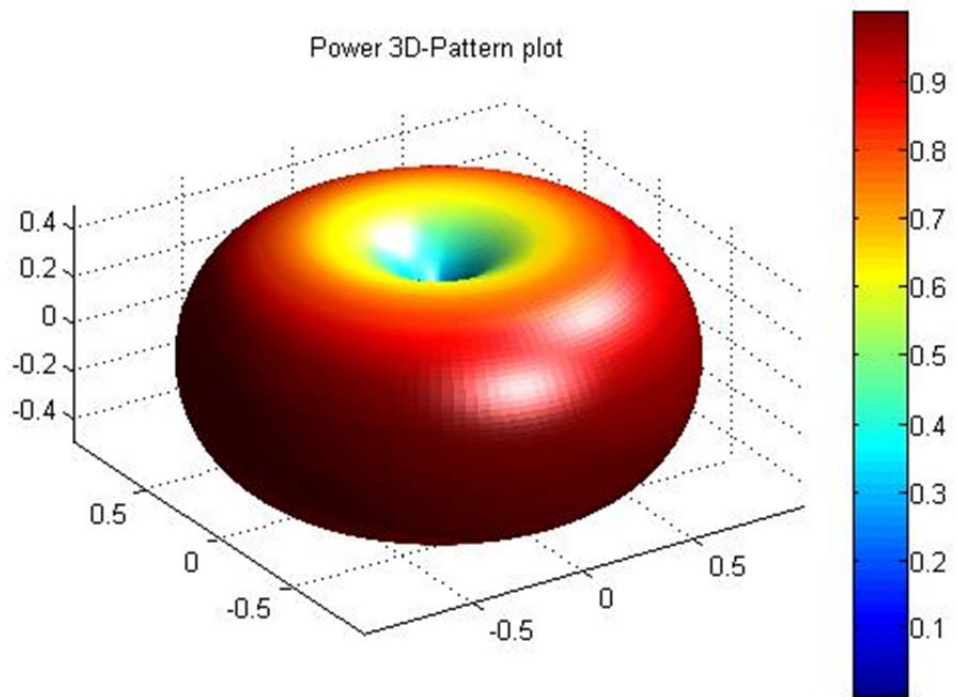


Figure 1: The 3D pattern of Poynting vector field that generated by a moving charge

Chapter 2: Poynting's Theorem

2.1 Poynting's theorem

To arrive to Poynting's theorem, the development begins with Ampere's Law, which is under the assumption that the medium may be conductive:

$$\nabla \times \vec{H} = -\frac{\partial \vec{D}}{\partial t} + \vec{J} \quad (2.1)$$

where \vec{H} is the magnetic field (A/m), \vec{D} is the electric displacement field (C/m^2), and \vec{J} is the conduction current density. Next, we dot multiply Ampere's Law with electric field \vec{E} on both sides of equation (2.1),

$$\vec{E} \cdot \nabla \times \vec{H} = -\frac{\partial \vec{D}}{\partial t} \cdot \vec{E} + \vec{E} \cdot \vec{J} \quad (2.2)$$

Then, we use the vector identity, which may be proved by expansion in rectangular coordinates:

$$\vec{E} \cdot \nabla \times \vec{H} = \vec{H} \cdot \nabla \times \vec{E} - \nabla \cdot (\vec{E} \times \vec{H}) \quad (2.3)$$

applying the vector identity to equation (2.2), we have

$$\vec{H} \cdot \nabla \times \vec{E} - \nabla \cdot (\vec{E} \times \vec{H}) = -\frac{\partial \vec{D}}{\partial t} \cdot \vec{E} + \vec{E} \cdot \vec{J} \quad (2.4)$$

From Faraday's law,

$$\nabla \times \vec{E} = -\frac{\partial \vec{B}}{\partial t} \quad (2.5)$$

After substituting (2.5) in (2.4), we have

$$-\nabla \cdot (\vec{E} \times \vec{H}) = \vec{J} \cdot \vec{E} + \vec{E} \cdot \frac{\partial \vec{D}}{\partial t} + \vec{H} \cdot \frac{\partial \vec{B}}{\partial t} \quad (2.6)$$

Next, let us assume that the fields are in an isotropic medium where the values of ϵ and μ are independent of time. Then we may substitute $\vec{D} = \epsilon \vec{E}$ and $\vec{B} = \mu \vec{H}$, and move ϵ and μ out of the time derivative to obtain

$$-\nabla \cdot (\vec{E} \times \vec{H}) = \vec{J} \cdot \vec{E} + \epsilon \vec{E} \cdot \frac{\partial \vec{E}}{\partial t} + \mu \vec{H} \cdot \frac{\partial \vec{H}}{\partial t} \quad (2.7)$$

The two derivative terms can be rewritten as:

$$\epsilon \vec{E} \cdot \frac{\partial \vec{E}}{\partial t} = \frac{\partial}{\partial t} \left(\frac{1}{2} \vec{D} \cdot \vec{E} \right) \quad (2.8)$$

and

$$\mu \vec{H} \cdot \frac{\partial \vec{H}}{\partial t} = \frac{\partial}{\partial t} \left(\frac{1}{2} \vec{B} \cdot \vec{H} \right) \quad (2.9)$$

With (2.8) and (2.9), equation (2.7) becomes

$$-\nabla \cdot (\vec{E} \times \vec{H}) = \vec{J} \cdot \vec{E} + \frac{\partial}{\partial t} \left(\frac{1}{2} \vec{D} \cdot \vec{E} \right) + \frac{\partial}{\partial t} \left(\frac{1}{2} \vec{B} \cdot \vec{H} \right) \quad (2.10)$$

Last, we integrate (2.10) over a volume:

$$\begin{aligned} - \int_{\text{vol}} \nabla \cdot (\vec{E} \times \vec{H}) \cdot d\mathbf{v} \\ = \int_{\text{vol}} \vec{J} \cdot \vec{E} d\mathbf{v} + \int_{\text{vol}} \frac{\partial}{\partial t} \left(\frac{1}{2} \vec{D} \cdot \vec{E} \right) d\mathbf{v} + \int_{\text{vol}} \frac{\partial}{\partial t} \left(\frac{1}{2} \vec{B} \cdot \vec{H} \right) d\mathbf{v} \end{aligned} \quad (2.11)$$

Then we apply divergence theorem to the left-hand side to change the volume integral into an integral over the surface that encloses the volume. It is assumed that the positive normal is the outward normal. For the right-hand side, we take the time differentiations out of the operations of spatial integration. Now we obtain

$$\begin{aligned} - \oint_S (\vec{E} \times \vec{H}) \cdot d\mathbf{S} = \\ \int_{\text{vol}} \vec{J} \cdot \vec{E} d\mathbf{v} + \frac{\partial}{\partial t} \int_{\text{vol}} \left(\frac{1}{2} \vec{D} \cdot \vec{E} \right) d\mathbf{v} + \frac{\partial}{\partial t} \int_{\text{vol}} \left(\frac{1}{2} \vec{B} \cdot \vec{H} \right) d\mathbf{v} \end{aligned} \quad (2.12)$$

Equation (2.12) is well known as Poynting's Theorem.

On the right-hand side, the result of integrating over the volume of the source is the power oozing out of the surface. For the first integral, $\int_{\text{vol}} \vec{J} \cdot \vec{E} d\mathbf{v}$ is the total instantaneous Joule loss within the volume. If sources exist in the volume and are delivering power to the volume, then

$$\int_{\text{vol}} \vec{J} \cdot \vec{E} d\mathbf{v} > 0$$

If sources exist in the volume and are transferring power out of the volume, then

$$\int_{\text{vol}} \vec{J} \cdot \vec{E} dv < 0$$

If there are no sources in the interested volume, $\int_{\text{vol}} \vec{J} \cdot \vec{E} dv$ is the total ohmic power that is dissipated in the volume. Moreover, if the fields are static, equation (2.12) becomes

$$-\oint_S (\vec{E} \times \vec{H}) \cdot dS = \int_{\text{vol}} \vec{J} \cdot \vec{E} dv \quad (2.13)$$

Equation (2.13) states that for static fields, the net power flowing through surface s into volume v is equal to the power loss in this certain volume.

Now, we move to the second and third terms in equation (2.12). $\frac{\epsilon E^2}{2}$ is the energy density in the electric field and $\frac{\mu H^2}{2}$ is the energy density in the magnetic field. $\int_{\text{vol}} (\frac{\epsilon E^2}{2} + \frac{\mu H^2}{2}) dv$ is the total energy stored in the electric and magnetic fields. Since time derivatives are taken of the second and third terms, $\frac{\partial}{\partial t} \int_{\text{vol}} (\frac{\epsilon E^2}{2} + \frac{\mu H^2}{2}) dv$ is the time rate of increase of energy stored within this volume, or the instantaneous power is going to increase the stored power. As a result, the sum of the expressions on the right-hand side, $\int_{\text{vol}} \vec{J} \cdot \vec{E} dv + \frac{\partial}{\partial t} \int_{\text{vol}} (\frac{\epsilon E^2}{2} + \frac{\mu H^2}{2}) dv$ is the total power flowing into the volume. In addition, the total power flowing out of the volume is thus

$$\oint_S (\vec{E} \times \vec{H}) \cdot dS \quad (2.14)$$

Therefore, Poynting's theorem can be interpreted thus: "the total power carried by electromagnetic fields that flows into a known volume is equal to the power converted into heat supplied by sources plus the increase in energy stored in the fields in the volume." The idea of Poynting's theorem is plotted in Figure 2. In a certain volume, V , which contains a current source, J , there is some power stored in the volume while some of the power is transferring out of the volume.

The power oozing out through the surface

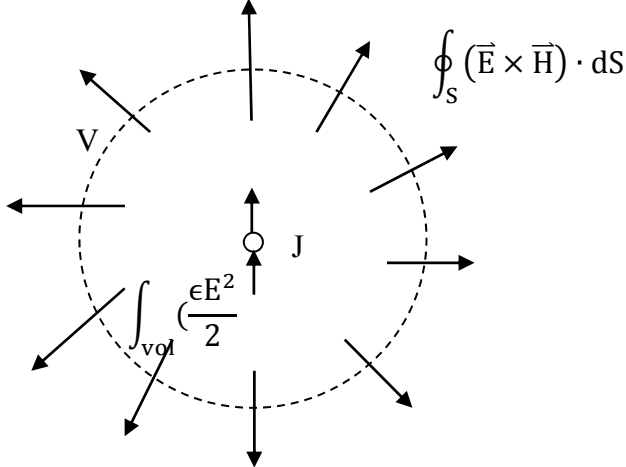


Figure 2: Illustration of the Poynting theorem

2.2 Poynting's vector

2.2.1 Definition

In Poynting's theorem, as shown in equation (2.12), the cross product $\vec{E} \times \vec{H}$ appears and is defined as the instantaneous Poynting's vector, \vec{P} ,

$$\vec{P} = \vec{E} \times \vec{H} \text{ (W/m}^2\text{)} \quad (2.15)$$

Poynting's vector can be interpreted as the energy flux, or an instantaneous local power strength of an electromagnetic wave. Luckily, the direction of Poynting's vector \vec{P} indicates that the direction of the instantaneous power flow at a specific location. By using this homonym, we can think of the Poynting's vector as a “pointing” vector, a vector that points the power flow direction. Since \vec{P} is the cross product of \vec{E} and \vec{H} , the direction of power flow is normal to both electric and magnetic fields at any point.

Now, equation (2.12) can be rewritten as

$$-\oint_S \vec{P} \cdot d\vec{S} = \int_{vol} \vec{J} \cdot \vec{E} dv + \frac{\partial}{\partial t} \int_{vol} \left(\frac{1}{2} \vec{D} \cdot \vec{E} \right) dv + \frac{\partial}{\partial t} \int_{vol} \left(\frac{1}{2} \vec{B} \cdot \vec{H} \right) dv \quad (2.16)$$

2.2.2 Time-average Poynting's vector

The time-average Poynting's vector is obtained by integrating the instantaneous Poynting's vector over a specific period and then dividing by this period. For the complex notation form, the time-average Poynting's vector (average power density) over one period can be expressed as

$$\langle \vec{P} \rangle = \langle \vec{E} \times \vec{H} \rangle = \frac{1}{2} \operatorname{Re}\{\vec{E} \times \vec{H}^*\} \quad (2.17)$$

The real part of it represents the real part of the power density and the imaginary part of it represents the reactive power. Let us derive the conservation of energy equation in complex forms to take a better look at the reactive power. From Table 1 we can rewrite the two Maxwell' equations in the complex forms:

$$\nabla \times \vec{H} = \vec{J} + j\omega\epsilon\vec{E} = \vec{J}_i + \sigma\vec{E} + j\omega\epsilon\vec{E} \quad (2.18)$$

$$\nabla \times \vec{E} = -j\omega\mu\vec{H} \quad (2.19)$$

Next, we dot multiply the equation (2.19) by \vec{H}^* , and take the conjugate on (2.18) first and then dot multiply by \vec{E} . We can rewrite those two equations as

$$\vec{E} \cdot (\nabla \times \vec{H}^*) = \vec{E} \cdot \vec{J}_i^* + \sigma\vec{E} \cdot \vec{E}^* - j\omega\epsilon\vec{E} \cdot \vec{E}^* \quad (2.20)$$

$$\vec{H}^* \cdot (\nabla \times \vec{E}) = -j\omega\mu\vec{H} \cdot \vec{H}^* \quad (2.21)$$

After we subtract (2.21) from (2.20), we have

$$\vec{E} \cdot (\nabla \times \vec{H}^*) - \vec{H}^* \cdot (\nabla \times \vec{E}) = \vec{E} \cdot \vec{J}_i^* + \sigma\vec{E} \cdot \vec{E}^* - j\omega\epsilon\vec{E} \cdot \vec{E}^* + j\omega\mu\vec{H} \cdot \vec{H}^* \quad (2.22)$$

Using the vector identity to rearrange (2.22) to

$$-\nabla \cdot (\vec{E} \times \vec{H}^*) = \vec{E} \cdot \vec{J}_i^* + \sigma|\vec{E}|^2 + j\omega(\mu|\vec{H}|^2 - \epsilon|\vec{E}|^2) \quad (2.23)$$

Taking volume integration on the both sides of (2.23) and dividing both sides by 2:

$$\begin{aligned} & - \iiint \nabla \cdot (\frac{1}{2} \vec{E} \times \vec{H}^*) dV \\ &= \frac{1}{2} \iiint \vec{E} \cdot \vec{J}_i^* dV + \frac{1}{2} \iiint \sigma|\vec{E}|^2 dV + j2\omega \iiint \left(\frac{1}{4}\mu|\vec{H}|^2 - \frac{1}{4}\epsilon|\vec{E}|^2 \right) dV \end{aligned} \quad (2.24)$$

Applying the divergence theorem to the left side to have

$$\begin{aligned}
 & -\oint\left(\frac{1}{2}\vec{E} \times \vec{H}^*\right) ds \\
 & = \frac{1}{2} \iiint \vec{E} \cdot \vec{J}_i^* dv + \frac{1}{2} \iiint \sigma |\vec{E}|^2 dv + j2\omega \iiint \left(\frac{1}{4}\mu|\vec{H}|^2 - \frac{1}{4}\varepsilon|\vec{E}|^2\right) dv
 \end{aligned} \tag{2.25}$$

If we have an electromagnetic source supplying power within an area, the supplied complex power is represented as the first term with a negative sign. The second term on the right side represents the dissipated real power, which is always real. The last two terms on the right side are in terms of time-average magnetic and electric fields, respectively, representing the reactive power associated with magnetic and electric fields, respectively being imaginary. The summation of terms on the right side describes the transmission of complex power in the system within a specific surface.

Note that if the permeabilities and permittivities are imaginary, the contributions from the imaginary parts represent the losses because they turn into real numbers after they are multiplied by j . Therefore, if we have a material with complex either permeability or permittivity, there will be real power losses during transmission.

Last but not least, we see that the Poynting's vector will be zero when either the electric or the magnetic field is zero, or when the two fields are parallel to each other. As a result, there is no power flowing in the close area of a static charges system, which only has an electric field. Another case that obtains zero Poynting's vector is that of a perfect conductor. By definition, a perfect conductor should have no tangential component of electric field at its surface. Thus, \vec{P} has zero normal component to the conductor and there is then no power flowing through a perfect conductor.

Chapter 3: Coaxial Waveguide (two-conductor)

A coaxial waveguide is a common two-conductor configuration, which provides transverse electromagnetic mode (TEM), TE, and TM modes. A coaxial waveguide is composed of a central conductor surrounded by a tubular outer conductor. The pair of conductors at $\rho = a$ and $\rho = b$ are assumed ideal, and the dielectric between them is assumed lossless, as shown in Figure 3.

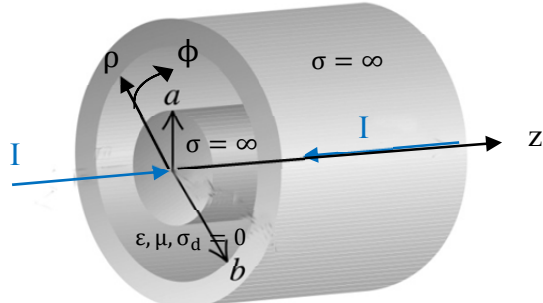


Figure 3: Coaxial waveguide

3.1 TEM mode

The current that flows in the inner conductor forms concentric magnetic field circles around the inner conductor, while the electric field points radially everywhere between the two conductors. The fields can be written as

$$\vec{E} = \frac{V_0}{\rho \ln(\frac{b}{a})} e^{-jkz} \hat{\rho} \quad (3.1)$$

$$\vec{H} = \frac{kV_0}{\rho \omega \mu \ln(\frac{b}{a})} e^{-jkz} \hat{\phi} \quad (3.2)$$

The distributions of fields are shown in Figure 4.

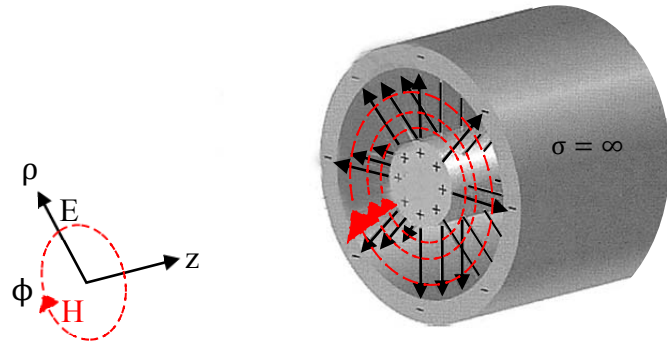


Figure 4: Fields distribution in a coaxial waveguide

Poynting's vector can be written as

$$\vec{P} = \frac{1}{2} \vec{E} \times \vec{H}^* = \frac{1}{2} \frac{V_0^2}{\eta \rho^2 \ln^2(\frac{b}{a})} \hat{z} \quad (3.3)$$

Since there are no fields flowing in the two ideal conductors, the power propagates along the cable (axial direction) in the dielectric region between the two conductors. From equation (3.3) we know that the power is the strongest at the inner conductor and becomes weaker toward the outer conductor. This is because Poynting's vector decays as a function of ρ^2 . For a coax with an inner radius of 1.75 cm and an outer radius of 3 cm, the power distribution for the TEM mode in a coaxial waveguide can be plotted by MATLAB, as shown as Figure 5.

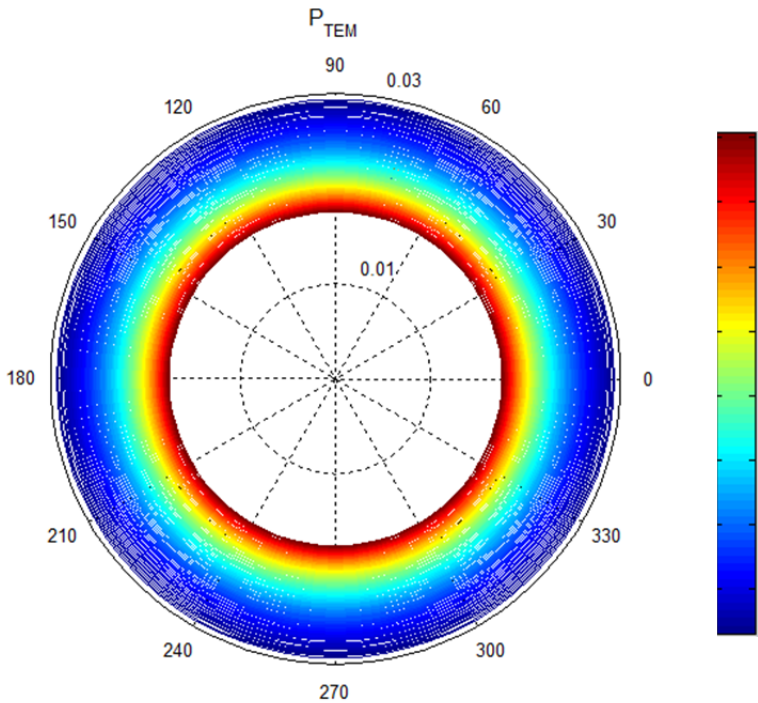


Figure 5: The TEM mode of Poynting vector for a coaxial waveguide

3.2 TM mode

A coaxial cable also supports higher-order modes if the operating frequency is above the cutoff frequency. All the propagating modes are solutions to the wave equations, which are the results from Maxwell's equations, and satisfy all the boundary conditions required for field continuity. First, we solve the wave equation for E_z by using the method of separation of variables:

$$\frac{1}{\rho} \frac{\partial}{\partial \rho} \left(\rho \frac{\partial E_z}{\partial \rho} \right) + \frac{1}{\rho^2} \frac{\partial^2 E_z}{\partial \phi^2} + k_{c,TM}^2 E_z = 0 \quad (3.4)$$

where

$$\beta_{TE} = \sqrt{k^2 - \left(\frac{m\pi}{a}\right)^2 - \left(\frac{n\pi}{b}\right)^2} = \sqrt{k^2 - k_{c,TM}^2} \quad (3.5)$$

And we get

$$E_z(\rho, \phi) = (A' \cos n\phi + B' \sin n\phi)[C' J_n(k_{c,TM}\rho) + D' N_n(k_{c,TM}\rho)] \quad (3.6)$$

Next, we select $\phi = 0$ so that we only have to deal with the cosine variation. We can rearrange equation (3.6) to get

$$E_z(\rho, \phi) = \cos n\phi[C J_n(k_{c,TM}\rho) + D N_n(k_{c,TM}\rho)] \quad (3.7)$$

We then apply boundary conditions at $\rho = a$ and $\rho = b$ to E_z :

$$E_z(a, \phi) = \cos n\phi[C J_n(k_{c,TM}a) + D N_n(k_{c,TM}a)] = 0 \quad (3.8)$$

$$E_z(b, \phi) = \cos n\phi[C J_n(k_{c,TM}b) + D N_n(k_{c,TM}b)] = 0 \quad (3.9)$$

We can now determine the values of $k_{c,TM}$ and most of the unknown constants by solving the Bessel-Neumann combination boundary condition:

$$J_n(k_{c,TM}a)N_n(k_{c,TM}b) - J_n(k_{c,TM}b)N_n(k_{c,TM}a) = 0 \quad (3.10)$$

For $b/a = 1.8$, we find the solutions for TM_{nl} modes by letting

$$x_{nl} = k_{c,TM_{nl}}a$$

We list the value of x_{nl} for $n = 0$ to $n = 9$, and $l = 1$ to $l = 4$ in Table 2.

Table 2: x_{nl} for TM_{nl} mode of coaxial waveguide ($b/a = 1.8$)

l	n									
	0	1	2	3	4	5	6	7	8	9
1	3.91	3.98	4.20	4.50	4.90	5.36	5.87	6.41	6.99	7.51
2	7.85	7.88	7.98	8.15	8.40	8.73	9.03	9.48	9.80	10.31
3	11.78	11.80	11.87	11.98	12.20	12.38	12.70	12.84	13.33	13.55
4	15.70	15.72	15.77	15.86	15.97	16.15	16.25	16.59	16.80	17.08

Finally, we obtain the solution for $E_z(\rho, \phi, z)$ after the values of $k_{c,TM_{nl}}$ have been determined:

$$E_z(\rho, \phi, z) = C \left[J_n(k_{c,TM}\rho) - \frac{J_n(k_{c,TM}b)}{N_n(k_{c,TM}b)} N_n(k_{c,TM}\rho) \right] \cos n\phi e^{-j\beta_{TM}z} \quad (3.11)$$

Since we are solving for TM modes, we can use $H_z = 0$ and the solution of E_z , as

shown in (3.11), to obtain other fields in different directions:

$$E_\rho(\rho, \phi, z) = -j \frac{\beta_{TM} C}{k_{c,TM}} \left[J'_n(k_{c,TM}\rho) - \frac{J_n(k_{c,TM}b)}{N_n(k_{c,TM}b)} N'_n(k_{c,TM}\rho) \right] \cos n\phi e^{-j\beta_{TM}z} \quad (3.12)$$

$$E_\phi(\rho, \phi, z) = j \frac{\beta_{TM} C}{\rho k_{c,TM}^2} \left[J_n(k_{c,TM}\rho) - \frac{J_n(k_{c,TM}b)}{N_n(k_{c,TM}b)} N_n(k_{c,TM}\rho) \right] \sin n\phi e^{-j\beta_{TM}z} \quad (3.13)$$

$$H_\rho(\rho, \phi, z) = -j \frac{\omega \epsilon n C}{\rho k_{c,TM}^2} \left[J_n(k_{c,TM}\rho) - \frac{J_n(k_{c,TM}b)}{N_n(k_{c,TM}b)} N_n(k_{c,TM}\rho) \right] \sin n\phi e^{-j\beta_{TM}z} \quad (3.14)$$

$$H_\phi(\rho, \phi, z) = -j \frac{\omega \epsilon C}{k_{c,TM}} \left[J'_n(k_{c,TM}\rho) - \frac{J_n(k_{c,TM}b)}{N_n(k_{c,TM}b)} N'_n(k_{c,TM}\rho) \right] \cos n\phi e^{-j\beta_{TM}z} \quad (3.15)$$

Then, the Poynting's vector of TM modes in a coaxial waveguide is:

$$\begin{aligned} \vec{P}_{TM} &= \frac{1}{2} \vec{E}_{TM} \times \vec{H}_{TM}^* \\ &= -j \frac{\omega \epsilon C^2}{2k_{c,TM}} \left[J_n(k_{c,TM}\rho) - \frac{J_n(k_{c,TM}b)}{N_n(k_{c,TM}b)} N_n(k_{c,TM}\rho) \right] \\ &\quad \cdot \left[J'_n(k_{c,TM}\rho) - \frac{J_n(k_{c,TM}b)}{N_n(k_{c,TM}b)} N'_n(k_{c,TM}\rho) \right] \cos^2 n\phi \hat{\rho} \\ &\quad + j \frac{\omega \epsilon n C^2}{2\rho k_{c,TM}^2} \left[J_n(k_{c,TM}\rho) - \frac{J_n(k_{c,TM}b)}{N_n(k_{c,TM}b)} N_n(k_{c,TM}\rho) \right]^2 \cos n\phi \sin n\phi \hat{\phi} \\ &\quad + \frac{\omega \epsilon \beta_{TM} C^2}{2k_{c,TM}^2} \left\{ \frac{n^2}{\rho^2 k_{c,TM}^2} \left[J_n(k_{c,TM}\rho) - \frac{J_n(k_{c,TM}b)}{N_n(k_{c,TM}b)} N_n(k_{c,TM}\rho) \right]^2 \sin^2 n\phi \right. \\ &\quad \left. + \left[J'_n(k_{c,TM}\rho) - \frac{J_n(k_{c,TM}b)}{N_n(k_{c,TM}b)} N'_n(k_{c,TM}\rho) \right]^2 \cos^2 n\phi \right\} \hat{z} \end{aligned} \quad (3.16)$$

For $n = 0$ and $l = 1$, the Poynting's vector of the lowest order TM mode can be written as

$$\begin{aligned}
\langle \vec{P} \rangle_{TM,01} = & -j \frac{\omega \epsilon C^2}{2k_{c,TM01}} \left[J_0(k_{c,TM01}\rho) - \frac{J_0(k_{c,TM01}b)}{N_0(k_{c,TM01}b)} N_0(k_{c,TM01}\rho) \right] \\
& \cdot \left[J'_0(k_{c,TM01}\rho) - \frac{J_0(k_{c,TM01}b)}{N_0(k_{c,TM01}b)} N'_0(k_{c,TM01}\rho) \right] \hat{\rho} \\
& + \frac{\omega \epsilon \beta_{TM01} C^2}{2k_{c,TM01}^2} \left[J'_0(k_{c,TM01}\rho) - \frac{J_0(k_{c,TM01}b)}{N_0(k_{c,TM01}b)} N'_0(k_{c,TM01}\rho) \right]^2 \hat{z}
\end{aligned} \tag{3.17}$$

Equation (3.17) shows that TM_{01} only obtains components in the z and ρ directions. The ρ component is always imaginary, and the z component is real as long as β_{TM01} is real. From equation (3.5) we know that $\omega^2 \mu \epsilon$ should then be equal or greater than $k_{c,TM01}^2$. Although the Poynting's vector is formed in both radial and axial directions, power only propagates in the axial direction because the power is reactive in the radial direction.

$J_n(x)$ is the Bessel's function of the first kind and $N_n(x)$, also known as $Y_n(x)$, is the Bessel's function of the second kind. The first 4 orders of $J_n(x)$ and $N_n(x)$ are plotted by MATLAB in Figure 6 and Figure 7.

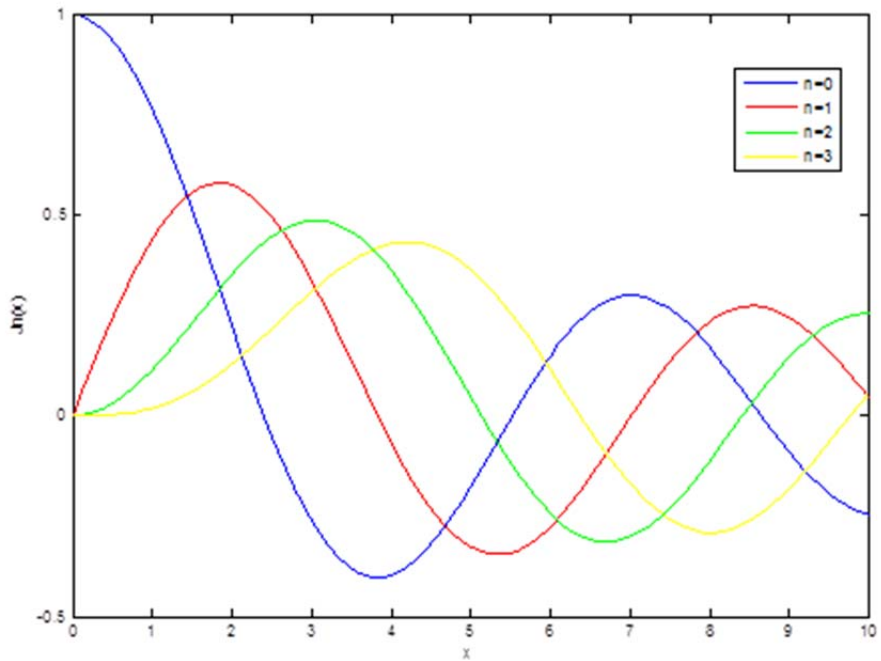


Figure 6: The first four orders of the Bessel's function of the first kind

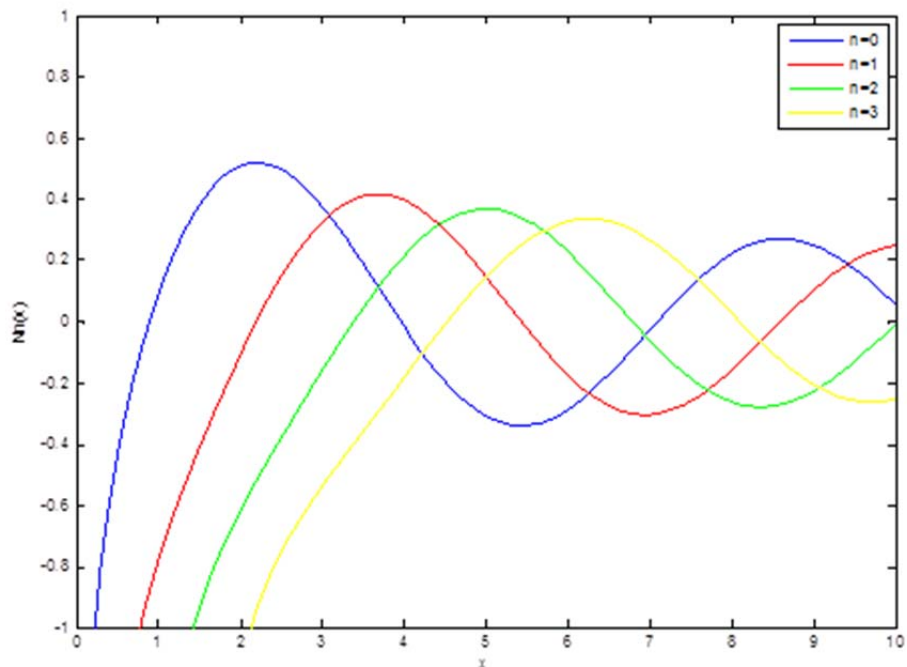


Figure 7: The first four orders of the Bessel's function of the second kind

The derivative of the Bessel's function of the first kind, $J'_n(x)$, and the derivative of the Bessel's function of the second kind, $N'_n(x)$, can be computed from the lower and higher orders of Bessel's function:

$$2J'_n(x) = J_{n-1}(x) - J_{n+1}(x) \quad (3.18)$$

$$2N'_n(x) = N_{n-1}(x) - N_{n+1}(x) \quad (3.19)$$

We can plot $J'_n(x)$ and $N'_n(x)$ by MATLAB, as shown in Figure 8 and Figure 9.

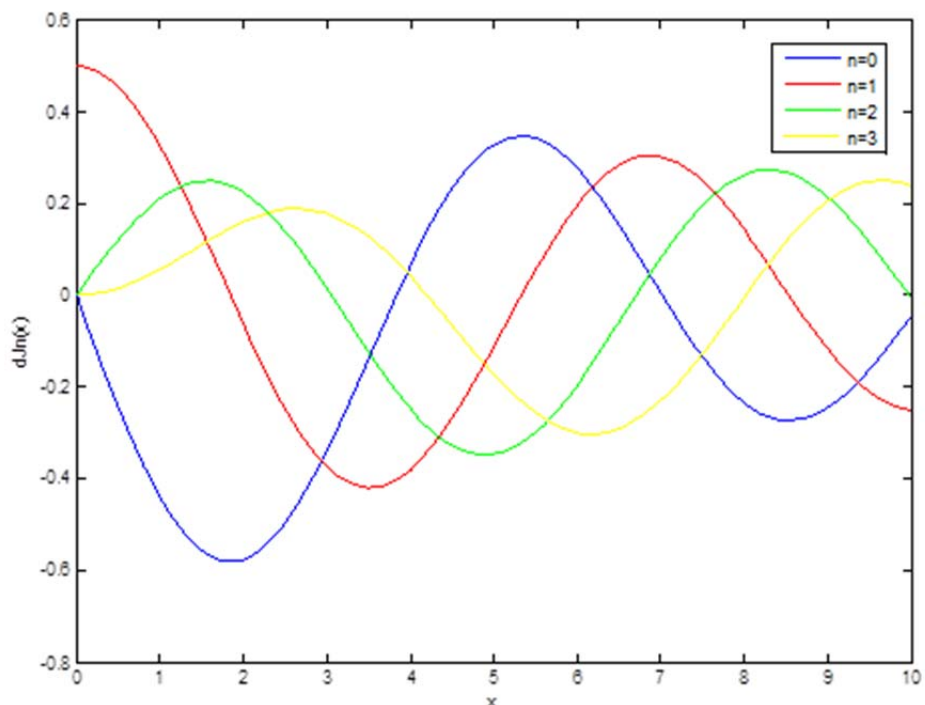


Figure 8: The derivative of the first four orders of the Bessel's function of the first kind

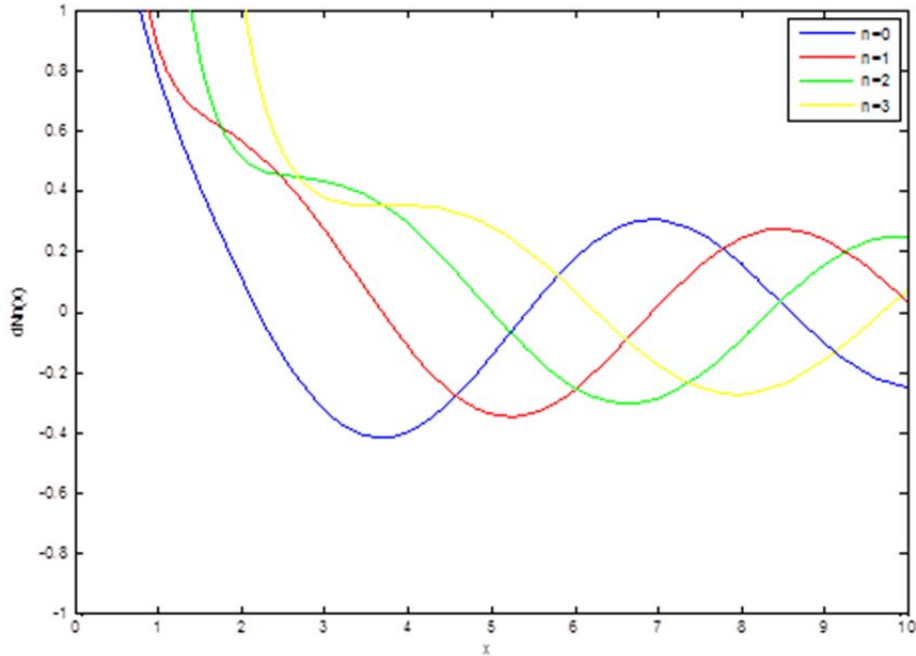


Figure 9: The derivative of the first four orders of the Bessel's function of the second kind

In order to demonstrate Poynting's vector more clearly, we use a coaxial waveguide with an inner conductor radius of 1.75 cm and an outer conductor radius of 3 cm as an example. Since $b/a = 3/1.75 = 1.714$, and from Table 2, $k_{c,TM01}$ can be now calculated:

$$k_{c,TM01} = \frac{3.130}{0.03 - 0.0175} = 250.4 \text{ (rad/m)}$$

The normalized magnitude of Poynting's vector along the radius can be plotted by using MATLAB, as shown in Figure 10.

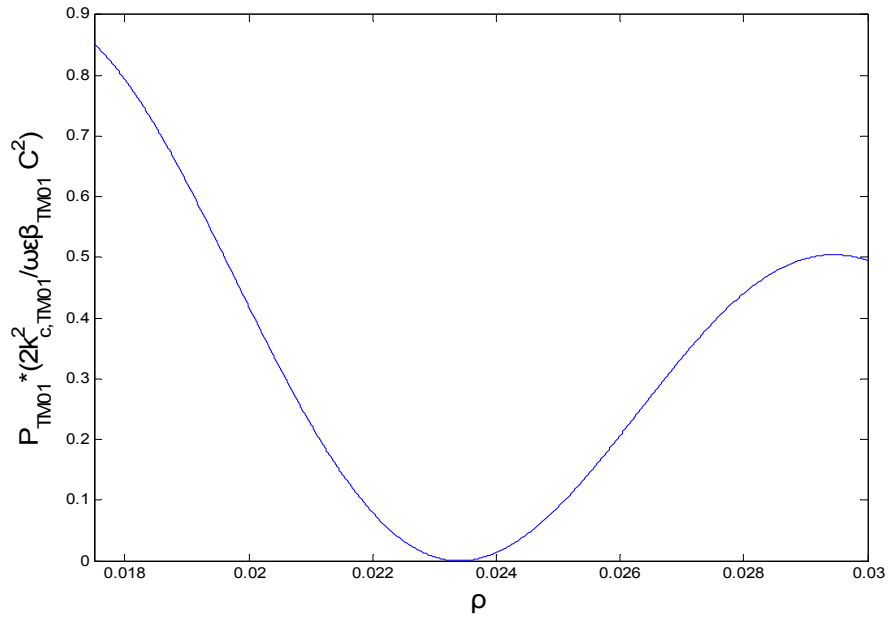


Figure 10: TM_{01} mode of Poynting's vector along the radius

In Figure 10, we know that there is no power transferring at $\rho = 0.0234$ m since the fields are zero at this location. The power configuration for the TM_{01} mode in a coaxial waveguide is shown in Figure 11.

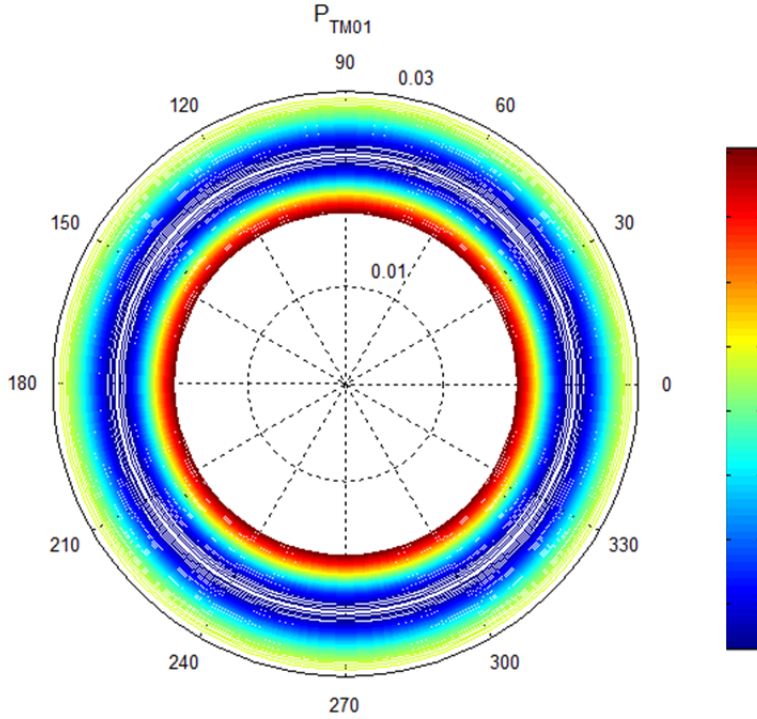


Figure 11: TM_{01} mode of Poynting vector for a coaxial waveguide

Figure 11 indicates that the maximum power density is located at the outer boundary of the inner conductor. The power delays along the radial axial and reaches zero when it hits $\rho = 0.0234$ m. The power begins to increase again, until it hits the boundary of the outer conductor; however, the value is smaller than the maximum. The results from Figure 11 match the results from Figure 10.

For the TM_{11} mode, the Poynting's vector is

$$\begin{aligned} \langle \vec{P} \rangle_{TM,11} = & \frac{\omega \epsilon \beta_{TM11} C^2}{2k_{c,TM11}^2} \left\{ \frac{1}{\rho^2 k_{c,TM11}^2} \left[J_1(k_{c,TM11}\rho) \right. \right. \\ & \left. \left. - \frac{J_1(k_{c,TM11}b)}{N_1(k_{c,TM11}b)} N_1(k_{c,TM11}\rho) \right]^2 \sin^2 \phi \right\} \hat{z} \\ & + \left[J'_1(k_{c,TM11}\rho) - \frac{J_1(k_{c,TM11}b)}{N_1(k_{c,TM11}b)} N'_1(k_{c,TM11}\rho) \right]^2 \cos^2 \phi \} \hat{z} \end{aligned} \quad (3.20)$$

The propagation vector at the cutoff frequency for the TM_{11} mode is

$$k_{c,TM11} = \frac{3.18}{0.03 - 0.0175} = 254.4 \text{ rad/m}$$

The power configuration for the TM_{11} mode can now be plotted, as shown in Figure 12.

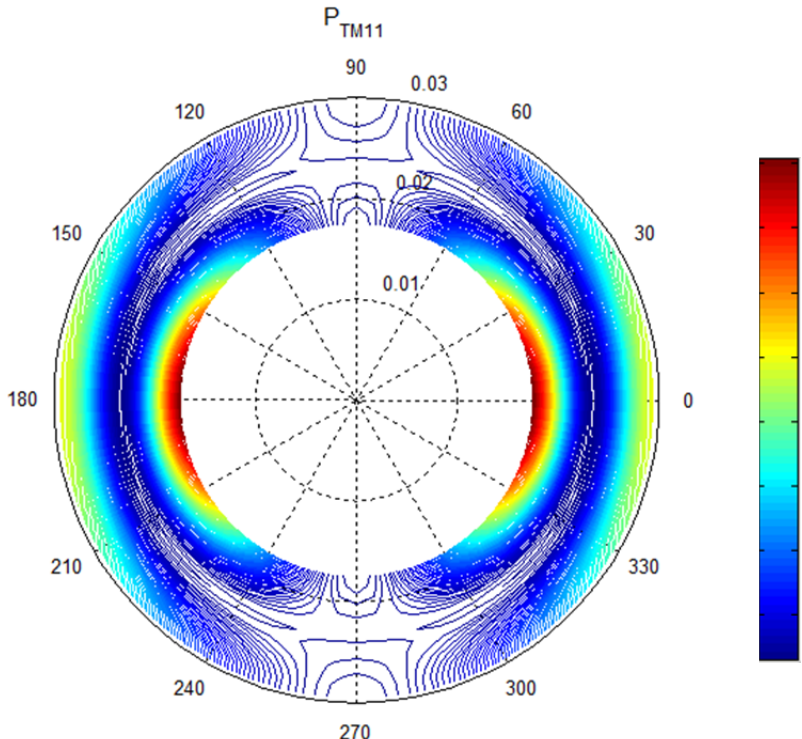


Figure 12: TM_{11} mode of Poynting vector for a coaxial waveguide

Figure 12 indicates that the two maximums occur at the boundary of the inner conductor at $\theta = 0, 180$. The power densities are very low at $\theta = 90, 270$ and there are no power flows at $\rho = 0.0234 \text{ m}$. The patterns of power density between $(\rho, \theta) = (0.0175, 0)$ and $(0.03, 0)$, and between $(\rho, \theta) = (0.0175, 180)$ and $(0.03, 180)$ show that the power density flow for the TM_{11} mode acts like the power density flow of the TM_{01} mode.

For the TM_{21} mode, the Poynting's vector is

$$\begin{aligned}
\langle \vec{P} \rangle_{TM,21} = & \frac{\omega \epsilon \beta_{TM21} C^2}{2k_{c,TM21}^2} \left\{ \frac{4}{\rho^2 k_{c,TM21}^2} \left[J_2(k_{c,TM21}\rho) \right. \right. \\
& \left. \left. - \frac{J_2(k_{c,TM21}b)}{N_2(k_{c,TM21}b)} N_2(k_{c,TM21}\rho) \right]^2 \sin^2 2\phi \right\} \hat{z} \\
& + \left[J'_2(k_{c,TM21}\rho) - \frac{J_2(k_{c,TM21}b)}{N_2(k_{c,TM21}b)} N'_2(k_{c,TM21}\rho) \right]^2 \cos^2 2\phi \quad (3.21)
\end{aligned}$$

The propagation vector at the cutoff frequency for the TM_{21} mode is

$$k_{c,TM21} = \frac{3.36}{0.03 - 0.0175} = 268.8 \text{ rad/m}$$

The power configuration for the TM_{21} mode can now be plotted, as shown in Figure 13.

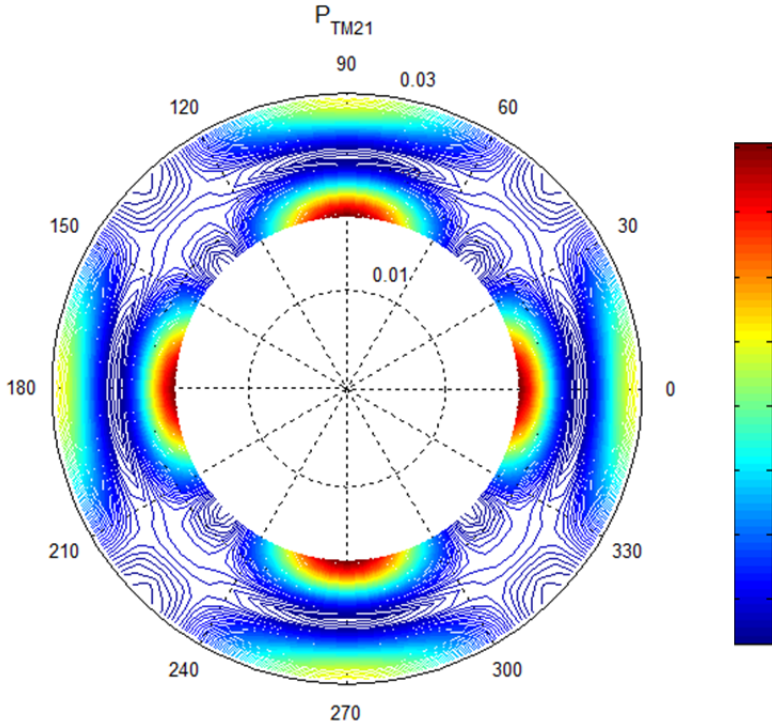


Figure 13: TM_{21} mode of Poynting vector for a coaxial waveguide

Figure 13 indicates that the four power density maximums occur at the boundary of the inner conductor at $\theta = 0, 90, 180, 270$. The power density reaches local

minimums at $\theta = 45, 135, 225, 315$, and is zero at $\rho = 0.0234$ m. The patterns of power density between $(\rho, \theta) = (0.0175, 0)$ and $(0.03, 0)$, between $(\rho, \theta) = (0.0175, 90)$ and $(0.03, 90)$, between $(\rho, \theta) = (0.0175, 180)$ and $(0.03, 180)$, and between $(\rho, \theta) = (0.0175, 270)$ and $(0.03, 270)$ show that the power density flow for the TM_{21} mode acts like the power density flow for the TM_{01} mode.

3.3 TE mode

From solving the wave equation for H_z by using the method of separation of variables, we get:

$$\frac{1}{\rho} \frac{\partial}{\partial \rho} \left(\rho \frac{\partial H_z}{\partial \rho} \right) + \frac{1}{\rho^2} \frac{\partial^2 H_z}{\partial \phi^2} + k_{c,TE}^2 H_z = 0 \quad (3.22)$$

We then apply boundary conditions to H_z , and determine the values of $k_{c,TE}$ and most of the unknown constants, as we did before for the TM modes, by solving the Bessel-Neumann derivative combination boundary condition:

$$J'_n(k_{c,TE}a)N'_n(k_{c,TE}b) - J'_n(k_{c,TE}b)N'_n(k_{c,TE}a) = 0 \quad (3.23)$$

For $b/a = 1.8$, we find the solutions for TE_{nl} by letting

$$x'_{nl} = k_{c,TE_{nl}}a$$

We list the values of x'_{nl} for $n = 0$ to $n = 9$, and $l = 1$ to $l = 4$ in Table 3.

Table 3: x'_{nl} for TE_{nl} mode of coaxial waveguide ($b/a = 1.8$)

l	n									
	0	1	2	3	4	5	6	7	8	9
1	3.98	0.72	1.44	2.14	2.82	3.48	4.11	4.73	5.34	5.94
2	7.88	4.05	4.27	4.62	5.07	5.62	6.22	6.87	7.55	8.24
3	11.80	7.92	8.02	8.20	8.44	8.75	9.11	9.52	9.99	10.5
4	15.72	11.82	11.89	12.01	12.18	12.38	12.63	12.92	13.25	13.62

Finally, we obtain the solution for $H_z(\rho, \phi, z)$, after the values of $k_{c,TE,nl}$ are determined, by finding the roots of the Bessel-Neumann derivate combination boundary condition:

$$H_z(\rho, \phi, z) = C \left[J_n(k_{c,TE}\rho) - \frac{j'_n(k_{c,TE}b)}{N'_n(k_{c,TE}b)} N_n(k_{c,TE}\rho) \right] \cos n\phi e^{-j\beta_{TE}z} \quad (3.24)$$

Since we are solving for the TE mode, we can use $E_z = 0$, and the solution of H_z , as shown in (3.24), to obtain other fields in different directions:

$$\begin{aligned} H_\rho(\rho, \phi, z) &= \\ &-j \frac{\beta_{TE} C}{k_{c,TE}} \left[J'_n(k_{c,TE}\rho) - \frac{j'_n(k_{c,TE}b)}{N'_n(k_{c,TE}b)} N'_n(k_{c,TE}\rho) \right] \cos n\phi e^{-j\beta_{TE}z} \end{aligned} \quad (3.25)$$

$$\begin{aligned} H_\phi(\rho, \phi, z) &= \\ &j \frac{\beta_{TE} n C}{\rho k_{c,TE}^2} \left[J_n(k_{c,TE}\rho) - \frac{j'_n(k_{c,TE}b)}{N'_n(k_{c,TE}b)} N_n(k_{c,TE}\rho) \right] \sin n\phi e^{-j\beta_{TE}z} \end{aligned} \quad (3.26)$$

$$E_\rho(\rho, \phi, z) = j \frac{\omega \mu n C}{\rho k_{c,TE}^2} \left[J_n(k_{c,TE}\rho) - \frac{j'_n(k_{c,TE}b)}{N'_n(k_{c,TE}b)} N_n(k_{c,TE}\rho) \right] \sin n\phi e^{-j\beta_{TE}z} \quad (3.27)$$

$$E_\phi(\rho, \phi, z) = j \frac{\omega \mu C}{k_{c,TE}} \left[J'_n(k_{c,TE}\rho) - \frac{j'_n(k_{c,TE}b)}{N'_n(k_{c,TE}b)} N'_n(k_{c,TE}\rho) \right] \cos n\phi e^{-j\beta_{TE}z} \quad (3.28)$$

Then, the Poynting's vector of the TE modes in a coaxial waveguide is:

$$\begin{aligned} \vec{P}_{TE} &= \frac{1}{2} \vec{E}_{TE} \times \vec{H}_{TE}^* \\ &= j \frac{\omega \mu C^2}{2 k_{c,TE}} \left[J_n(k_{c,TE}\rho) - \frac{j'_n(k_{c,TE}b)}{N'_n(k_{c,TE}b)} N_n(k_{c,TE}\rho) \right] \\ &\quad \cdot \left[J'_n(k_{c,TE}\rho) - \frac{j'_n(k_{c,TE}b)}{N'_n(k_{c,TE}b)} N'_n(k_{c,TE}\rho) \right] \cos^2 n\phi \hat{\rho} \\ &+ j \frac{\omega \mu n C^2}{2 \rho k_{c,TE}^2} \left[J_n(k_{c,TE}\rho) - \frac{j'_n(k_{c,TE}b)}{N'_n(k_{c,TE}b)} N_n(k_{c,TE}\rho) \right]^2 \cos n\phi \sin n\phi \hat{\phi} \\ &+ \frac{\omega \mu \beta_{TE} C^2}{2 k_{c,TE}^2} \left\{ \frac{n^2}{\rho^2 k_{c,TE}^2} \left[J_n(k_{c,TE}\rho) - \frac{j'_n(k_{c,TE}b)}{N'_n(k_{c,TE}b)} N_n(k_{c,TE}\rho) \right]^2 \sin^2 n\phi \right. \\ &\quad \left. + \left[J'_n(k_{c,TE}\rho) - \frac{j'_n(k_{c,TE}b)}{N'_n(k_{c,TE}b)} N'_n(k_{c,TE}\rho) \right]^2 \cos^2 n\phi \right\} \hat{z} \end{aligned} \quad (3.29)$$

The same coaxial waveguide as we used for the TM modes is now used to demonstrate Poynting's vector in the TE modes. For TE_{11} mode, the Poynting's vector is

$$\begin{aligned} \langle \vec{P} \rangle_{TE,11} = & \frac{\omega\mu\beta_{TE}C^2}{2k_{c,TE11}^2} \left\{ \frac{1}{\rho^2 k_{c,TE11}^2} \left[J_1(k_{c,TE11}\rho) \right. \right. \\ & \left. \left. - \frac{J'_1(k_{c,TE11}b)}{N'_1(k_{c,TE11}b)} N_1(k_{c,TE11}\rho) \right]^2 \sin^2 \phi \right. \\ & \left. + \left[J'_1(k_{c,TE11}\rho) - \frac{J'_1(k_{c,TE11}b)}{N'_1(k_{c,TE11}b)} N'_1(k_{c,TE11}\rho) \right]^2 \cos^2 \phi \right\} \hat{z} \end{aligned} \quad (3.30)$$

The power configuration for the TE_{11} mode is shown in Figure 14.

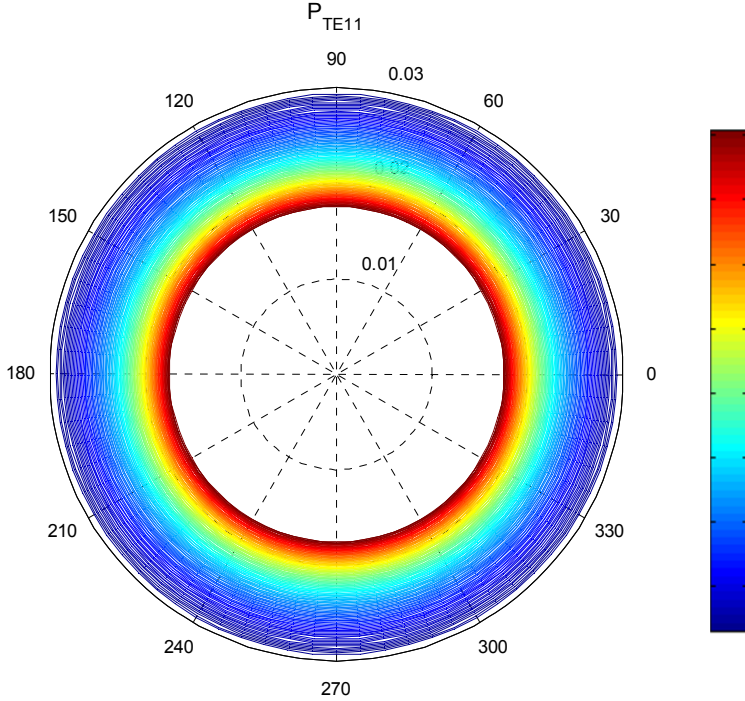


Figure 14: TE_{11} mode of Poynting vector for a coaxial waveguide

Figure 14 indicates that the maximum of power density is at the outer boundary of the inner conductor. The power delays along the radial axial and reaches zero when it hits the inner boundary of the outer conductor.

For TE_{21} mode, the Poynting's vector is

$$\begin{aligned} \langle \vec{P} \rangle_{TE,21} = & \frac{\omega\mu\beta_{TE}C^2}{2k_{c,TE21}^2} \left\{ \frac{4}{\rho^2 k_{c,TE21}^2} \left[J_2(k_{c,TE21}\rho) \right. \right. \\ & - \frac{J'_2(k_{c,TE21}b)}{N'_2(k_{c,TE21}b)} N_2(k_{c,TE21}\rho) \left. \right]^2 \sin^2 2\phi \\ & + \left. \left[J'_2(k_{c,TE21}\rho) - \frac{J'_2(k_{c,TE21}b)}{N'_2(k_{c,TE21}b)} N'_2(k_{c,TE21}\rho) \right]^2 \cos^2 2\phi \right\} \hat{z} \end{aligned} \quad (3.31)$$

The power configuration for the TE_{21} mode is shown in Figure 15.

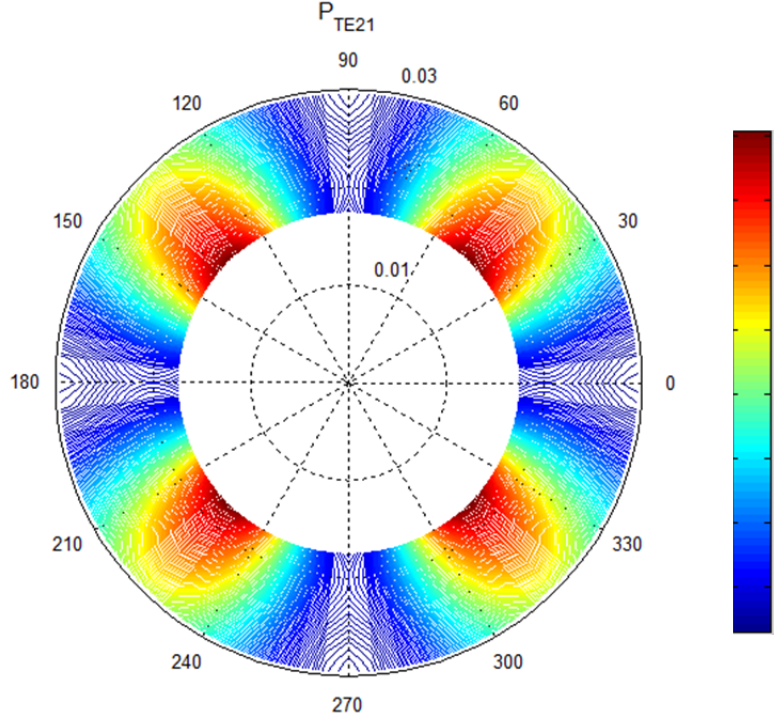


Figure 15: TE_{21} mode of Poynting vector for a coaxial waveguide

Figure 15 indicates that the four power density maximums occur on the boundary of the inner conductor at $\theta = 45, 135, 225, 315$, and the power density reaches minimums at $\theta = 0, 90, 180, 270$.

For the TE_{31} mode, the Poynting's vector is

$$\begin{aligned}
\langle \vec{P} \rangle_{TE,31} = & \frac{\omega \mu \beta_{TE} C^2}{2k_{c,TE31}^2} \left\{ \frac{9}{\rho^2 k_{c,TE31}^2} \left[J_3(k_{c,TE31}\rho) \right. \right. \\
& \left. \left. - \frac{J'_3(k_{c,TE31}b)}{N'_3(k_{c,TE31}b)} N_3(k_{c,TE31}\rho) \right]^2 \sin^2 3\phi \right. \\
& \left. + \left[J'_3(k_{c,TE31}\rho) - \frac{J'_3(k_{c,TE31}b)}{N'_3(k_{c,TE31}b)} N'_3(k_{c,TE31}\rho) \right]^2 \cos^2 3\phi \right\} \hat{z}
\end{aligned} \tag{3.32}$$

The power configuration for the TE_{31} mode is shown in Figure 16.

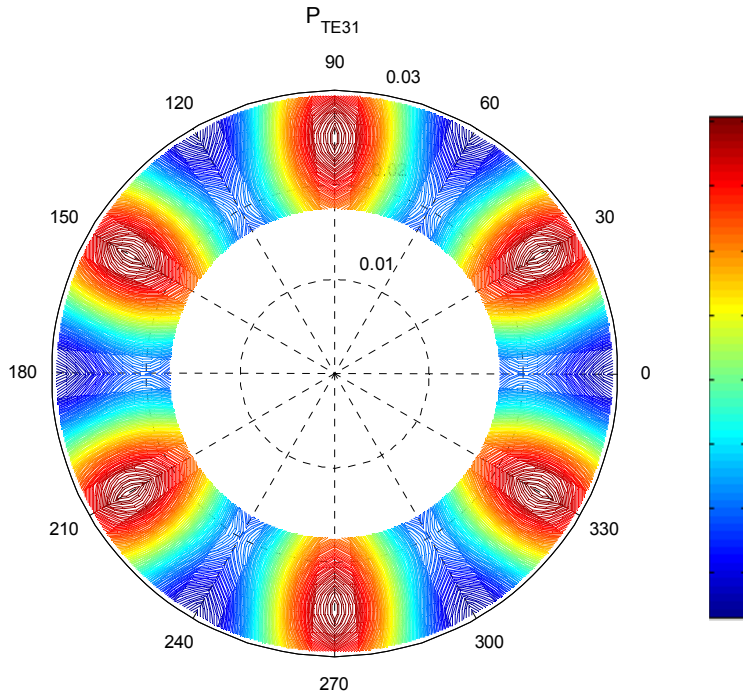
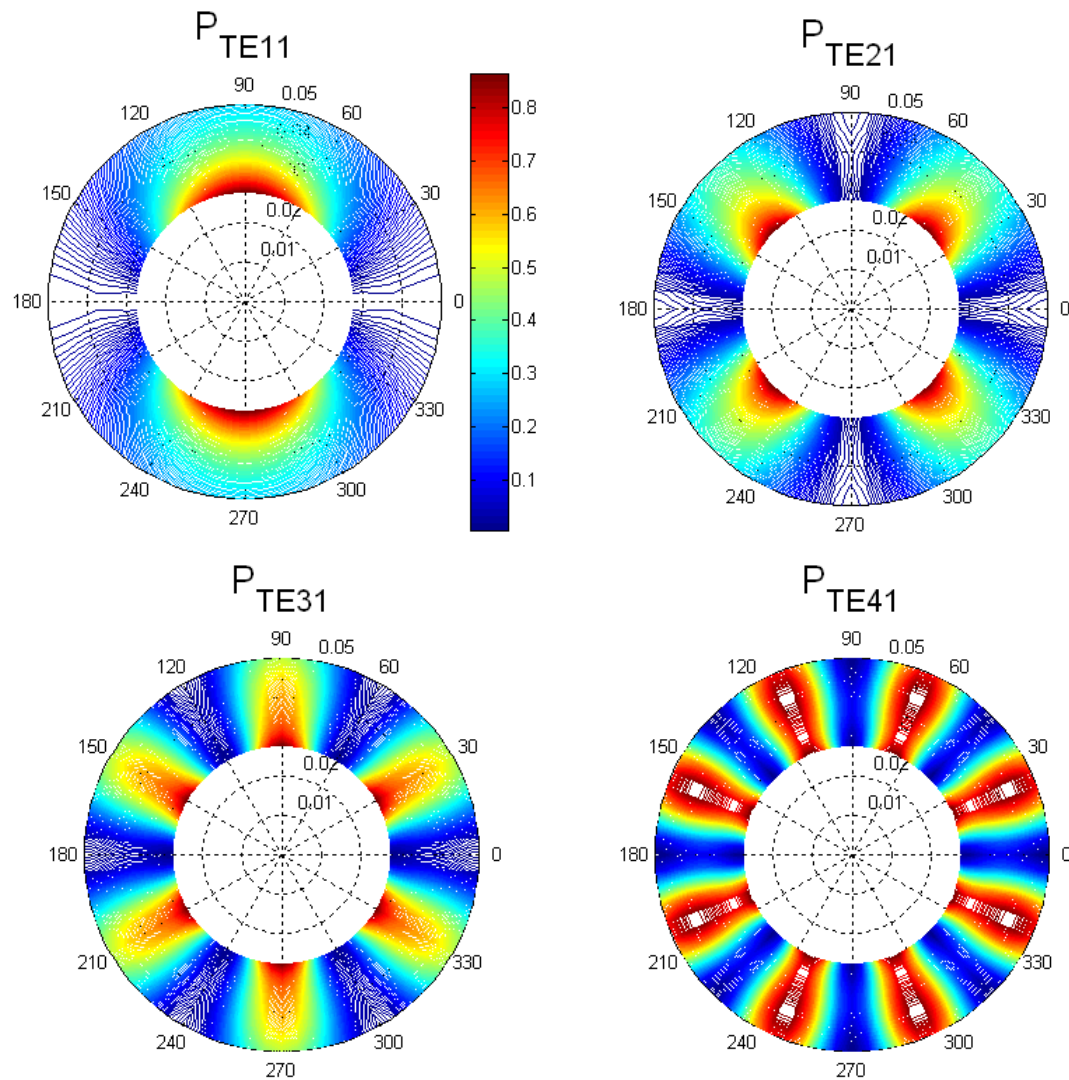


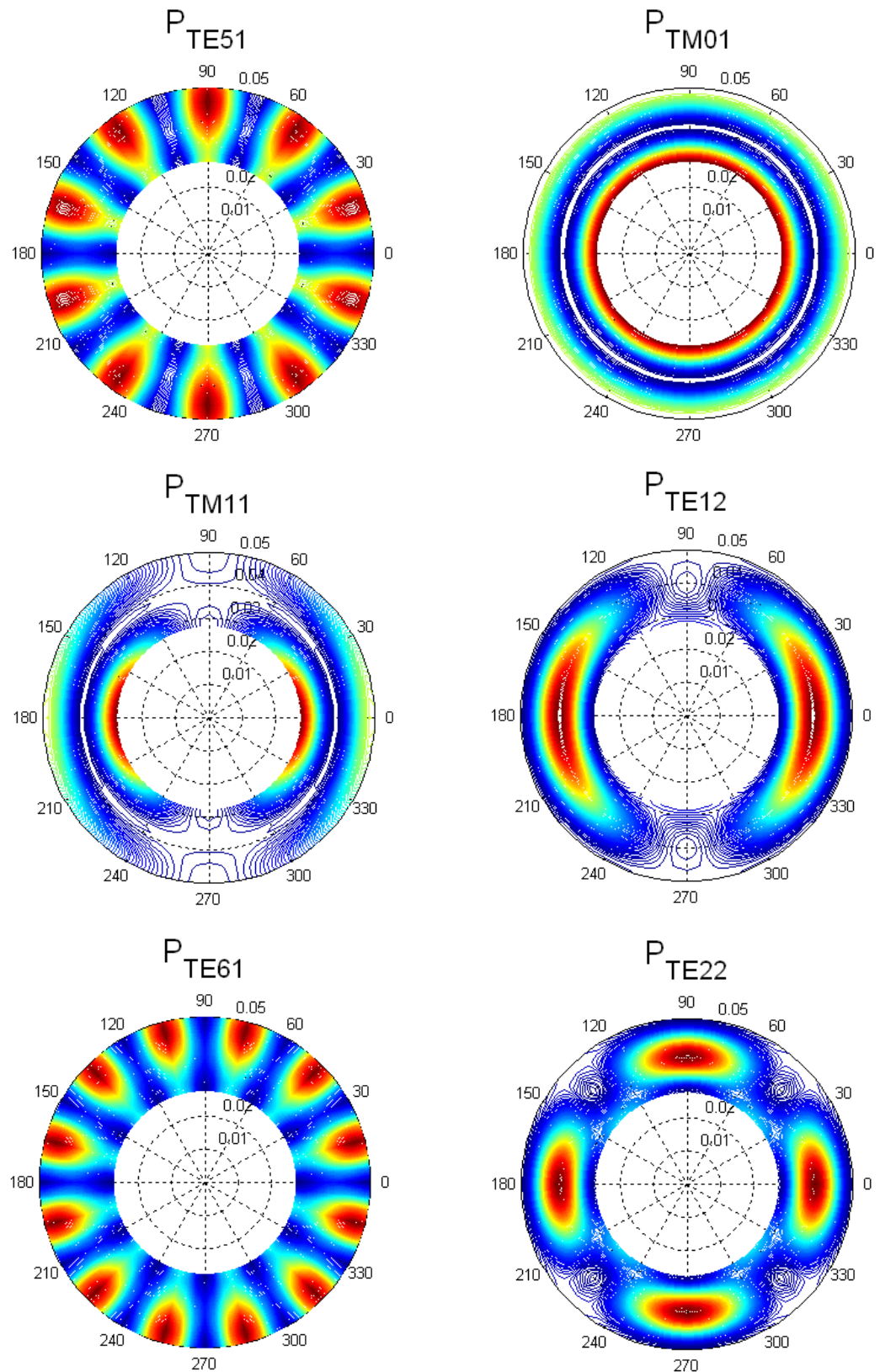
Figure 16: TE_{31} mode of Poynting vector for a coaxial waveguide

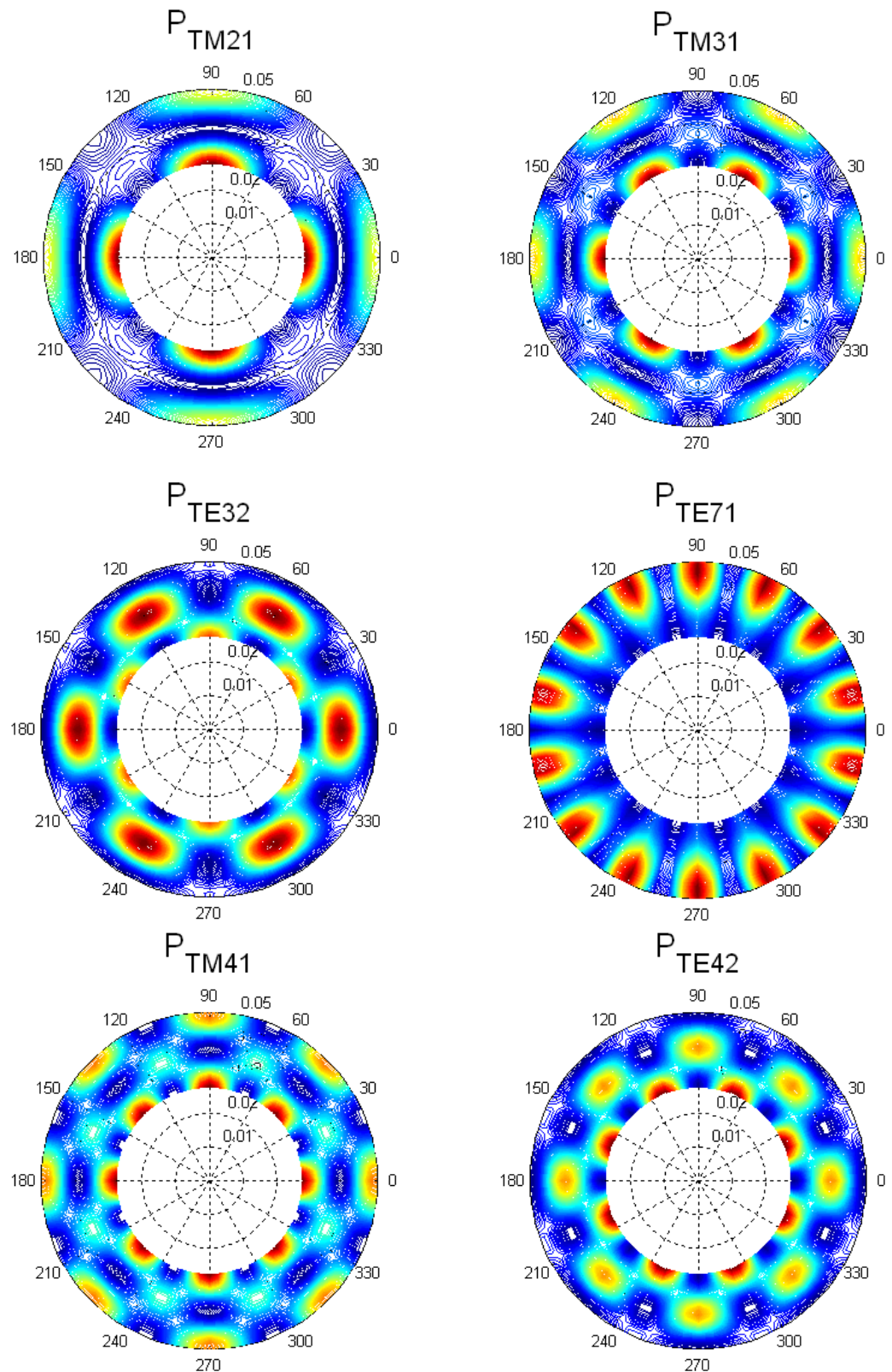
Figure 16 indicates that the six maximums of power density occur at $(\rho, \theta) = (2.55, 30), (2.55, 90), (2.55, 150), (2.55, 210), (2.55, 270)$ and $(2.55, 330)$. The power density reaches minimums at $\theta = 0, 60, 120, 180, 240, 300$. The power maximum does not show on the boundary of the inner conductor. Instead, it occurs between the two conductors.

3.4 First 16 modes

According to Table 2 and Table 3, we can find the mode order from determining the order of operation frequency (from low to high) for different values of m and n. Given $b/a = 1.8$, the time-average Poynting's vector (power flow) configurations for the first 16 modes in a coaxial waveguide are plotted:







Chapter 4: Rectangular Waveguide (one-conductor)

A rectangular waveguide with width a , height b and open-ended in z is shown in Figure 17. In contrast to the coaxial waveguides that we studied in Chapter 3, the waveguides we discuss here are single conductor waveguides. In a single conductor waveguide, the TEM mode cannot exist because the solution for the boundary condition is trivial. Thus, we start by studying the TE mode directly.

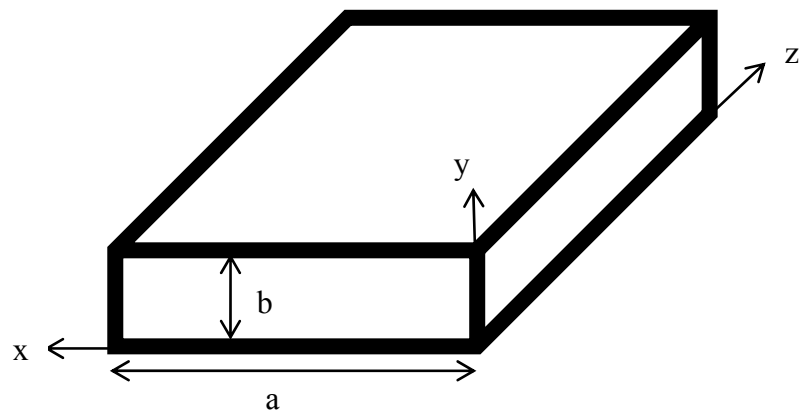


Figure 17: A rectangular waveguide with width a , height b and open-ended in z

4.1 TE mode

The process of finding solution for the TE modes in a rectangular waveguide is similar to the process for a coaxial waveguide. The only difference is that we use rectangular instead of spherical coordinates for the transverse coordinates in the wave equation. Therefore, we start by solving the wave equation for H_z :

$$\frac{\partial^2 H_z}{\partial x^2} + \frac{\partial^2 H_z}{\partial y^2} + k_{c,TE}^2 H_z = 0 \quad (4.1)$$

By using the method of separating the variables, we get

$$H_z(x, y) = (A' \cos k_x x + B' \sin k_x x)(C' \cos k_y y + D' \sin k_y y) \quad (4.2)$$

We apply boundary conditions at $x = 0$ and $y = 0$; this then requires that $B' = 0$

and $D' = 0$. On the side wall at $x = a$,

$$E_y(a, y) = -j \frac{\omega \mu k_y}{k_{c,TE}^2} A' C' \sin k_x a \cos k_y y = 0 \quad (4.3)$$

The only nontrivial solution is

$$\sin k_x a = 0 \quad \text{or} \quad k_x = \frac{m\pi}{a}, \quad m=0,1,2,\dots \quad (4.4)$$

Similarly, for $y = b$:

$$E_x(x, b) = j \frac{\omega \mu k_y}{k_{c,TE}^2} A' C' \cos k_x x \sin k_y b = 0 \quad (4.5)$$

This requires

$$\sin k_y b = 0 \quad \text{or} \quad k_y = \frac{n\pi}{b}, \quad n=0,1,2,\dots \quad (4.6)$$

We then have electric and magnetic fields as shown below:

$$H_z(x, y, z) = A \cos \frac{m\pi}{a} x \cos \frac{n\pi}{b} y e^{-j\beta_{TE} z} \quad (4.7)$$

$$E_x(x, y, z) = j \frac{\omega \mu (\frac{n\pi}{b}) A}{b k_{c,TE}^2} \cos \frac{m\pi}{a} x \sin \frac{n\pi}{b} y e^{-j\beta_{TE} z} \quad (4.8)$$

$$E_y(x, y, z) = -j \frac{\omega \mu (\frac{m\pi}{a}) A}{k_{c,TE}^2} \sin \frac{m\pi}{a} x \cos \frac{n\pi}{b} y e^{-j\beta_{TE} z} \quad (4.9)$$

$$H_x(x, y, z) = j \frac{\beta_{TE} (\frac{m\pi}{a}) A}{k_{c,TE}^2} \sin \frac{m\pi}{a} x \cos \frac{n\pi}{b} y e^{-j\beta_{TE} z} \quad (4.10)$$

$$H_y(x, y, z) = j \frac{\beta_{TE} (\frac{n\pi}{b}) A}{k_{c,TE}^2} \cos \frac{m\pi}{a} x \sin \frac{n\pi}{b} y e^{-j\beta_{TE} z} \quad (4.11)$$

where

$$\beta_{TE} = \sqrt{k^2 - \left(\frac{m\pi}{a}\right)^2 - \left(\frac{n\pi}{b}\right)^2} = \sqrt{k^2 - k_{c,TE}^2} \quad (4.12)$$

and

$$k_{c,TE}^2 = \left(\frac{m\pi}{a}\right)^2 + \left(\frac{n\pi}{b}\right)^2 \quad (4.13)$$

A is a constant that can be determined by the feeding source that drives the waveguide.

In a rectangular waveguide with $a > b$, the TE_{10} mode, or say dominant mode, is the lowest mode since it has the lowest attenuation of all modes. For a rectangular waveguide, either m or n can be zero, but not both. The electric and magnetic fields of the dominate mode can be plotted in different planes as in Figure 18, Figure 19 and Figure 20.

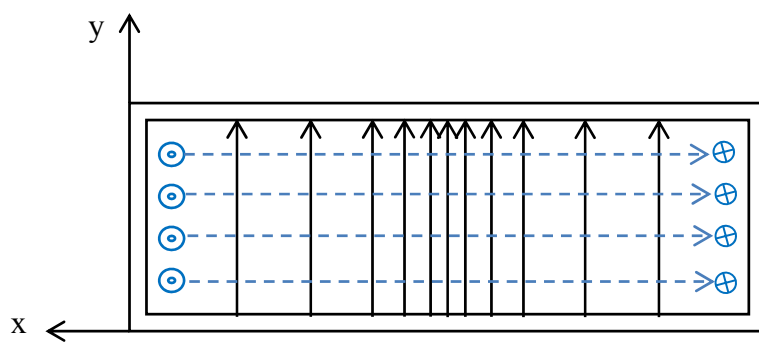


Figure 18: The electromagnetic field configuration of TE_{10} mode for a rectangular waveguide in the x-y plane

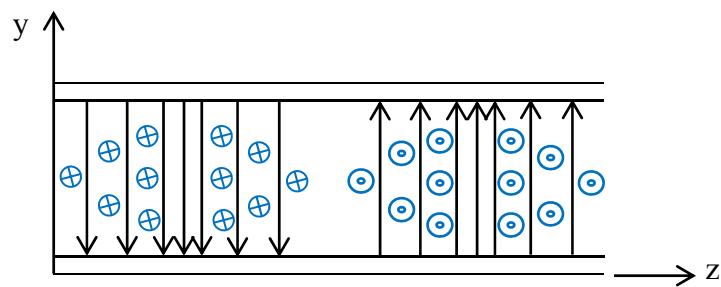


Figure 19: The electromagnetic field configuration in the z-y plane

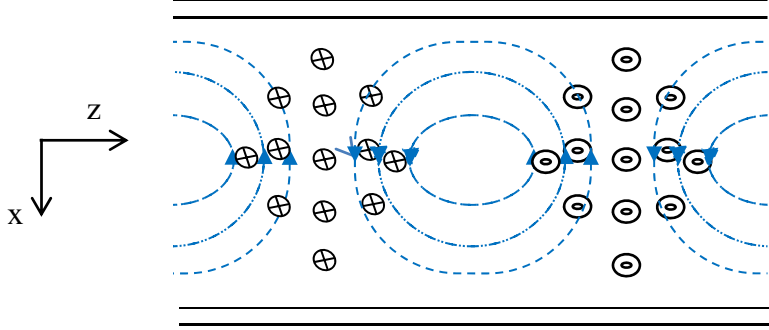


Figure 20: The electromagnetic field configuration in the x-z plane

After we obtain the electric and magnetic fields, we can calculate Poynting's vector:

$$\begin{aligned}
 \vec{P} = \frac{1}{2} \vec{E} \times \vec{H}^* &= \frac{1}{2} \frac{\omega \mu \pi^2}{k_{c,TE}^4} \sqrt{k^2 - k_{c,TE}^2} A^2 \left(\frac{m^2}{a^2} \sin^2 \left(\frac{m\pi}{a} x \right) \cos^2 \left(\frac{n\pi}{b} y \right) \right. \\
 &\quad \left. + \frac{n^2}{b^2} \cos^2 \left(\frac{m\pi}{a} x \right) \sin^2 \left(\frac{n\pi}{b} y \right) \right) \hat{z} \\
 &- j \frac{1}{2} \frac{\omega \mu A^2}{k_{c,TE}^2} \left(\frac{m}{a} \sin \left(\frac{m\pi}{a} x \right) \cos \left(\frac{m\pi}{a} y \right) \cos^2 \left(\frac{n\pi}{b} y \right) \hat{x} \right. \\
 &\quad \left. + \frac{n}{b} \cos^2 \left(\frac{m\pi}{a} x \right) \sin \left(\frac{n\pi}{b} y \right) \cos \left(\frac{n\pi}{b} y \right) \hat{y} \right), m, n = 0, 1, 2, 3, \dots \quad (4.14)
 \end{aligned}$$

Also, the time-average Poynting's vector:

$$\begin{aligned}
 \langle \vec{P} \rangle &= \frac{1}{2} \frac{\omega \mu \pi^2}{k_{c,TE}^4} \sqrt{k^2 - k_{c,TE}^2} A^2 \left(\frac{m^2}{a^2} \sin^2 \left(\frac{m\pi}{a} x \right) \cos^2 \left(\frac{n\pi}{b} y \right) \right. \\
 &\quad \left. + \frac{n^2}{b^2} \cos^2 \left(\frac{m\pi}{a} x \right) \sin^2 \left(\frac{n\pi}{b} y \right) \right) \hat{z} \quad (4.15)
 \end{aligned}$$

For the TE_{10} mode, the time-average Poynting's vector is

$$\langle \vec{P}_{TE_{10}} \rangle = \frac{1}{2} \frac{\omega \mu a^2}{\pi^2} \sqrt{k^2 - (\frac{\pi}{a})^2} A^2 \sin^2 \left(\frac{\pi}{a} x \right) \hat{z} \quad (4.16)$$

For a rectangular waveguide with $a = 2$ and $b = 1$, the power configuration of the TE_{10} mode is shown in Figure 21.

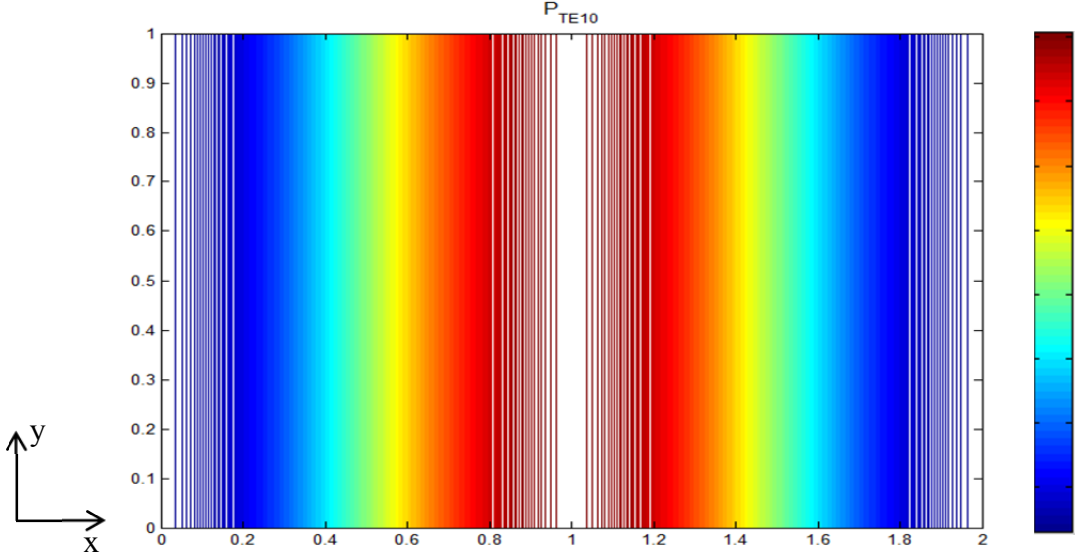


Figure 21: TE_{10} mode of Poynting vector for a rectangular waveguide

Figure 21 indicates that the maximum power density occurs at $x = 1$ (the middle of the width) and the magnitude reaches zero at $x = 0$ and $x = a$ (on the side walls). If we plot the magnitude of Poynting's vector on the x-y plane, it will be a sinusoidal function with half wave length.

For the TE_{11} mode, the Poynting's vector is

$$\begin{aligned} \langle \vec{P}_{TE_{11}} \rangle &= \frac{1}{2} \frac{\omega \mu \pi^2}{k_{c,TE}^4} \sqrt{k^2 - k_{c,TE}^2} A^2 \left(\frac{1}{a^2} \sin^2 \left(\frac{\pi}{a} x \right) \cos^2 \left(\frac{\pi}{b} y \right) \right. \\ &\quad \left. + \frac{1}{b^2} \cos^2 \left(\frac{\pi}{a} x \right) \sin^2 \left(\frac{\pi}{b} y \right) \right) \hat{z} \end{aligned} \quad (4.17)$$

The power configuration for the TE_{11} mode is shown in Figure 22.

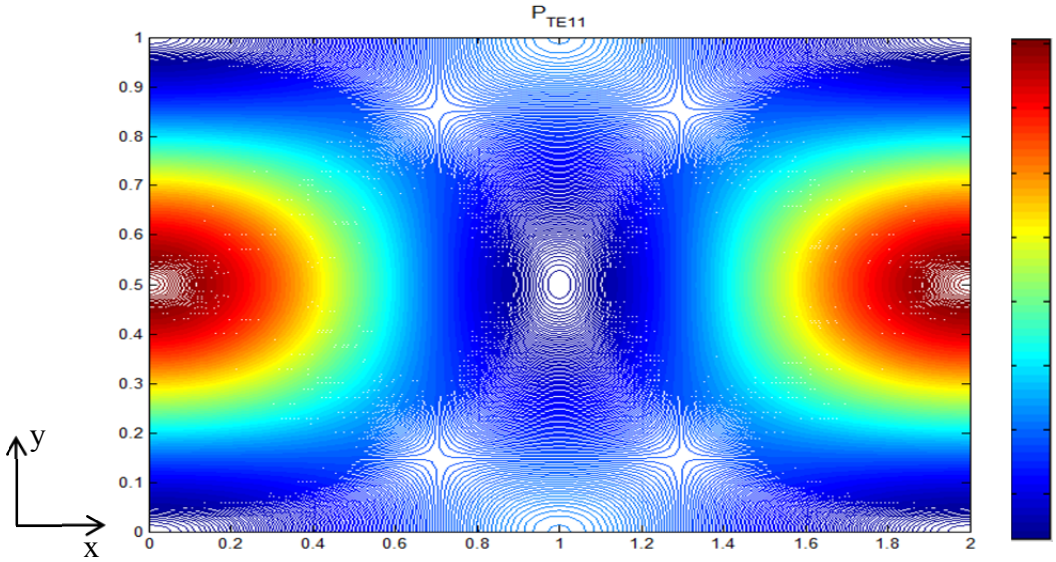


Figure 22: TE_{11} mode of Poynting vector for a rectangular waveguide

Figure 22 indicates that the two maximum power densities occur at $(x,y) = (0,0.5)$ and $(2,0.5)$ (in the middle of the side walls), and the power density reaches zero at the center and the four corners, which are $(x,y) = (0,0)$, $(0,1)$, $(1,0.5)$, $(2,0)$ and $(2,1)$. Note that there are two local maximums at $(x,y) = (1,0)$ and $(1,1)$.

For the TE_{21} mode, the Poynting's vector is

$$\begin{aligned} \langle \vec{P}_{TE_{21}} \rangle &= \frac{1}{2} \frac{\omega \mu \pi^2}{k_{c,TE}^4} \sqrt{k^2 - k_{c,TE}^2} A^2 \left(\frac{2^2}{a^2} \sin^2 \left(\frac{2\pi}{a} x \right) \cos^2 \left(\frac{\pi}{b} y \right) \right. \\ &\quad \left. + \frac{1}{b^2} \cos^2 \left(\frac{2\pi}{a} x \right) \sin^2 \left(\frac{\pi}{b} y \right) \right) \hat{z} \end{aligned} \quad (4.18)$$

The power configuration for the TE_{21} mode is shown in Figure 23.

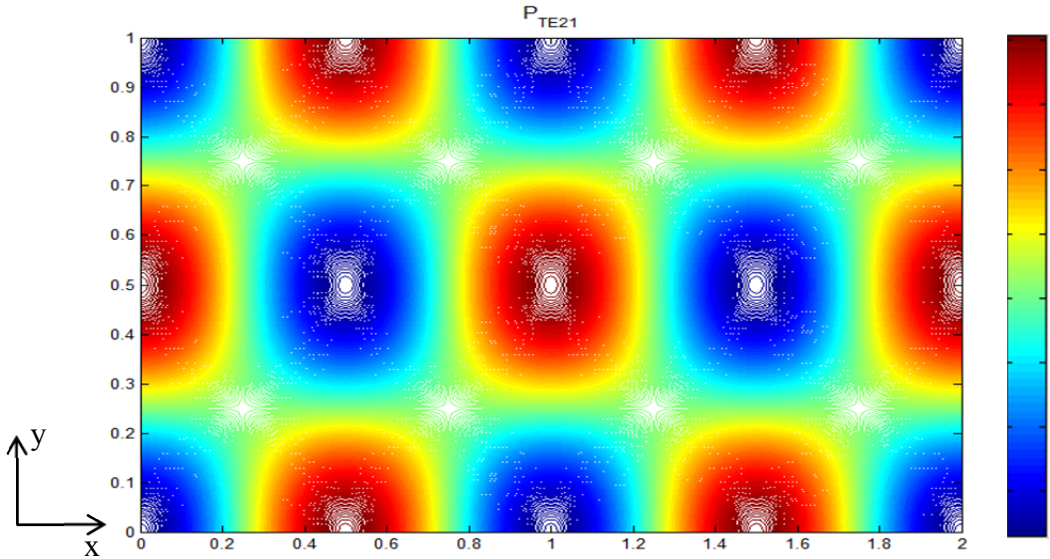


Figure 23: TE_{21} mode of Poynting vector for a rectangular waveguide

Figure 23 indicates that the seven maximum power densities occur at $(x,y) = (0,0.5)$, $(0.5,0)$, $(0.5,1)$, $(1,0.5)$, $(1.5,0)$, $(1.5,1)$ and $(2,0.5)$, and the power density reaches zero at $(x,y) = (0,0)$, $(0,1)$, $(0.5,0.5)$, $(1,0)$, $(1,1)$, $(1.5,0.5)$, $(2,0)$ and $(2,1)$.

4.2 TM mode

As what we've done for the TE mode, we can determine the electric and magnetic fields for the TM mode as below:

$$E_z(x, y, z) = B \sin \frac{m\pi}{a} x \sin \frac{n\pi}{b} y e^{-j\beta_{TM}z} \quad (4.19)$$

$$E_x(x, y, z) = -j \frac{\beta_{TM}(\frac{m\pi}{a})}{k_{c,TM}^2} B \cos \frac{m\pi}{a} x \sin \frac{n\pi}{b} y e^{-j\beta_{TM}z} \quad (4.20)$$

$$E_y(x, y, z) = -j \frac{\beta_{TE}(\frac{n\pi}{b})}{k_{c,TM}^2} B \sin \frac{m\pi}{a} x \cos \frac{n\pi}{b} y e^{-j\beta_{TM}z} \quad (4.21)$$

$$H_x(x, y, z) = j \frac{\omega \epsilon(\frac{n\pi}{b})}{k_{c,TM}^2} B \sin \frac{m\pi}{a} x \cos \frac{n\pi}{b} y e^{-j\beta_{TM}z} \quad (4.22)$$

$$H_y(x, y, z) = -j \frac{\omega \epsilon (\frac{m\pi}{a})}{k_{c,TM}^2} B \cos \frac{m\pi}{a} x \sin \frac{n\pi}{b} y e^{-j\beta_{TM} z} \quad (4.23)$$

where

$$\beta_{TM} = \sqrt{k^2 - \left(\frac{m\pi}{a}\right)^2 - \left(\frac{n\pi}{b}\right)^2} = \sqrt{k^2 - k_{c,TM}^2} \quad (4.24)$$

and

$$k_{c,TM}^2 = \left(\frac{m\pi}{a}\right)^2 + \left(\frac{n\pi}{b}\right)^2 \quad (4.25)$$

B is a constant that can be determined by the feeding source that drives the waveguide.

For the TM modes, $m = 0$ and $n = 0$ are not possible since the solution is trivial. Thus, TM_{11} is the lowest possible TM mode. The field configuration can be plotted in different planes, as shown in Figure 24 and Figure 25.

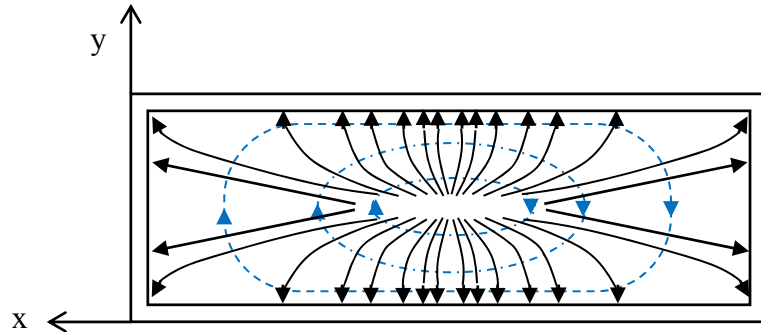


Figure 24: The electromagnetic field configuration of the TM_{11} mode for a rectangular waveguide in the x-y plane

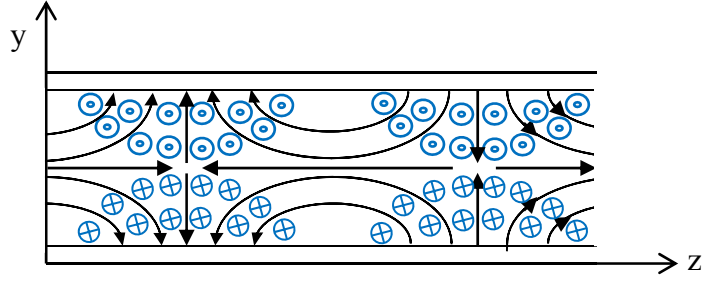


Figure 25: The electromagnetic field configuration in the z-y

The Poynting's vector is

$$\begin{aligned}
 \vec{P} = \frac{1}{2} \vec{E} \times \vec{H}^* = \\
 \frac{1}{2} \frac{\omega \epsilon \pi^2}{k_{c,TM}^4} \sqrt{k^2 - k_{c,TM}^2} B^2 \left(\frac{m^2}{a^2} \cos^2 \left(\frac{m\pi}{a} x \right) \sin^2 \left(\frac{n\pi}{b} y \right) \right. \\
 \left. + \frac{n^2}{b^2} \sin^2 \left(\frac{m\pi}{a} x \right) \cos^2 \left(\frac{n\pi}{b} y \right) \right) \hat{z} \\
 + j \frac{1}{2} \frac{\omega \epsilon B^2}{k_{c,TM}^2} \left(\frac{m}{a} \sin \left(\frac{m\pi}{a} x \right) \sin^2 \left(\frac{n\pi}{b} y \right) \cos \left(\frac{m\pi}{a} x \right) \hat{x} \right. \\
 \left. + \frac{n}{b} \sin^2 \left(\frac{m\pi}{a} x \right) \sin \left(\frac{n\pi}{b} y \right) \cos \left(\frac{n\pi}{b} y \right) \hat{y} \right), \quad m, n = 0, 1, 2, 3, \dots \dots \quad (4.26)
 \end{aligned}$$

The time-average Poynting's vector is

$$\langle \vec{P} \rangle = \frac{1}{2} \frac{\omega \epsilon \pi^2}{k_{c,TM}^4} \sqrt{k^2 - k_{c,TM}^2} B^2 \left(\frac{m^2}{a^2} \cos^2 \left(\frac{m\pi}{a} x \right) \sin^2 \left(\frac{n\pi}{b} y \right) \right. \\
 \left. + \frac{n^2}{b^2} \sin^2 \left(\frac{m\pi}{a} x \right) \cos^2 \left(\frac{n\pi}{b} y \right) \right) \hat{z} \quad (4.27)$$

Finally, the time average Poynting's vector for the TM_{11} mode is

$$\langle \vec{P}_{TM_{11}} \rangle = \frac{1}{2} \frac{\omega \epsilon \pi^2}{k_{c,TM}^4} \sqrt{k^2 - k_{c,TM}^2} B^2 \left(\frac{1}{a^2} \cos^2 \left(\frac{\pi}{a} x \right) \sin^2 \left(\frac{\pi}{b} y \right) \right. \\
 \left. + \frac{1}{b^2} \sin^2 \left(\frac{\pi}{a} x \right) \cos^2 \left(\frac{\pi}{b} y \right) \right) \hat{z} \quad (4.28)$$

The power configuration for the TM_{11} mode is shown in Figure 26.

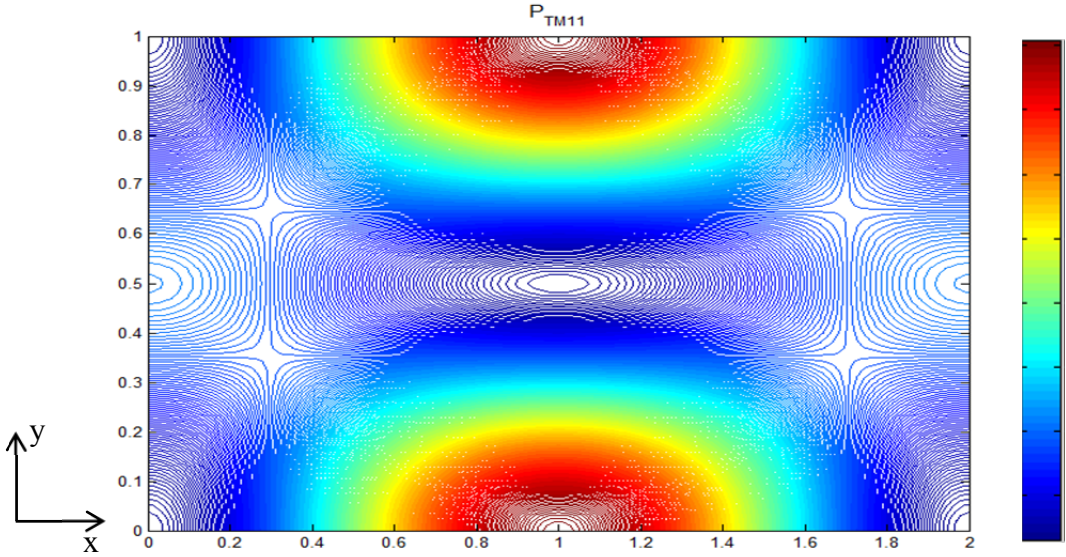


Figure 26: TM_{11} mode of Poynting vector for a rectangular waveguide

Figure 26 indicates that the two maximum power densities occur at $(x,y) = (1,0)$ and $(1,1)$, and the power density reaches zero at the center and four corners of the waveguide. Note that there are two local maximums at $(x, y) = (0, 0.5)$ and $(2,0.5)$ (in the middle of the side walls).

For the TM_{21} mode, the Poynting's vector is

$$\begin{aligned} \langle \vec{P}_{TM_{21}} \rangle &= \frac{1}{2} \frac{\omega \epsilon \pi^2}{k_{c,TM}^4} \sqrt{k^2 - k_{c,TM}^2} B^2 \left(\frac{2^2}{a^2} \cos^2 \left(\frac{2\pi}{a} x \right) \sin^2 \left(\frac{\pi}{b} y \right) \right. \\ &\quad \left. + \frac{1}{b^2} \sin^2 \left(\frac{2\pi}{a} x \right) \cos^2 \left(\frac{\pi}{b} y \right) \right) \hat{z} \end{aligned} \quad (4.29)$$

The power configuration for the TM_{21} mode is shown in Figure 27.

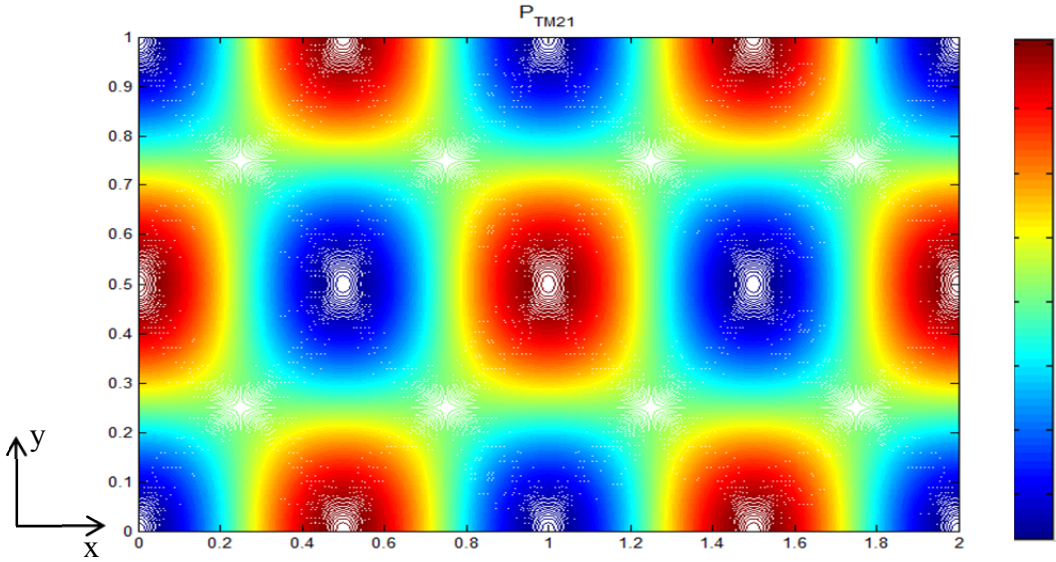


Figure 27: TM_{21} mode of Poynting vector for a rectangular waveguide

Figure 27 indicates that the seven maximum power densities occur at $(x, y) = (0, 0.5)$, $(0.5, 0)$, $(0.5, 1)$, $(1, 0.5)$, $(1.5, 0)$, $(1.5, 1)$ and $(2, 0.5)$, and the power density reaches zero at $(x, y) = (0, 0)$, $(0, 1)$, $(0.5, 0.5)$, $(1, 0)$, $(1, 1)$, $(1.5, 0.5)$, $(2, 0)$ and $(2, 1)$. From Figure 23, we learn that the TM_{21} mode shares the same power density configuration with the TE_{21} mode. The longitudinal propagation constant and the operation frequency for the two modes are the same. This kind of propagation is called to be degenerate. For a rectangular waveguide, the TM_{mn} is degenerate to the TE_{mn} mode for the same value of m and n .

For the TM_{22} mode, the Poynting's vector is

$$\langle \vec{P}_{TM_{22}} \rangle = \frac{1}{2} \frac{\omega \epsilon \pi^2}{k_{c,TM}^4} \sqrt{k^2 - k_{c,TM}^2} B^2 \left(\frac{2^2}{a^2} \cos^2 \left(\frac{2\pi}{a} x \right) \sin^2 \left(\frac{2\pi}{b} y \right) + \frac{2^2}{b^2} \sin^2 \left(\frac{2\pi}{a} x \right) \cos^2 \left(\frac{2\pi}{b} y \right) \right) \hat{z} \quad (4.30)$$

The power configuration for the TM_{22} mode is shown in Figure 28.

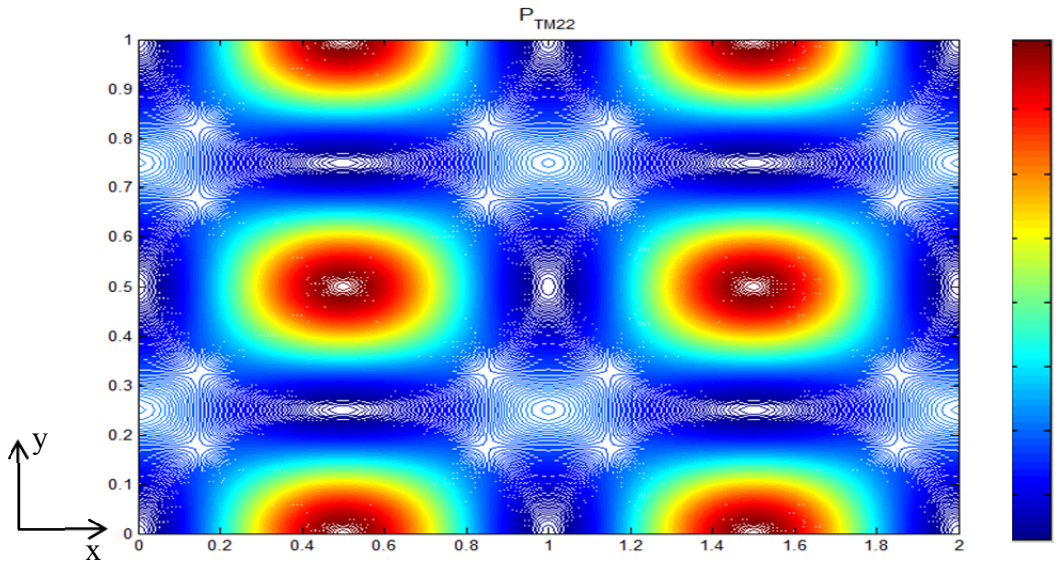
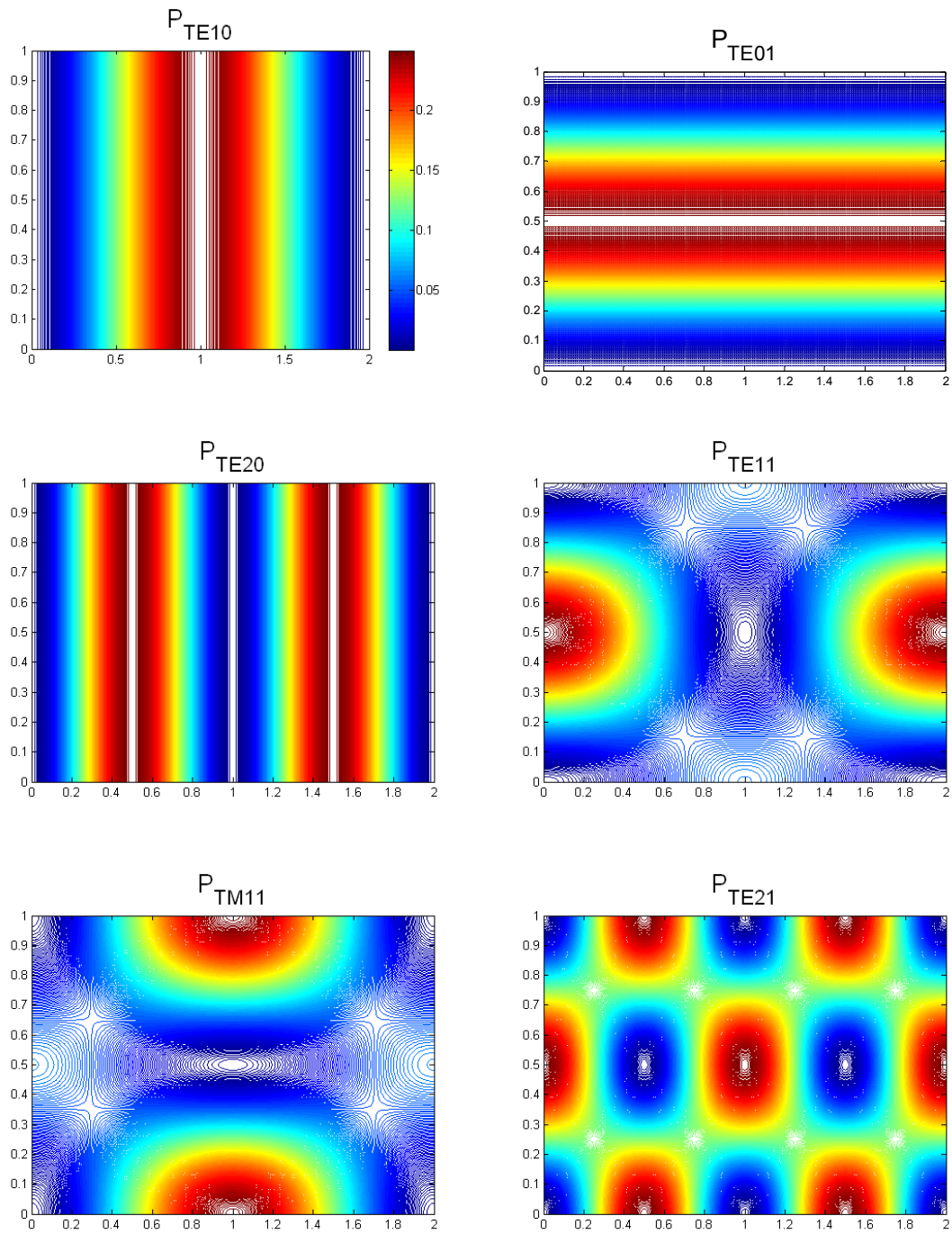


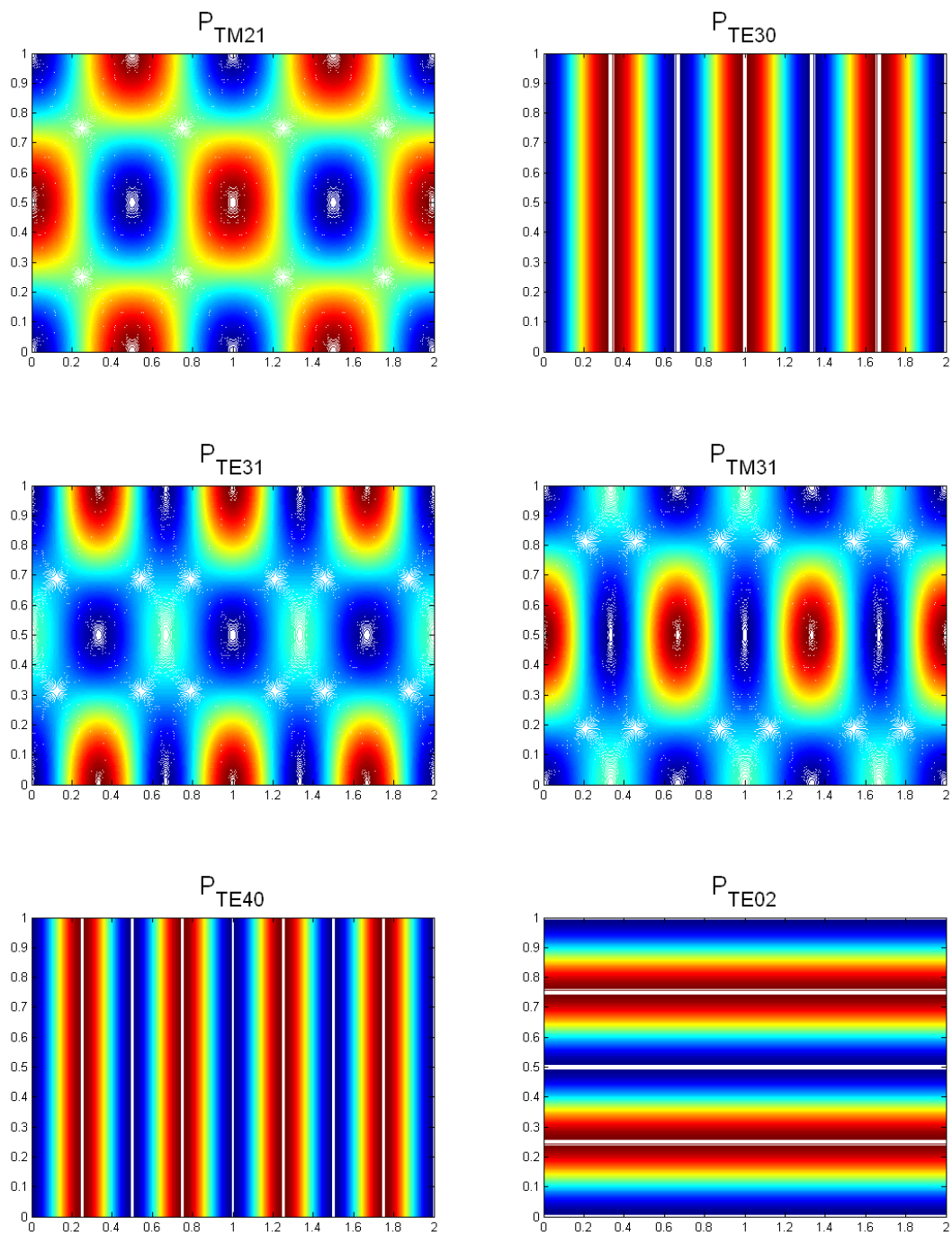
Figure 28: TM_{22} mode of Poynting vector for a rectangular waveguide

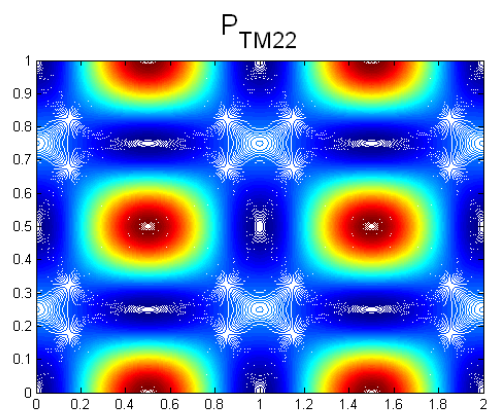
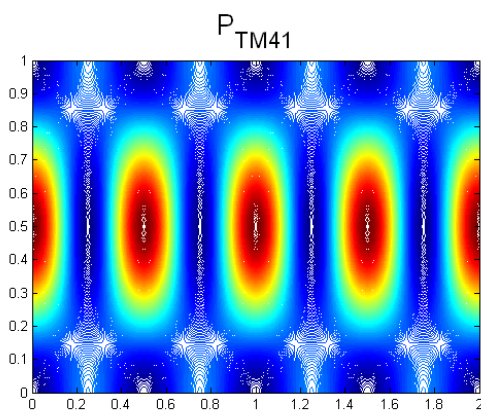
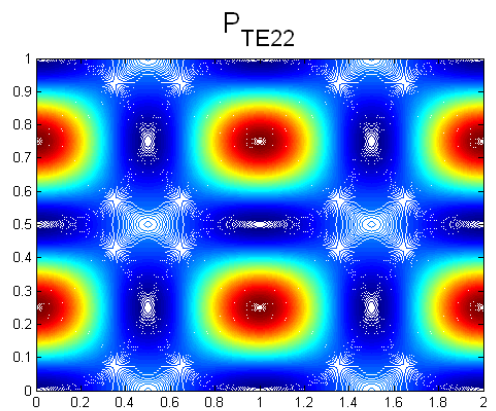
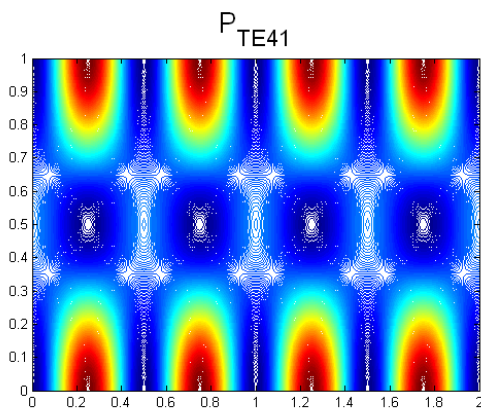
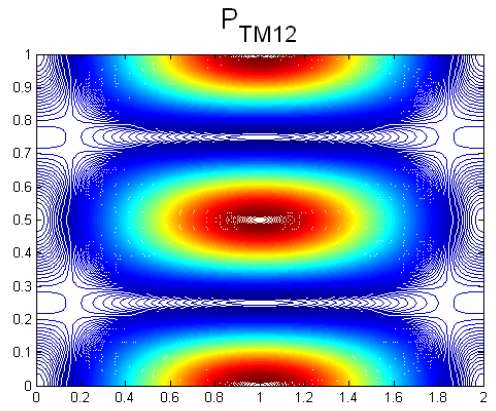
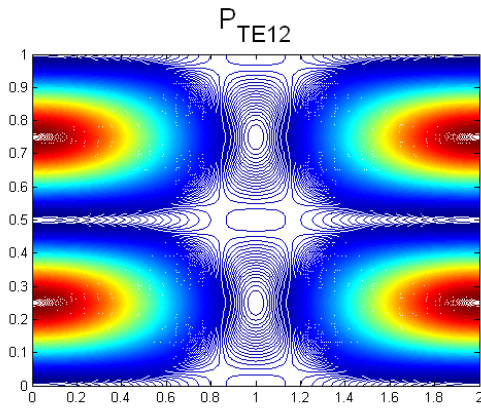
Figure 28 indicates that the six maximum power densities occur at $(x,y) = (0.5,0)$, $(0.5,0.5)$, $(0.5,1)$, $(1.5,0)$, $(1.5,0.5)$, and $(1.5,1)$, and the power density reaches zero at $(x,y) = (0,0)$, $(0,0.5)$, $(0,1)$, $(0.5,0.25)$, $(0.5,0.75)$, $(1,0)$, $(1,0.5)$, $(1,1)$, $(1.5,0.25)$, $(1.5,0.75)$, $(2,0)$, $(2,0.5)$ and $(2,1)$.

4.3 First 18 modes

According to equation (4.24), we can find the mode order by determining the order of operation frequency (from low to high) for different values of m and n . Given $a/b = 2$, the time-average Poynting's vector (power flow) configurations for the first 18 modes in a rectangular waveguide are plotted on the next pages:







Chapter 5: Circular Waveguide (one-conductor)

5.1 TE mode

To obtain the Poynting's vector for a circular waveguide, we repeat all the steps we've done for the coaxial waveguide. First, we solve the wave equation for H_z by using the method of separation of variables:

$$\frac{1}{\rho} \frac{\partial}{\partial \rho} \left(\rho \frac{\partial H_z}{\partial \rho} \right) + \frac{1}{\rho^2} \frac{\partial^2 H_z}{\partial \phi^2} + k_{c,TE}^2 H_z = 0 \quad (5.1)$$

we get

$$H_z(\rho, \phi) = (A' \cos n\phi + B' \sin n\phi) [C' J_n(k_{c,TE} \rho) + D' N_n(k_{c,TE} \rho)] \quad (5.2)$$

Next, we select $\phi = 0$ so that we only have to deal with the cosine variation. We also set $D' = 0$ to keep the fields finite since $N_n(0) = -\infty$ for every n . We rearrange equation (5.2) to get

$$H_z(\rho, \phi) = A J_n(k_{c,TE} \rho) \cos n\phi \quad (5.3)$$

Next, we apply boundary conditions to equation (5.3), and we get:

$$j \frac{\omega \mu}{k_{c,TE}} A J'_n(k_{c,TE} a) \cos n\phi = 0 \quad (5.4)$$

We can now determine the values of $k_{c,TE}$ and most of the unknown constants, by solving the derivative of the Bessel function evaluated at $\rho = a$:

$$J'_n(k_{c,TE} a) \quad (5.5)$$

Now, we obtain the values of $k_{c,TE_{nl}}$ by setting

$$p'_{nl} = k_{c,TE_{nl}} a$$

where the values of p'_{nl} are the l th-nonzero roots of the derivative of nth-order Bessel functions ($J'_n(p'_{nl}) = 0$, $p'_{nl} \neq 0$). These are given in Table 4 for $n = 0$ to $n = 7$ and $l = 1$ to $l = 4$.

Table 4: p'_{nl} for TE_{nl} mode of a circular waveguide (a=3 cm)

l	n							
	0	1	2	3	4	5	6	7
1	3.83	1.84	3.05	4.20	5.32	6.42	7.50	8.58
2	7.02	5.33	6.71	8.02	9.28	10.52	11.74	12.93
3	10.17	8.54	9.97	11.35	12.68	13.99	15.27	16.53
4	13.32	11.71	13.17	14.59	15.96	17.31	18.64	19.94

Finally, for a single hollow cylindrical tube, we obtain the solution for the magnetic field of the TE modes after $k_{c,TE_{nl}}$ is determined by finding the values of p'_{nl} :

$$H_z(\rho, \phi, z) = AJ_n(k_{c,TM}\rho) \cos n\phi e^{-j\beta_{TM}z} \quad (5.6)$$

Since we are solving for the TE mode, we can use $E_z = 0$ and H_z to obtain other fields in different directions.

$$H_\rho(\rho, \phi, z) = -j \frac{\beta_{TE} A}{k_{c,TE}} J'_n(k_{c,TE}\rho) \cos n\phi e^{-j\beta_{TE}z} \quad (5.7)$$

$$H_\phi(\rho, \phi, z) = j \frac{\beta_{TE} n A}{\rho k_{c,TE}^2} J_n(k_{c,TE}\rho) \sin n\phi e^{-j\beta_{TE}z} \quad (5.8)$$

$$E_\rho(\rho, \phi, z) = j \frac{\omega \mu n A}{\rho k_{c,TE}^2} J_n(k_{c,TE}\rho) \sin n\phi e^{-j\beta_{TE}z} \quad (5.9)$$

$$E_\phi(\rho, \phi, z) = j \frac{\omega \mu A}{k_{c,TE}} J'_n(k_{c,TE}\rho) \cos n\phi e^{-j\beta_{TE}z} \quad (5.10)$$

The Poynting's vector for the TE modes in a circular waveguide is

$$\begin{aligned} \vec{P}_{TE} &= \frac{1}{2} \vec{E}_{TE} \times \vec{H}_{TE}^* = \\ &j \frac{\omega \mu A^2}{2 k_{c,TE}} J_n(k_{c,TE}\rho) \cdot J'_n(k_{c,TE}\rho) \cos^2 n\phi \hat{\rho} \\ &+ j \frac{\omega \mu n A^2}{2 \rho k_{c,TE}^2} J_n^2(k_{c,TE}\rho) \cos n\phi \sin n\phi \hat{\phi} \\ &+ \frac{\omega \mu \beta_{TE} A^2}{2 k_{c,TE}^2} \left\{ \frac{n^2}{\rho^2 k_{c,TE}^2} J_n^2(k_{c,TE}\rho) \sin^2 n\phi + [J'_n(k_{c,TE}\rho)]^2 \cos^2 n\phi \right\} \hat{z} \end{aligned} \quad (5.11)$$

For $n = 0$ and $l = 1$, the Poynting's vector of the lowest order TM mode can be written as

$$\langle \vec{P} \rangle_{TE,01} = \frac{\omega \mu \beta_{TE} A^2}{2k_{c,TE}^2} [J'_0(k_{c,TE}\rho)]^2 \hat{z} \quad (5.12)$$

We use 3 cm for the radius of the conductor to demonstrate the power density flow in a circular waveguide. The power configuration for the TE_{01} mode is shown in Figure 29.

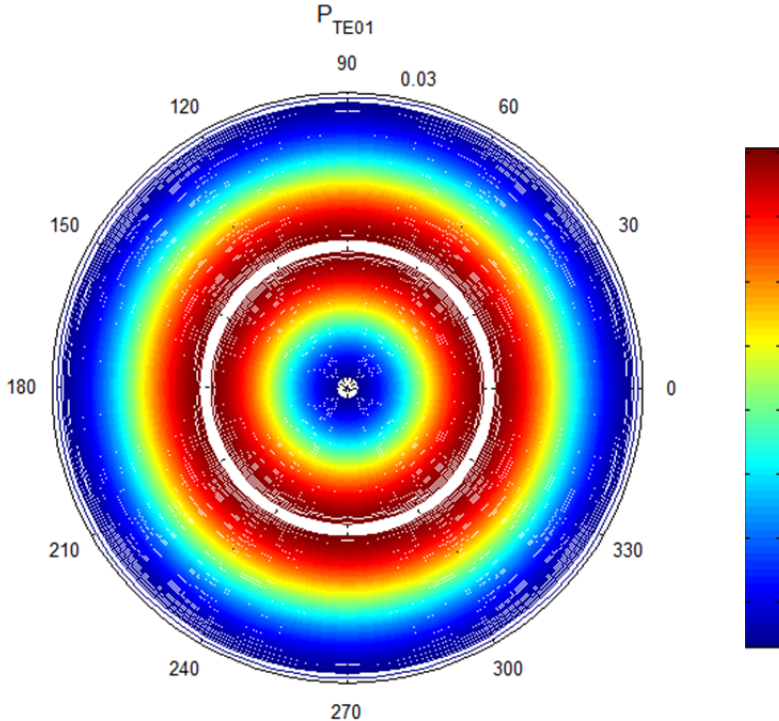


Figure 29: TE_{01} mode of Poynting vector for a rectangular waveguide

Figure 29 indicates that the maximum power density occurs at $\rho = 1.4$ cm and the power in the center of the waveguide is zero because $J'_0(0)$ is equal to zero. The power increases along the radial axial from the center and reaches maximum at $\rho = 1.4$ cm. It starts decreasing from here, until it hits the boundary of outer conductor.

For the TE_{11} mode, the Poynting's vector is

$$\langle \vec{P} \rangle_{TE,11} = \frac{\omega \mu \beta_{TE} A^2}{2k_{c,TE}^2} \left\{ \frac{1^2}{\rho^2 k_{c,TE}^2} J_1^2(k_{c,TE}\rho) \sin^2 \phi + [J'_1(k_{c,TE}\rho)]^2 \cos^2 \phi \right\} \hat{z} \quad (5.13)$$

The power configuration for the TE_{11} mode is shown in Figure 30.

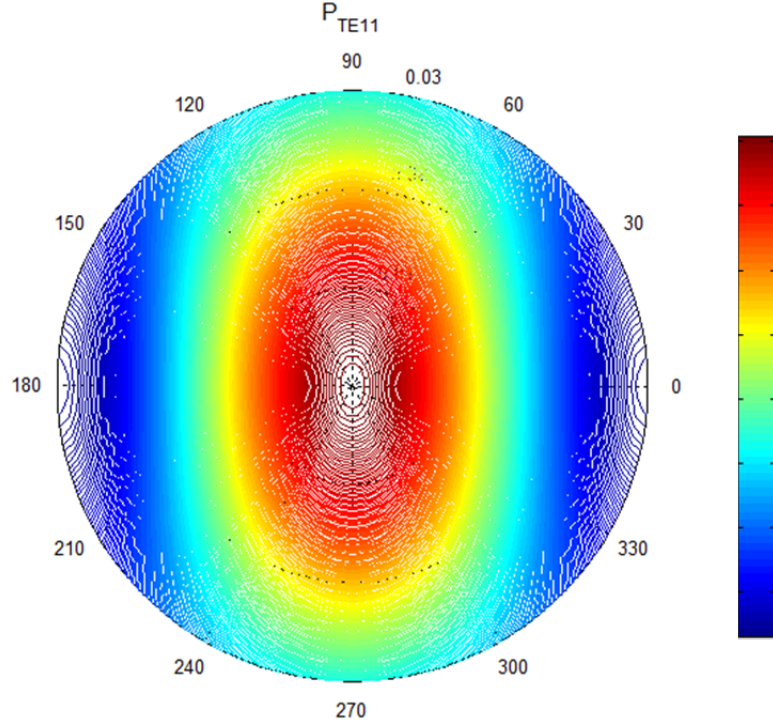


Figure 30: TE_{11} mode of Poynting vector for a rectangular waveguide

Figure 30 indicates that the maximum power density occurs at the center, and the power density reaches zero at the boundary of the conductor at $\theta = 0, 180$.

For the TE_{21} mode, the Poynting's vector is

$$\begin{aligned} \langle \vec{P} \rangle_{TE,21} = & \frac{\omega \mu \beta_{TE} A^2}{2k_{c,TE}^2} \left\{ \frac{2^2}{\rho^2 k_{c,TE}^2} J_2^2(k_{c,TE}\rho) \sin^2 2\phi \right. \\ & \left. + [J'_2(k_{c,TE}\rho)]^2 \cos^2 2\phi \right\} \hat{z} \end{aligned} \quad (5.14)$$

The power configuration for the TE_{21} mode is shown in Figure 31.

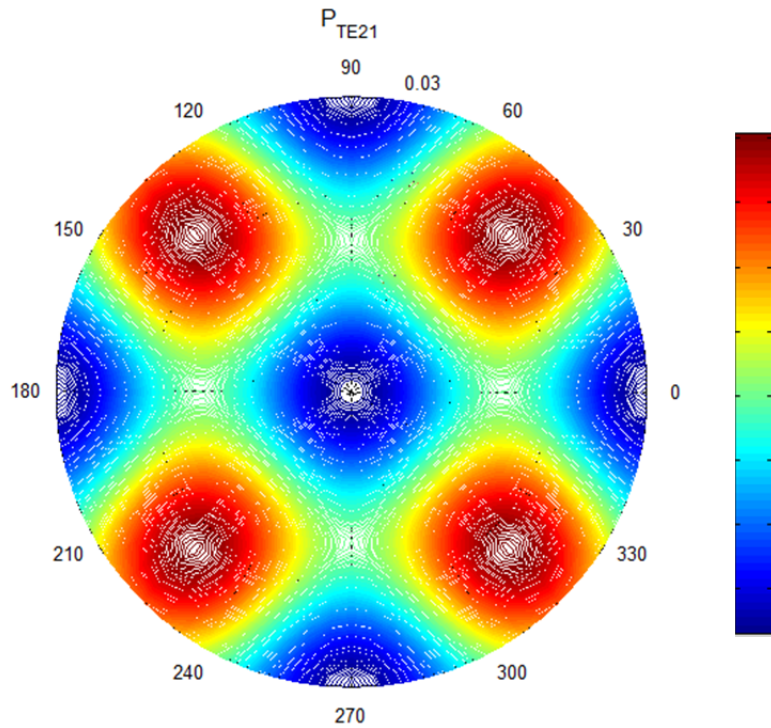


Figure 31: TE_{21} mode of Poynting vector for a rectangular waveguide

Figure 31 indicates that four maximums of power density occur at $(\rho, \theta) = (0.023, 45), (0.023, 135), (0.023, 225)$ and $(0.023, 315)$, and the power reaches zero at the center and on the boundary of the conductor at $\theta = 0, 90, 180, 270$.

5.2 TM mode

The process of finding the solution for these modes is similar to the process for the TM modes discussed in the previous chapter. Therefore, we start by finding the values for p_{nl} , and we obtain the values for $k_{c,TE_{nl}}$ by setting

$$p_{nl} = k_{c,TM_{nl}} a$$

where the values of p_{nl} are the l th-nonzero roots of the n th-order Bessel function of the first kind ($J_n(p_{nl}) = 0$, $p_{nl} \neq 0$). These are given in Table 5 for $n = 0$ to $n = 7$ and $l = 1$ to $l = 4$.

Table 5: p_{nl} for TM_{nl} mode of a circular waveguide ($a=3$ cm)

l	n							
	0	1	2	3	4	5	6	7
1	2.40	3.83	5.14	6.38	7.59	8.77	9.94	11.09
2	5.52	7.02	8.42	9.76	11.07	12.34	13.59	14.82
3	8.65	10.17	11.62	13.02	14.37	15.7	17.00	18.29
4	11.79	13.32	14.80	16.22	17.62	18.98	20.32	21.64

For a single hollow cylindrical tube, the electric field of the TM modes can be derived as:

$$E_z(\rho, \phi, z) = AJ_n(k_{c,TM}\rho) \cos n\phi e^{-j\beta_{TM}z} \quad (5.15)$$

We then apply boundary conditions to E_z to determine the values of $k_{c,TM}$ and most of the unknown constants.

Since we are solving for the TM mode, we can use $H_z = 0$ and E_z to obtain other fields in different directions:

$$E_\rho(\rho, \phi, z) = -j \frac{\beta_{TM} A}{k_{c,TM}} J'_n(k_{c,TM}\rho) \cos n\phi e^{-j\beta_{TM}z} \quad (5.16)$$

$$E_\phi(\rho, \phi, z) = j \frac{\beta_{TM} n A}{\rho k_{c,TM}^2} J_n(k_{c,TM}\rho) \sin n\phi e^{-j\beta_{TM}z} \quad (5.17)$$

$$H_\rho(\rho, \phi, z) = -j \frac{\omega \epsilon n A}{\rho k_{c,TM}^2} J_n(k_{c,TM}\rho) \sin n\phi e^{-j\beta_{TM}z} \quad (5.18)$$

$$H_\phi(\rho, \phi, z) = -j \frac{\omega \epsilon A}{k_{c,TM}} J'_n(k_{c,TM}\rho) \cos n\phi e^{-j\beta_{TM}z} \quad (5.19)$$

Poynting's vector is

$$\begin{aligned}
\vec{P}_{TM} &= \frac{1}{2} \vec{E}_{TM} \times \vec{H}_{TM}^* \\
&= j \frac{\omega \epsilon A^2}{2k_{c,TM}} J_n(k_{c,TM}\rho) \cdot J'_n(k_{c,TM}\rho) \cos^2 n\phi \hat{\rho} \\
&\quad + j \frac{\omega \epsilon n A^2}{2\rho k_{c,TM}^2} J_n^2(k_{c,TM}\rho) \cos n\phi \sin n\phi \hat{\phi} \\
&\quad + \frac{\omega \epsilon \beta_{TM} A^2}{2k_{c,TM}^2} \left\{ \frac{n^2}{\rho^2 k_{c,TM}^2} J_n^2(k_{c,TM}\rho) \sin^2 n\phi + [J'_n(k_{c,TM}\rho)]^2 \cos^2 n\phi \right\} \hat{z} \quad (5.20)
\end{aligned}$$

For $n = 0$, $l = 1$, the Poynting's vector of the lowest order TM mode, TM_{01} , can be written as

$$\langle \vec{P} \rangle_{TM,01} = \frac{\omega \epsilon \beta_{TM} A^2}{2k_{c,TM}^2} [J'_0(k_{c,TM}\rho)]^2 \hat{z} \quad (5.21)$$

Again, we use 3 cm for the radius of the conductor to demonstrate the power density flow in a circular waveguide. Note that $J'_0(0) = 0$, so the power in the center of the waveguide is zero.

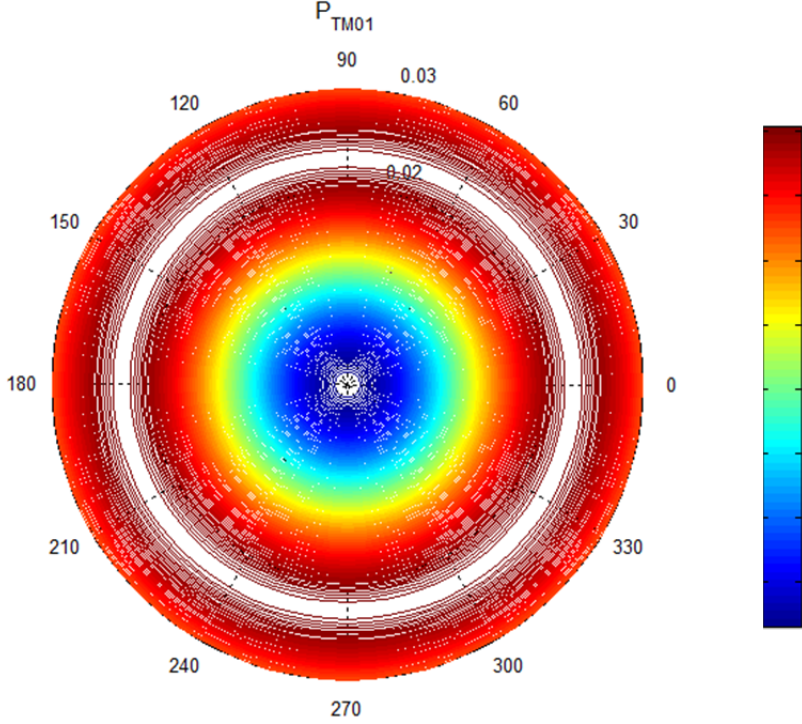


Figure 32: TM_{01} mode of Poynting vector for a rectangular waveguide

Figure 32 indicates that the maximum power density for the TM_{01} mode in a circular waveguide occurs at $\rho = 2.34$ cm and the power reaches zero at the center of the waveguide. Power increases along radial axial from the center and reaches maximum at $\rho = 2.34$ cm. Power decreases from here until it hits the boundary of outer conductor.

For the TM_{11} mode, the Poynting's vector is

$$\begin{aligned} \langle \vec{P} \rangle_{TM,11} = & \frac{\omega\epsilon\beta_{TM}A^2}{2k_{c,TM}^2} \left\{ \frac{1^2}{\rho^2 k_{c,TM}^2} J_1^2(k_{c,TM}\rho) \sin^2 \phi \right. \\ & \left. + [J'_1(k_{c,TM}\rho)]^2 \cos^2 \phi \right\} \hat{z} \end{aligned} \quad (5.22)$$

The power configuration for the TM_{11} mode is shown in Figure 33.

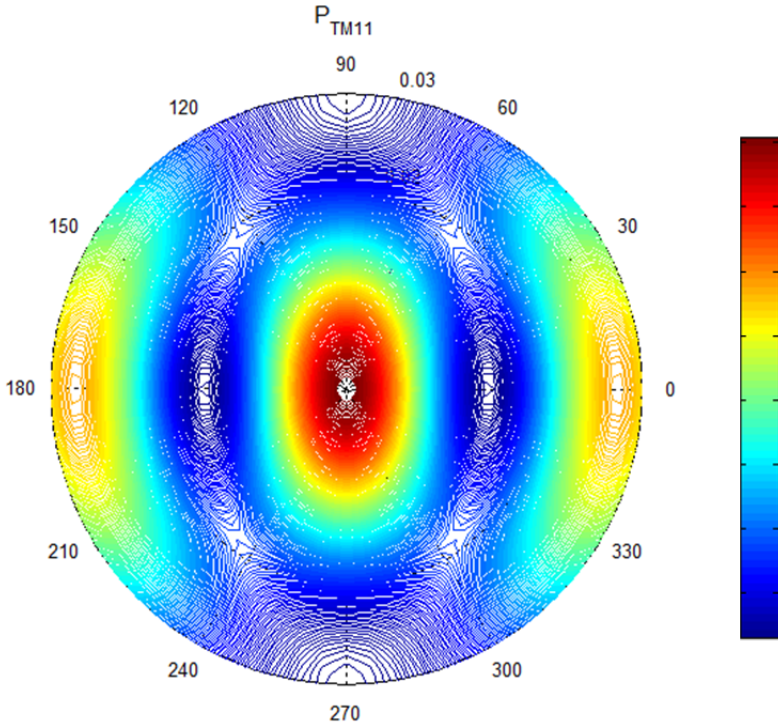


Figure 33: TM_{11} mode of Poynting vector for a rectangular waveguide

Figure 33 indicates that the maximum power density occurs at the center of the waveguide, and the power density reaches zero at $\theta = 90, 270$ on the boundary of the outer conductor.

For the TM_{21} mode, the Poynting's vector is

$$\begin{aligned} \langle \vec{P} \rangle_{TM,21} = & \frac{\omega \epsilon \beta_{TM} A^2}{2k_{c,TM}^2} \left\{ \frac{2^2}{\rho^2 k_{c,TM}^2} J_2^2(k_{c,TM}\rho) \sin^2 2\phi \right. \\ & \left. + [J'_2(k_{c,TM}\rho)]^2 \cos^2 2\phi \right\} \hat{z} \end{aligned} \quad (5.23)$$

The power configuration for the TM_{21} mode is shown in Figure 34.

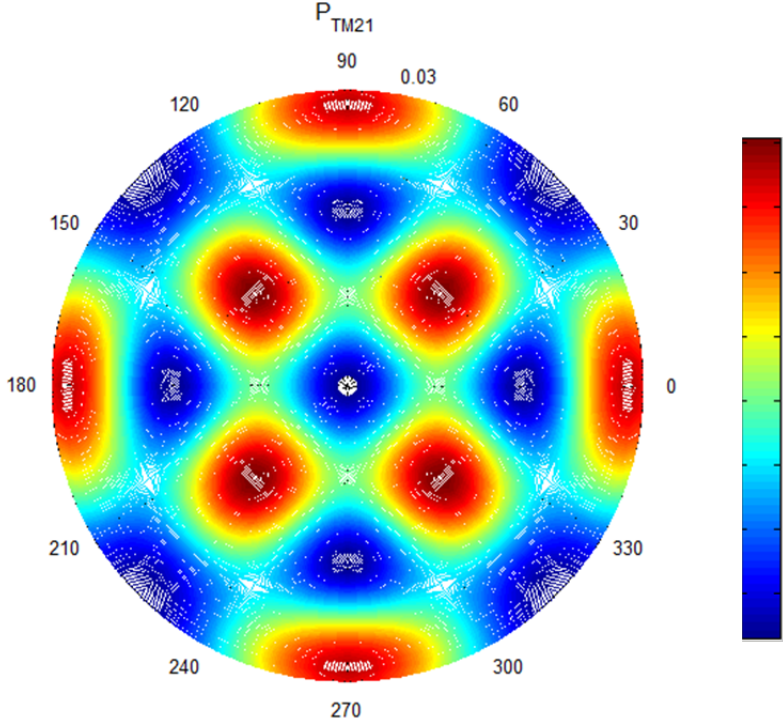
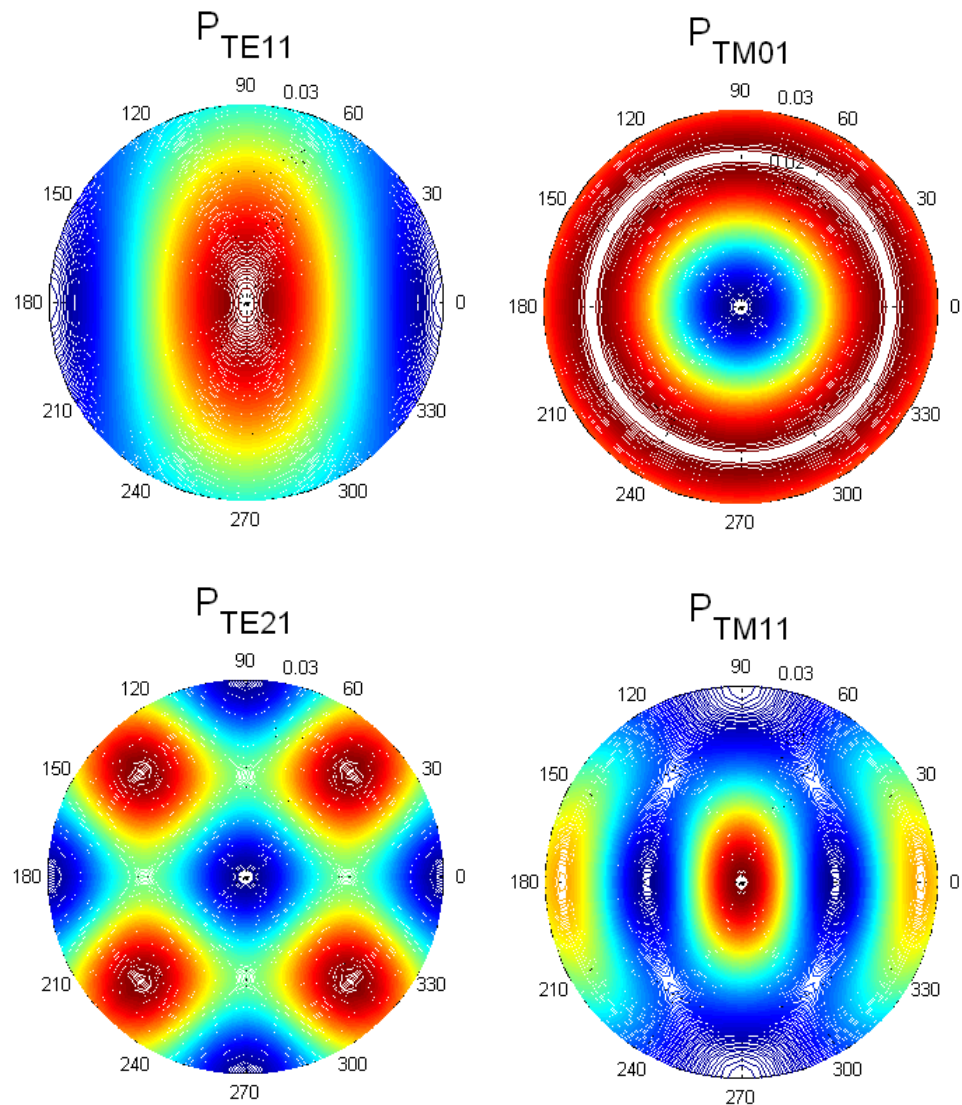


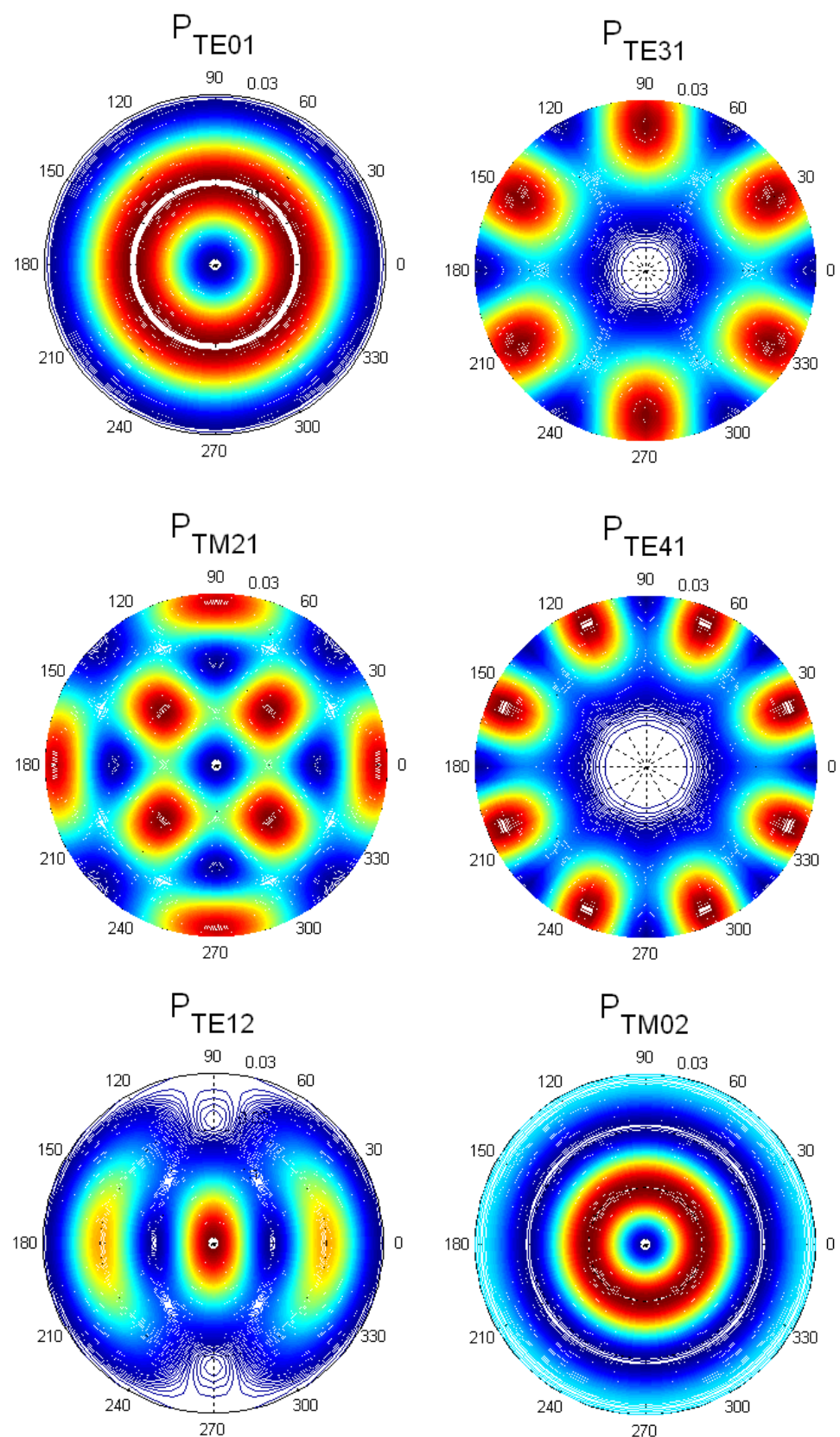
Figure 34: TM_{21} mode of Poynting vector for a rectangular waveguide

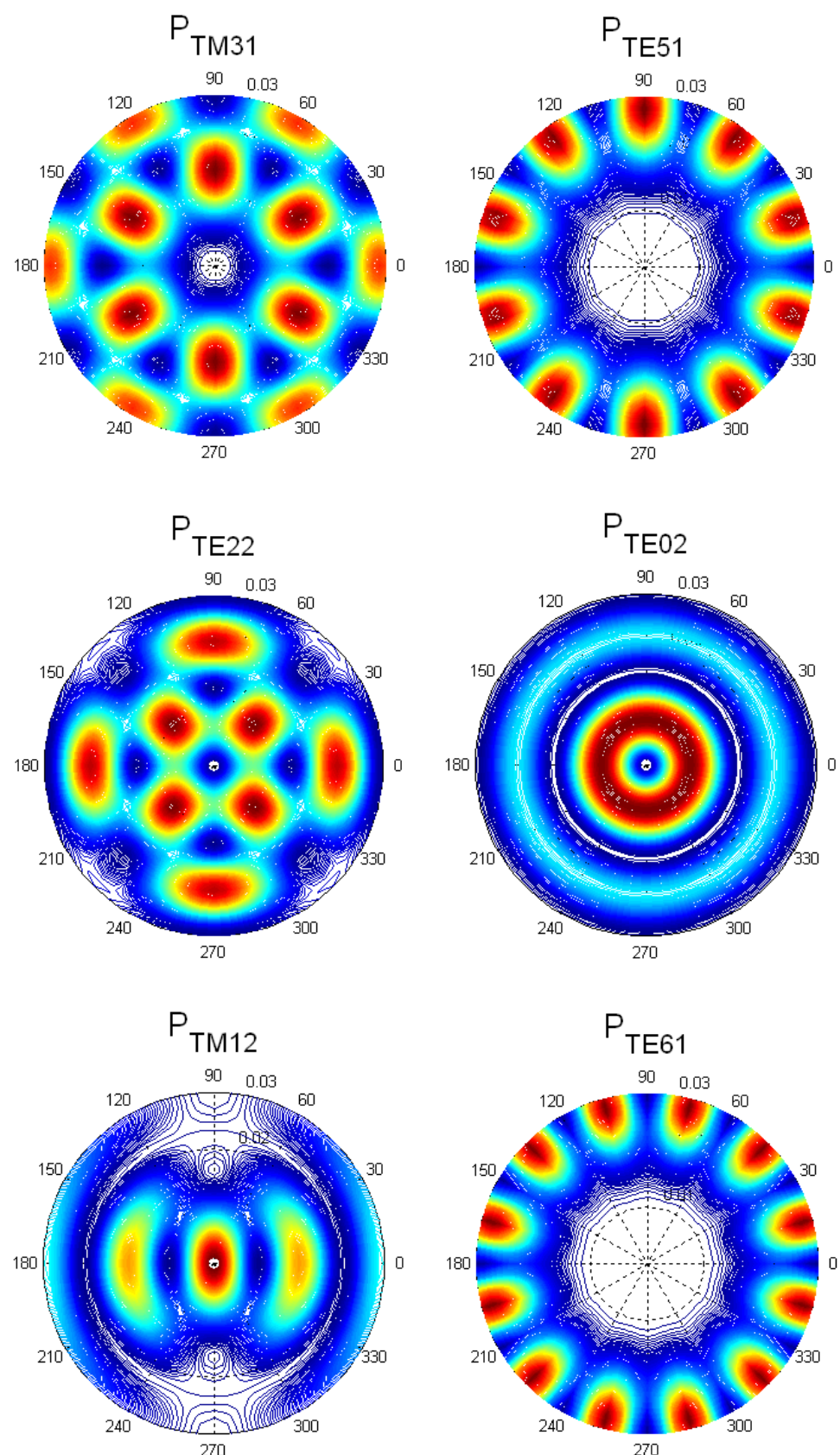
Figure 34 indicates that four maximums of power density occur at $(\rho, \theta) = (0.013, 45), (0.013, 135), (0.013, 225)$ and $(0.013, 315)$, and four local maximums occur near the boundary of the outer conductor at $\theta = 0, 90, 180, 270$. The power density reaches zero at the boundary of the outer conductor at $\theta = 45, 135, 225, 315$ and the center. The four local minimums occur at $(\rho, \theta) = (0.018, 0), (0.018, 90), (0.018, 180)$ and $(0.018, 270)$.

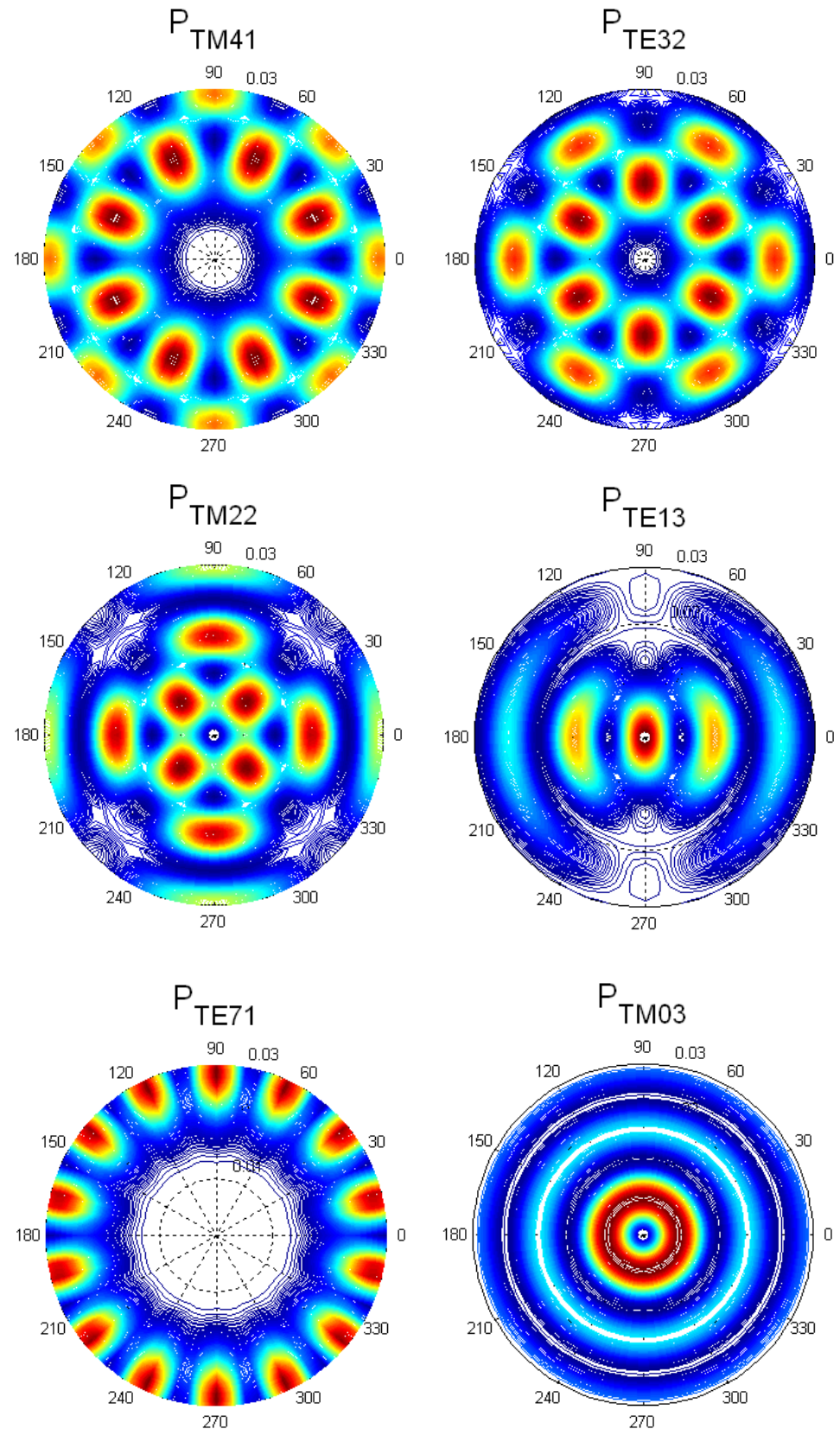
5.3 First 30 modes

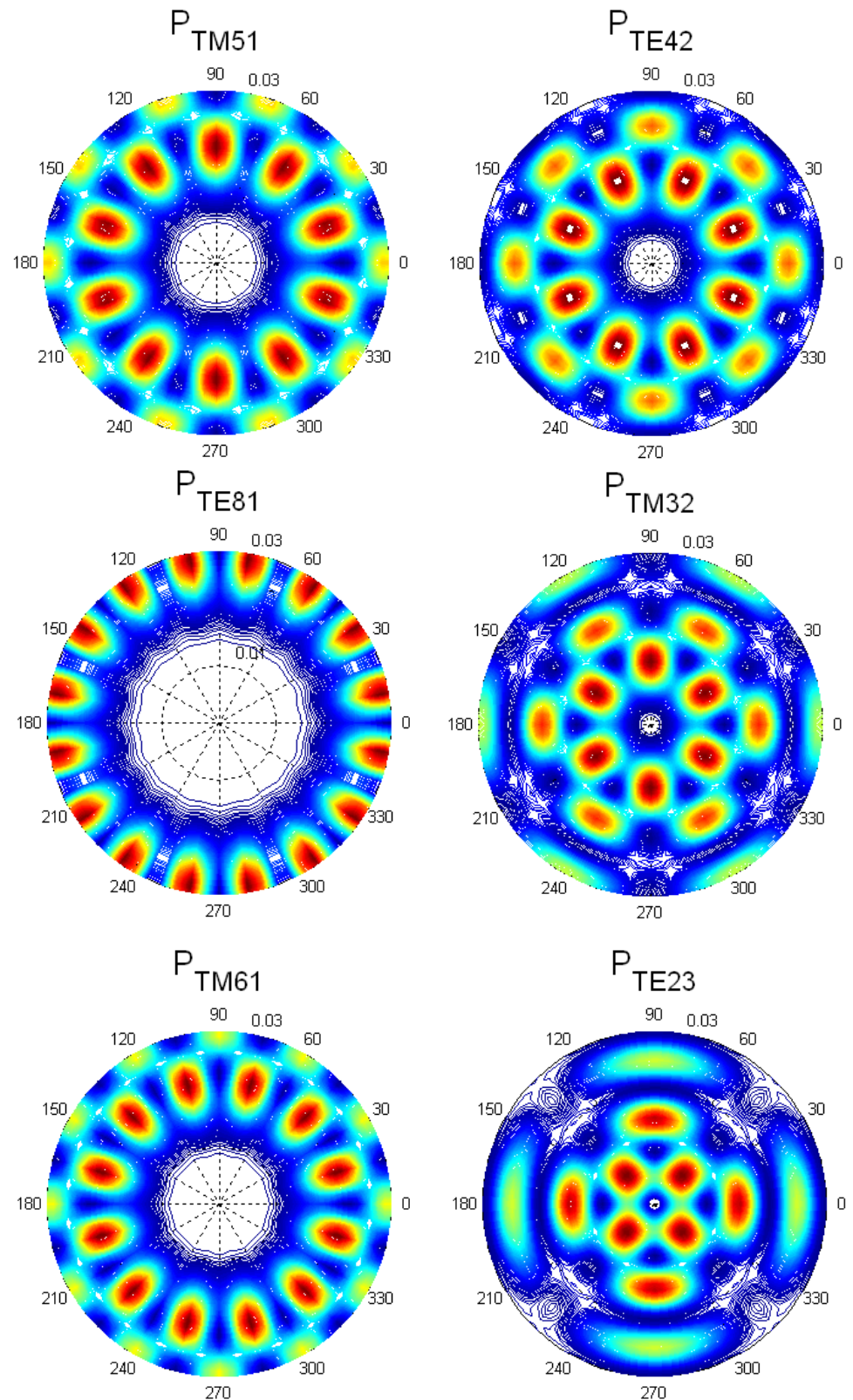
According to Table 4 and Table 5, we can derive the mode order by determining the order of operation frequency (from low to high) for different values of m and n. Using the value $a = 3$ cm, the time-average Poynting's vector (power flow) configurations for the first 30 modes in a circular waveguide are plotted on the following pages:

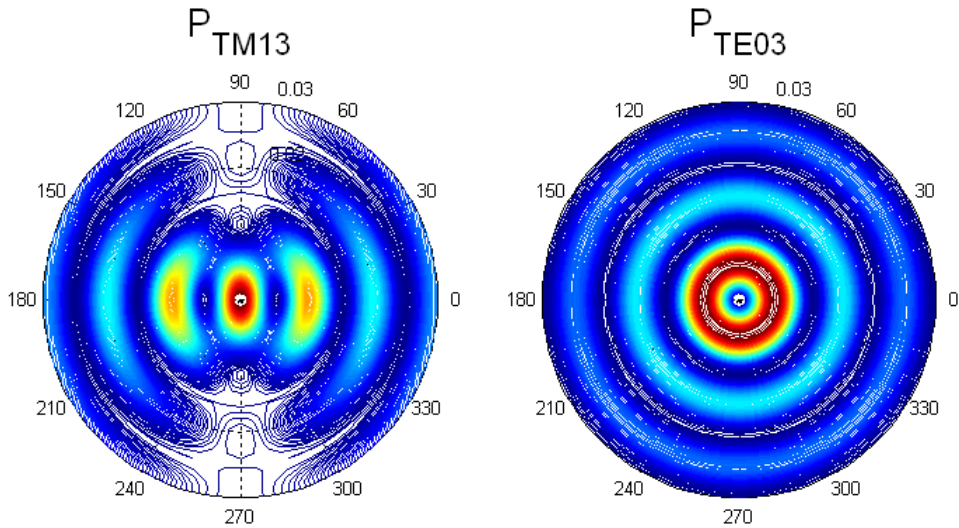












5.4 Mixed modes

If the operating frequency is above the lowest cutoff frequency, two or more modes can be formed in a waveguide. For example, for a rectangular waveguide with the same dimensions we used in Chapter 4, the cutoff frequency of the second lowest mode (TE_{01}) is:

$$\omega_{c,TE_{01}} = \frac{1}{\sqrt{\mu\epsilon}} \sqrt{\left(\frac{m\pi}{a}\right)^2 + \left(\frac{n\pi}{b}\right)^2} = \frac{1}{\sqrt{\mu\epsilon}} \sqrt{\left(\frac{0\pi}{2}\right)^2 + \left(\frac{1\pi}{1}\right)^2} = 9.4 \times 10^8 \quad (5.24)$$

Now, TE_{01} and TE_{10} (the dominate mode) both propagate in the waveguide if the operating frequency right above 940 MHz. The time-average Poynting's vector for the two mixed modes can be plotted as shown in Figure 35.

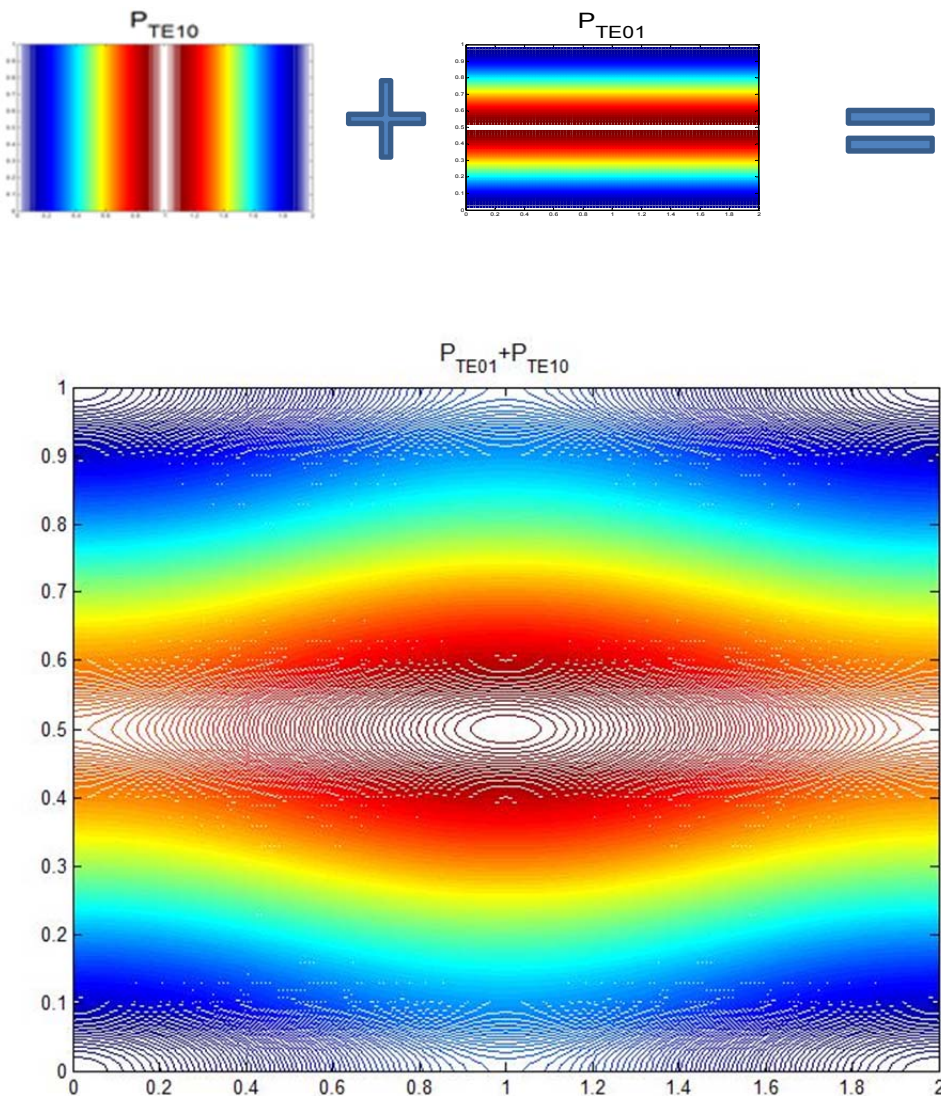


Figure 35: The power density when TE_{01} and TE_{10} modes are both excited in a rectangular waveguide

Another example of mixed-mode is presented in Figure 36. Under a proper frequency, the TE_{11} and TM_{01} modes both propagate in a circular waveguide.

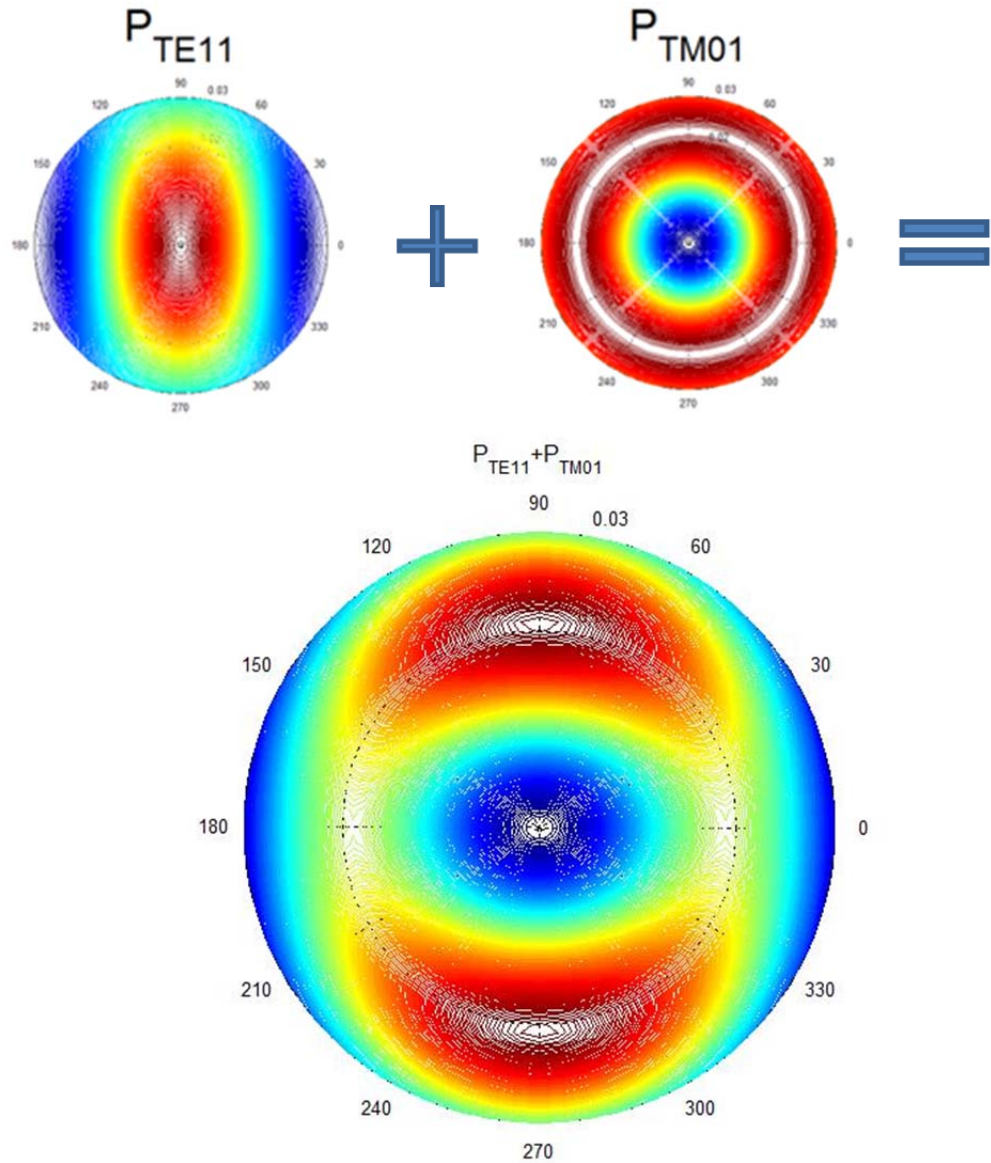


Figure 36: The power density when TE_{11} and TM_{01} modes are both excited in a circular waveguide

Chapter 6: Several Examples Illustrating the Energy Flow Using the Poynting's Vector

6.1 Single conductor carrying a current

A common demonstration of power transmission, interpreted by the Poynting's vector, is the application of a current carrying wire. Consider a round conductor with direct current, \vec{I} , flowing in the positive z direction, as indicated in Figure 37. According to Ampere's Law, and the general approximation of the current density, we know that the electric field and the current density at the surface of the cylindrical

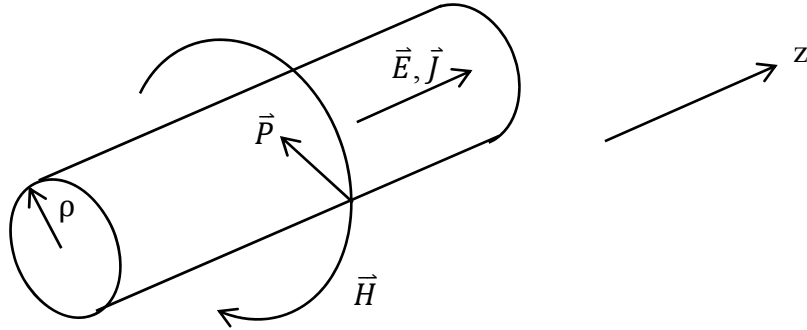


Figure 37: The Poynting's vector $\vec{P} = \vec{E} \times \vec{H}$ near a single conductor Carrying a current

conductor can be written as

$$\vec{E} = \frac{J}{\sigma} \hat{z} \text{ or } \vec{J} = \sigma \vec{E} \quad (6.1)$$

$$\vec{J} = \frac{I}{\pi a^2} \hat{z} \quad (6.2)$$

And the magnetic field inside the wire is given by

$$\vec{H} = \frac{I\rho}{2\pi a^2} \hat{\phi} \quad (6.3)$$

where σ is the conductivity, \vec{J} is the current density, and a is the radius of the conductor. Therefore, the Poynting's vector at $\rho = a$ can be indicated as

$$\vec{P} = \vec{E} \times \vec{H} = \frac{I}{\sigma 2\pi a} (-\hat{\rho}) \quad (6.4)$$

The power flow points in the $-\hat{\rho}$ direction, which means the power comes from the external field, perpendicular to the surface, and then goes into the conductor. Now, if we take surface integration on the Poynting's vector over a cylindrical surface of length l and radius ρ , we get

$$\begin{aligned} \left| - \oint_S \mathcal{P} \cdot dS \right| &= \\ - \oint_S \frac{I}{\sigma 2\pi a} |(-\hat{\rho}) \cdot dS| &= \frac{1}{\sigma \pi a^2} \frac{I}{2\pi a} 2\pi a l = I^2 \frac{l}{\sigma \pi a^2} = I^2 R \end{aligned} \quad (6.5)$$

where R is the resistance of the conductor.

There is no flow through the end of the wire since \vec{P} does not have any components that are normal to the ends. Therefore, all the power flows through the cylindrical surface and then inward, in the amount of I^2R . I^2R is the Joule loss of the conductor, which is supplied by the external field feeding the power into the surface of the conductor. It is also the amount of thermal energy that is generated due to the heat dissipated in the conductor. The Poynting's vector, therefore, is in agreement with circuit theory in this case. Moreover, the first term on the right-hand side in the Poynting's theorem can be calculated as:

$$\begin{aligned} \int_{\text{vol}} \mathbf{J} \cdot \mathbf{E} dv &= \int_{\text{vol}} \vec{J} \cdot \frac{\vec{J}}{\sigma} dv = \\ \int_{\text{vol}} \frac{1}{\sigma} \left(\frac{I}{\pi a^2} \right)^2 dv &= \frac{1}{\sigma} \left(\frac{I}{\pi a^2} \right)^2 (\pi a^2 l) = \frac{I^2}{\sigma \pi a^2} = I^2 R \end{aligned} \quad (6.6)$$

We have assumed that the electric field and magnetic field are not changing with time so that:

$$\frac{\partial}{\partial t} \int_{\text{vol}} \left(\frac{\epsilon E^2}{2} + \frac{\mu H^2}{2} \right) dv = 0 \quad (6.7)$$

From (6.6) and (6.7), we can rewrite the Poynting's theorem as

$$\int_{vol} \vec{J} \cdot \vec{E} dv + \frac{\partial}{\partial t} \int_{vol} \left(\frac{1}{2} \vec{D} \cdot \vec{E} \right) dv + \frac{\partial}{\partial t} \int_{vol} \left(\frac{1}{2} \vec{B} \cdot \vec{H} \right) dv = I^2 R \quad (6.8)$$

The results in equation (6.8) and (6.5) match one another, according to the Poynting's vector theorem.

6.2 Poynting's vector illustrating the propagation of energy along a transmission line connecting a battery to a load

After this discussion of the Poynting's vector in a conductor, we next consider connecting a battery to a resistive load by intermediary of two wires. Would power flow inside the wires from the battery to the conductor? Consider that a load is connected to a battery via two wires. It is intuitive to assume that the fields travel inside the metal wires and transmit power to the load. However, it is unclear exactly how power moves from a battery to a load.

To answer this question, we have to consider surface charges, which provide a radial component to the electric field outside the wire. Note that the charges on the wires are not uniform; the voltage is higher when it is closer to the battery.

Because of the voltage drop, the two wires carry equal currents in magnitude, in opposite directions. The electric potential of the wire that is connected between the cathode and the load is higher than the wire connected between the anode and the load. The voltage difference between the two wires creates an electric field that points from the higher voltage to the lower voltage between the wires. Also, the current flowing in the wires creates a circling magnetic field around them. Therefore, at every point in space, we find that the Poynting's vector points from the battery to the load, which means the power created by the battery is actually going from the battery to the load in the tridimensional space surrounding the wires.

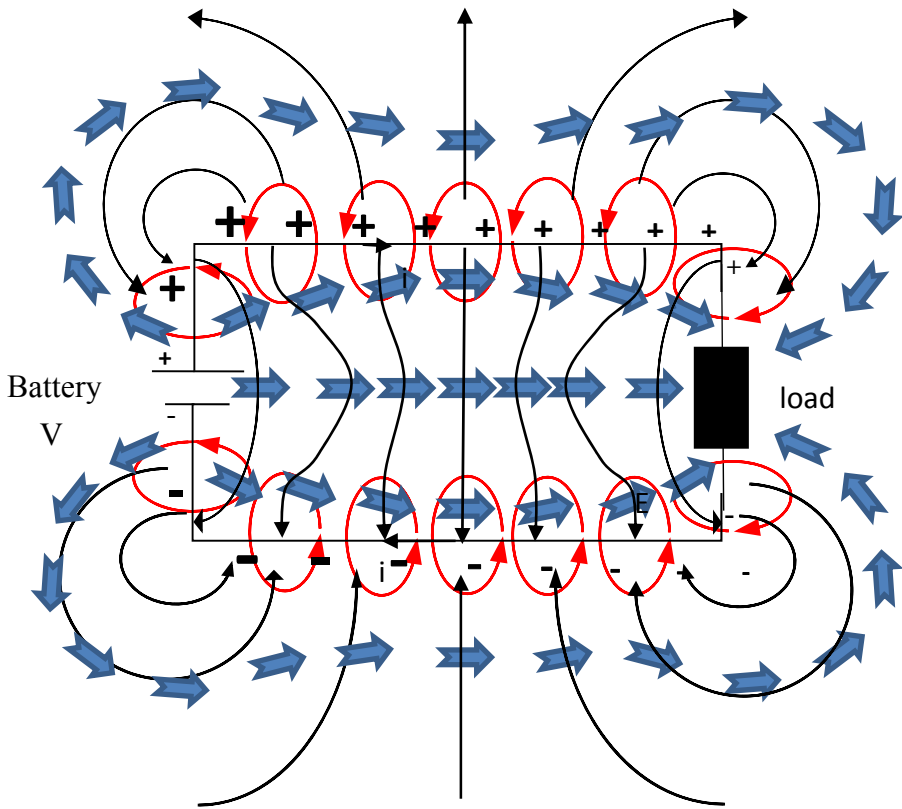


Figure 38: Poynting vector flow from a battery to a load

The component of the Poynting's vector that runs parallel to the wire is a result of the radial electric field and the circling magnetic field around the wire. The component of the Poynting's vector that goes into the wire is responsible for the Joule loss, as given by the equation of the Poynting's vector above. Since the fields are smaller further away from the battery, the Poynting's vector also becomes smaller and smaller further along the wire. The gradual reduction of the Poynting's vector means that some power has already been dissipated; therefore, the power that flows down the rest of the wire is smaller.

As indicated in Figure 38, the wires act like a wave guide for the electric and magnetic fields traveling towards the load. Why, then, is the power not transmitted though the wires? This is because for an ideal wire, the conductivity σ is infinity. As a result, the electric field within the wire is zero. Since \vec{E} field is equal to zero in the

wire, $\bar{P} = \frac{1}{2} \bar{E} \times \bar{H}^*$ is equal to zero in the wire as well. In this case, since power is carried in the electromagnetic field and transmitted into the air, why do we need wires to connect the source and load? The pair of wires is used to guide the electromagnetic field in transmitting from the battery to the load. In this physical phenomenon, we know that as long as there is a closed loop formed, the electromagnetic field is present and carrying power.

6.3 Simple circuit (battery plus two resistors)

The Poynting's vector in a simple circuit has been discussed in [6]. In this paper, they use the "relaxation method" to demonstrate the electric potential around a simple circuit with a battery and two resistors. These are considered point-like, as illustrated in Figure 39.

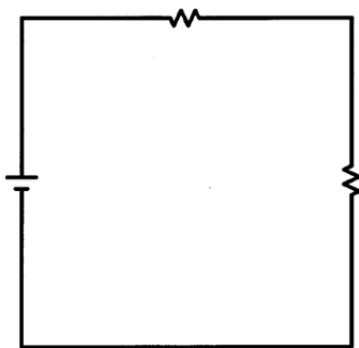


Figure 39: A simple circuit with a battery and two resistors

We next implement numerical derivatives by MATHEMATICA to obtain the electric field. Figure 40 displays the contour plot of the electric potential overlaid on the direction of the electric field. The electric potential is higher when it is closer to the anode of the battery.

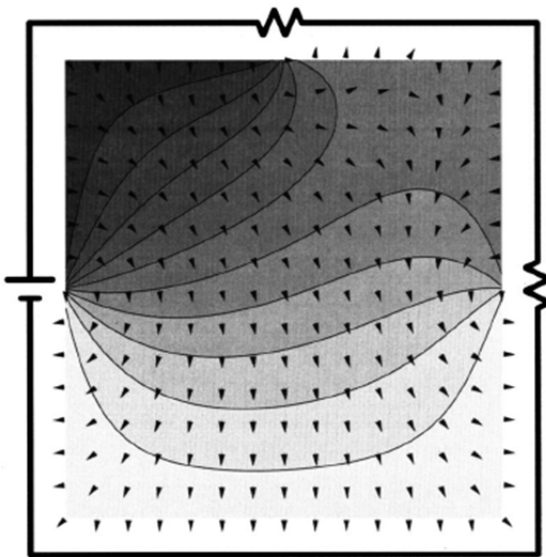


Figure 40: The contour plot of the electric potential for a simple circuit with a battery and two resistors

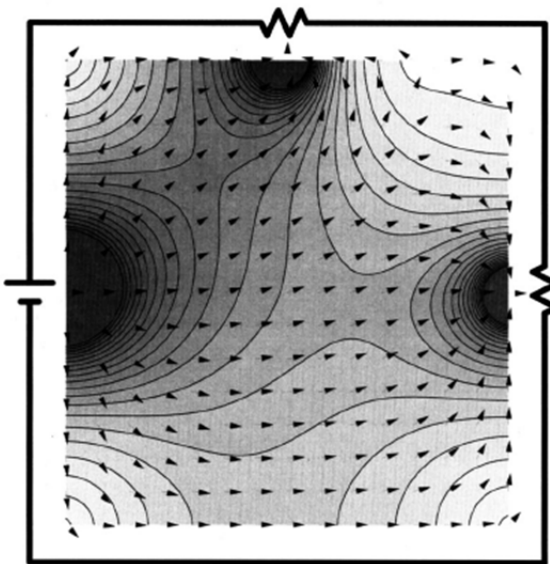


Figure 41: The magnitude of Poynting vector

As shown in Figure 41, the Poynting's vector can then be computed after the magnetic field is found by

$$\vec{B} = \mu_0 I / L \quad (6.9)$$

Basically, the Poynting's vector points at the resistors from the battery. This means

that the power and energy flow to the elements through the space from the battery.

6.4 Leaky coaxial cable

A coaxial cable is an electrical cable consists of two conductors that share a common axis. The center conductor is surrounded by insulation and the outer conductor serves as a ground. The energy flows through the insulation layer. In this way, the design provides shielding against noise from the outside of the cable and keeps the signal inside the cable.

An ideal battery that provides constant voltage V connects to one end of the conductors, as shown in Figure 42. The imperfect dielectric between the cable shield and the center conductor has conductivity σ_d and permeability μ_0 . The electric field in the dielectric is equal to

$$\vec{E}(r) = \frac{V}{r \ln(\frac{b}{a})} \hat{r} \quad (6.10)$$

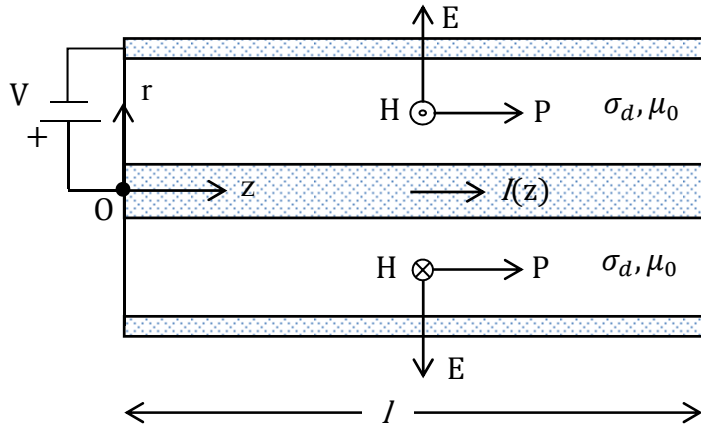


Figure 42: A coaxial cable with applied voltage V

The magnetic field is generated by the symmetric current distribution $I(z)$ in the cable. The magnetic field between the cable conductors can be expressed as

$$\vec{H}(r, z) = \frac{I(z)}{2\pi r} \hat{\phi} \quad (6.11)$$

The Poynting's vector in the cable is then

$$\vec{P}(r, z) = \vec{E}(r) \times \vec{H}(r, z) = \frac{VI(z)}{2\pi r^2 \ln(\frac{b}{a})} \hat{r} \times \hat{\phi} \quad (6.12)$$

where

$$I(z) = \frac{2\pi\sigma_d}{\ln(\frac{b}{a})} V(l - z) \quad (6.13)$$

Therefore, the Poynting's vector can be rewritten:

$$\vec{P}(r, z) = \frac{\sigma_d V^2 (l - z)}{r^2 \ln^2(\frac{b}{a})} \hat{z} \quad (6.14)$$

The magnitude of the Poynting's vector indicates that the amount of flux of energy flowing in the dielectric material. As shown in the equation (6.14) and Figure 43, the power flux is higher at locations closer to the center conductor and the battery. The direction of power flux is from the battery toward the rest of the cable. We note that there is no power flux outside the cable because the field outside the cable is zero.

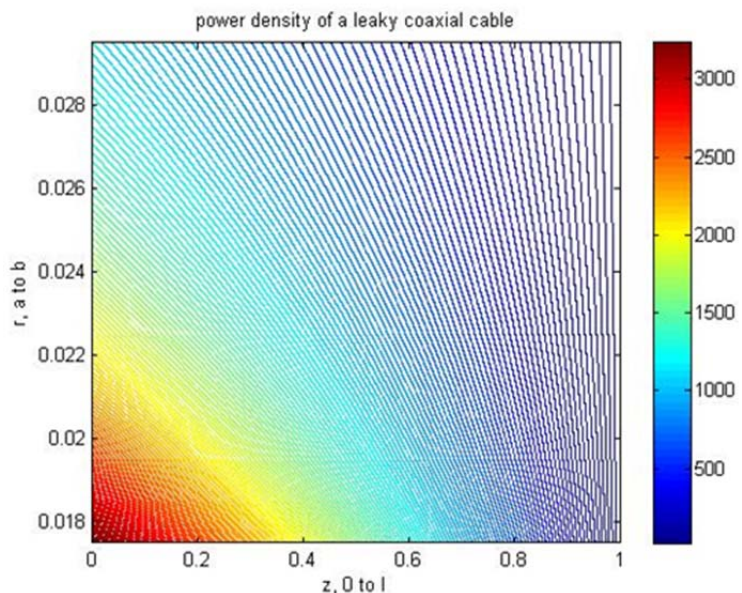


Figure 43: The power density inside a leaky coaxial cable along the axial

Chapter 7: Examples illustrating the Poynting's vector transmission of energy in time-varying cases

7.1 Time Harmonic Plane Wave

7.1.1 Introduction

A plane wave is a common and intuitive way to interpret electromagnetic waves. Although a traveling wave, in the real world, is not a uniform plane wave but spherical wave, when an observer is far away enough from the source, it is approximated as a plane wave. The approximation is considered satisfactory when the distance from a source is two wavelengths or greater.

7.1.2 Fields and the Poynting's vector

A time-harmonic plane wave propagating in the z direction, as shown in Figure 44, is generally expressed by an electric and magnetic fields pair

$$\vec{E} = E_0 \cos(\omega t - \beta z) \hat{x} \quad (7.1)$$

$$\vec{H} = \frac{E_0}{\eta} \cos(\omega t - \beta z) \hat{y} \quad (7.2)$$

The power density is

$$\vec{P} = \vec{E} \times \vec{H} = \frac{E_0^2}{\eta} \cos^2(\omega t - \beta z) \hat{z} \quad (7.3)$$

For a specific time, we can plot the instantaneous Poynting's vector pattern pointing in the z direction, as shown in Figure 44. The width of line for the Poynting's vector represents the strength of power density at a location z , as plotted on the top of Figure 44.

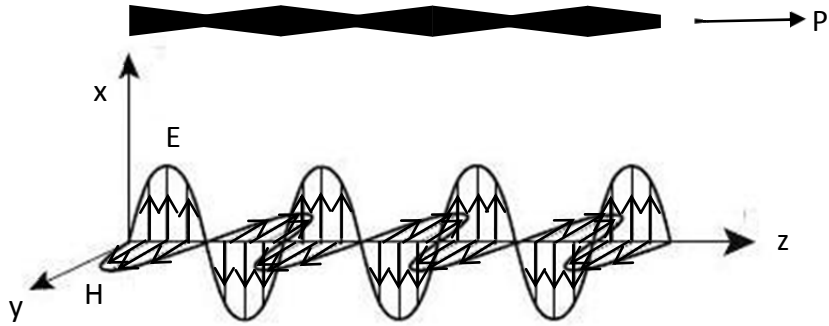


Figure 44: The electromagnetic fields and the magnitude of Poynting's vector of plane wave

The power density varies with both time and location. The average power flow is constant, which can be proven by the time-averaged Poynting's vector:

$$\langle \vec{P} \rangle = \overline{\vec{E} \times \vec{H}} \\ = \overline{\frac{E_0^2}{\eta} \cos^2(\omega t - \beta z)} = \frac{|E_0|^2}{\eta} \overline{\frac{1}{2} + \frac{1}{2} \cos(2\omega t - 2\beta z)} = \frac{1}{2} \frac{|E_0|^2}{\eta} \hat{z} \quad (7.4)$$

From the field theory point of view, the time-average Poynting's vector is constant for a uniform plane wave in free space because the value of the electric and magnetic fields are uniform on the transverse coordinates. (TEM waves)

The time-averaged Poynting's vector is obtained by integration over one period and division by period the duration T of the entire cycle.

$$\langle \vec{P} \rangle = \frac{1}{T} \int_0^T (\vec{E} \times \vec{H}) dt = \frac{1}{T} \int_0^T \frac{E_0^2}{\eta} \cos^2(\omega t - \beta z) dt \\ = \frac{1}{T} \frac{E_0^2}{\eta} \int_0^T \frac{1}{2} + \frac{1}{2} \cos(2\omega t - 2\beta z) dt \\ = \frac{1}{2T} \frac{E_0^2}{\eta} \left[t + \frac{1}{2\omega} \sin(2\omega t - 2\beta z) \right]_0^T = \frac{1}{2} \frac{|E_0|^2}{\eta} \quad (\text{W/m}^2) \quad (7.5)$$

To simplify this complicated math, we use phasor notation to represent steady state time harmonic signals. The general phasor representation of the time harmonic electromagnetic plane wave for the positive z traveling wave components is

$$\vec{E} = E_0 e^{-jkz} \hat{x} \quad (7.6)$$

$$\vec{H} = \frac{E_0}{\eta} e^{-jkz} \hat{y} \quad (7.7)$$

Then, the instantaneous Poynting's vector in phasor notation is defined as

$$\vec{P} = \frac{1}{2} \vec{E} \times \vec{H}^* \quad (7.8)$$

The time averaged power flow:

$$\text{Re}\{\vec{P}\} = \langle \vec{P} \rangle = \overline{\vec{E} \times \vec{H}} = \frac{1}{2} \frac{|E_0|^2}{\eta} \hat{z} \quad (7.9)$$

Now we calculate

$$\langle \vec{P} \rangle = \frac{1}{2} \text{Re}\{\vec{E} \times \vec{H}^*\} = \frac{1}{2} \text{Re} \left\{ E_0 e^{-j\beta z} \left(\frac{E_0}{\eta} e^{-j\beta z} \right)^* \right\} \hat{x} \times \hat{y} = \frac{1}{2} \frac{|E_0|^2}{\bar{\eta}} \hat{z} \quad (7.10)$$

The result in equation (7.10) matches the statement in (7.5), obtained with the real part of the Poynting's vector.

7.1.3 Example

A uniform plane wave is excited with a frequency of 300 MHz in vacuum; the electric field is determined by

$$\vec{E} = 5 \times 10^{-3} e^{-j6.8z} \hat{x} \quad (7.11)$$

Since the electric field is only in the x direction, the magnetic field can be calculated from equation (7.7)

$$\vec{H} = \frac{E_0}{\eta} e^{-jkz} \hat{y} = \frac{5 \times 10^{-3}}{377} e^{-j6.8z} \hat{y} = 1.33 \times 10^{-5} e^{-j6.8z} \hat{y} \quad (7.12)$$

Next, from (7.8) the Poynting's vector is

$$\begin{aligned} \vec{P} &= \frac{1}{2} \vec{E} \times \vec{H}^* = \frac{1}{2} \times 5 \times 10^{-3} e^{-j6.8z} \times 1.33 \times 10^{-5} e^{+j6.8z} (\hat{x} \times \hat{y}) \\ &= 3.325 \times 10^{-8} \hat{z} \text{ W/m}^2 = 33.25 \hat{z} \text{ nW/m}^2 \end{aligned} \quad (7.13)$$

From equation (7.13), we know the power is flowing only in the z direction, with magnitude in the scale of 3.325×10^{-8} watts per square meter. The signal strength for low-power systems, such as cellphones, is usually 1mV/m. In this case, the

Poynting's vector for the low-power system is in nano-watts, which is much smaller than the safe level, 100-500 mW/m².

7.2 Two plane waves traveling in opposite directions

Consider two waves are both polarized with \vec{E} in the y direction. Assume that one wave is traveling in the positive direction with magnitude E_+ while the other wave is traveling in the negative direction with magnitude E_- . In this case, E_y can be written as

$$\vec{E} = [E_+ \sin(\omega t - \beta x) + E_- \sin(\omega t + \beta x)]\hat{y} \quad (7.14)$$

We can find H_z from

$$\frac{\partial E_y}{\partial x} = -\mu \frac{\partial H_z}{\partial t} \quad (7.15)$$

And we have

$$\vec{H} = \left[\sqrt{\frac{\epsilon}{\mu}} E_+ \sin(\omega t - \beta x) - \sqrt{\frac{\epsilon}{\mu}} E_- \sin(\omega t + \beta x) \right] \hat{z} \quad (7.16)$$

The Poynting's vector is

$$\vec{P} = \vec{E} \times \vec{H} = \sqrt{\frac{\epsilon}{\mu}} [E_+^2 \sin^2(\omega t - \beta x) - E_-^2 \sin^2(\omega t + \beta x)] \hat{x} \quad (7.17)$$

According to (7.17) the resultant Poynting's vector is the difference between the two traveling waves, and is in the positive x direction if $E_+ > E_-$.

Assume that the wave traveling to the positive x direction is the incident wave on a plane boundary at $x = 0$, and the wave traveling to the negative x direction is a reflected wave. If the medium at $x > 0$ is a perfect conductor, we have a boundary condition of $E_- = -E_+$. This leads to a pure standing wave at $x < 0$. Note that the net Poynting's vector is zero under this condition, which means there is no power transmitted through the boundary.

Now, we will examine the condition of a pure standing wave in more detail from the perspective of energy localization. The electric energy density of a pure standing wave is

$$\begin{aligned} w_e &= \frac{1}{2}\epsilon E^2 = \frac{1}{2}\epsilon [E_+ \sin(\omega t - \beta x) + E_- \sin(\omega t + \beta x)]^2 \\ &= \frac{1}{2}\epsilon [(E_+ + E_-) \sin \omega t \cos \beta x - (E_+ - E_-) \cos \omega t \sin \beta x] \end{aligned} \quad (7.18)$$

If we take $x = 0$ to be the boundary between the two media, the boundary condition from the tangential component of the electric field requires that $E_y = 0$, therefore $E_+ = -E_-$ at the boundary. Thus (7.18) becomes

$$w_e = 2\epsilon E_-^2 \cos^2 \omega t \sin^2 \beta x \quad (7.19)$$

Substituting $\sqrt{\frac{\epsilon}{\mu}} E_+ = H_-$ in (7.16) yields

$$H_z = -2H_- \sin \omega t \cos \beta x \quad (7.20)$$

The magnetic energy density of a pure standing wave is

$$w_m = 2\mu H_-^2 \sin^2 \omega t \cos^2 \beta x \quad (7.21)$$

By comparing equation (7.19) and (7.21), we can see that the electric energy density is a maximum when the magnetic is zero and the magnetic energy density is a maximum when the electric is zero. Moreover, the points of maximum are $\frac{\lambda}{4}$ apart. In

this case we have a pure resonator. The energy bounces back and forth from electric form to magnetic form. This kind of energy is called reactive energy which is not transmitted but transforms from one form to another. As shown in Figure 45, the energy densities are plotted at three different instants of time, $t = 0, T/8$, and $T/4$. The blue curves show the instantaneous electric energy density w_e as calculated from equation (7.19) and the red curves show the instantaneous magnetic energy w_m as calculated from equation (7.21).

Finally, we can calculate the Poynting's vector for a pure standing wave

$$\begin{aligned}
\vec{P} &= \vec{E} \times \vec{H} = 2E_- \cos \omega t \sin \beta x \times (-)2H_- \sin \omega t \cos \beta x \hat{x} \\
&= -4 \sqrt{\frac{\epsilon}{\mu}} E_-^2 \cos \omega t \sin \beta x \sin \omega t \cos \beta x \hat{x}
\end{aligned} \tag{7.22}$$

From equation (7.22) we find the maximum for the Poynting's vector at $t = T/8$ with the peak value of $\sqrt{\epsilon/\mu} E_-^2$. At $t = T/8$, the position of one maximum is at $\beta x = \pi/4$ and is pointing in the negative x direction. The other maximum at $\beta x = 3\pi/4$ is pointing in the positive x direction. As the arrows indicate in Figure 46, the energy flows from the electric energy density regions to the magnetic energy density region. As mentioned before, there is no net energy transmission in a pure standing wave, instead, the energy locations oscillate back and forth.

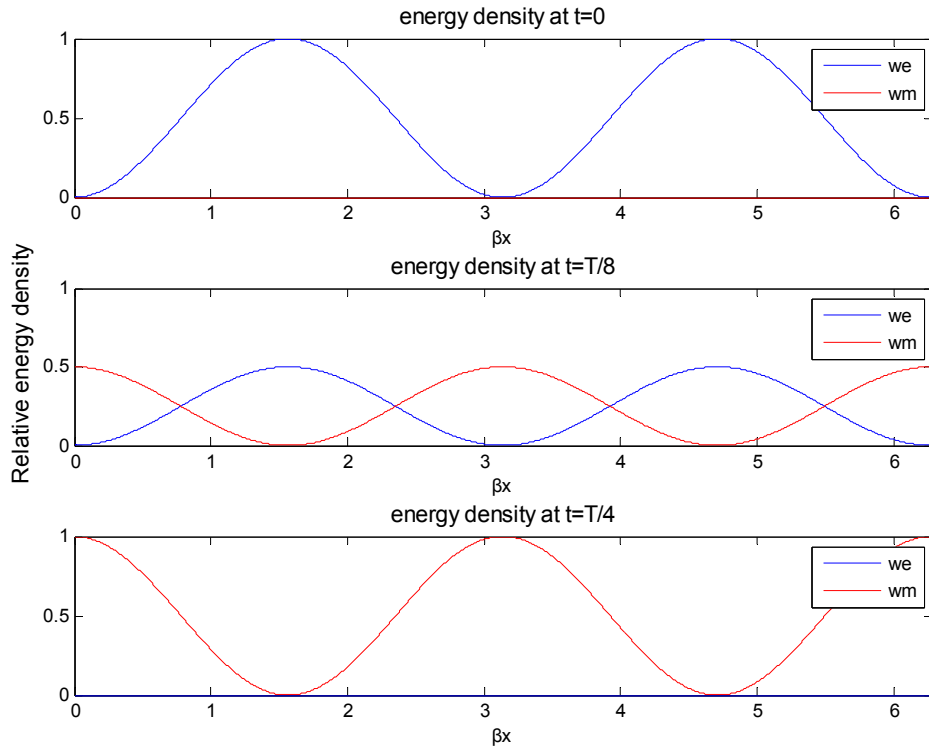


Figure 45: The energy density at $t = 0, T/8$, and $T/4$

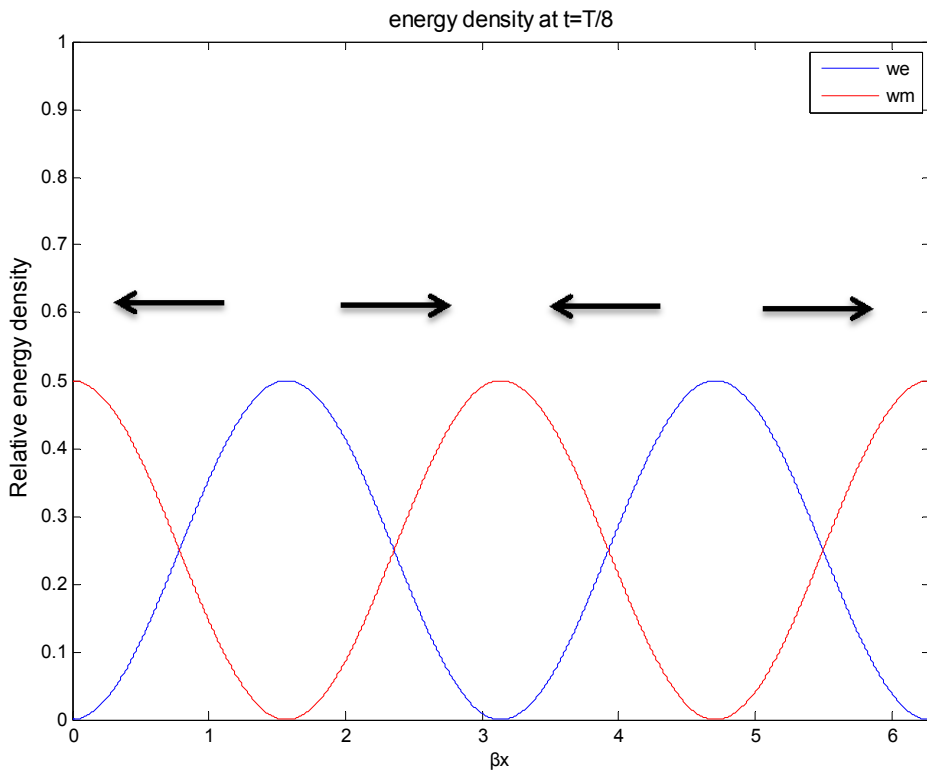


Figure 46: The direction of energy flow at $t = T/8$

7.3 Poynting's vector in a resonator

7.3.1 Introduction

In chapter 7.2, we have already discussed standing waves that result from the superposition of two waves of equal magnitude traveling in opposite directions. For a parallel-plate resonator consisting of two perfect infinite planes, the electric field is zero at distances of integral multiples of $\lambda/2$ from the perfect conductor. Thus, if we place a perfect conductor at these points, there will be no effect on the fields, voltage or current at any other points. Moreover, if we have a dielectric medium between two perfectly conducting plates that are parallel to each other, and that contain stored energy, this energy will act as standing waves which have wavelengths of $l = n\lambda_n/2$, where $n = 1, 2, 3, \dots$ with the corresponding frequencies of $\omega_n = n\pi v_p/l$.

7.3.2 Electromagnetic field in a resonator

Consider a resonator system of two infinite, parallel, perfectly conducting plates with a perfect dielectric between them. The energy is stored in the form of standing waves and has field components E_x and H_y as shown in Figure 47. The expressions

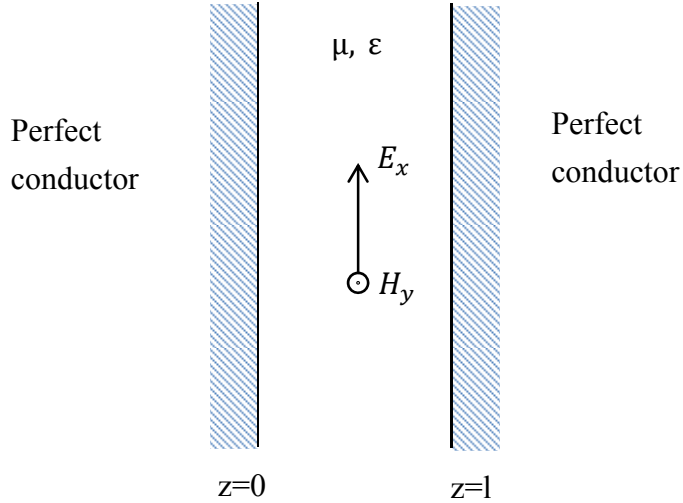


Figure 47: The electromagnetic fields in a resonator system

for the fields that satisfy the boundary conditions at $z = 0$ and $z = 1$ for all t can be written as

$$E_x(z, t) = 2E_0 \sin \frac{n\pi z}{l} \sin \frac{n\pi t}{l\sqrt{\mu\epsilon}} \quad (7.23)$$

$$H_y(z, t) = 2 \frac{E_0}{\eta} \cos \frac{n\pi z}{l} \cos \frac{n\pi t}{l\sqrt{\mu\epsilon}} \quad (7.24)$$

The instantaneous electric and magnetic stored energy density that are associated with these fields are

$$w_e(z, t) = \frac{1}{2} \epsilon E_x^2 = 2\epsilon E_0^2 \sin^2 \frac{n\pi z}{l} \sin^2 \frac{n\pi t}{l\sqrt{\mu\epsilon}} \quad (7.25)$$

$$w_m(z, t) = \frac{1}{2} \mu H_y^2 = 2\mu E_0^2 \cos^2 \frac{n\pi z}{l} \cos^2 \frac{n\pi t}{l\sqrt{\mu\epsilon}} \quad (7.26)$$

Consider a simple case, $n = 1$. The standing waves in this case have one-half wavelength between the two plates. The relative energy densities as a function of z at

different times are sketched in Figure 48. We know from Figure 48 that the stored energy density is entirely electric at all points where $t = l\sqrt{\mu\epsilon}/2, 3l\sqrt{\mu\epsilon}/2, \dots$ and entirely magnetic at $t = 0, l\sqrt{\mu\epsilon}, \dots$. Most of the electric energy is stored close to half way between the plates, and most of the magnetic energy is stored close to the conducting plates. The total energy density stored in the electric and magnetic fields in the system is a constant, with respect to time, since there is no power transferring.

We can write

$$\begin{aligned}
 w(t) &= \int_{z=0}^l (w_e(z, t) + w_m(z, t)) dz \\
 &= \int_{z=0}^l \left(2\epsilon E_0^2 \sin^2 \frac{n\pi z}{l} \sin^2 \frac{n\pi t}{l\sqrt{\mu\epsilon}} + 2\epsilon E_0^2 \cos^2 \frac{n\pi z}{l} \cos^2 \frac{n\pi t}{l\sqrt{\mu\epsilon}} \right) dz \\
 &= \frac{2\epsilon E_0^2 l}{2} \left(\sin^2 \frac{n\pi t}{l\sqrt{\mu\epsilon}} + \cos^2 \frac{n\pi t}{l\sqrt{\mu\epsilon}} \right) = \epsilon E_0^2 l
 \end{aligned} \tag{7.27}$$

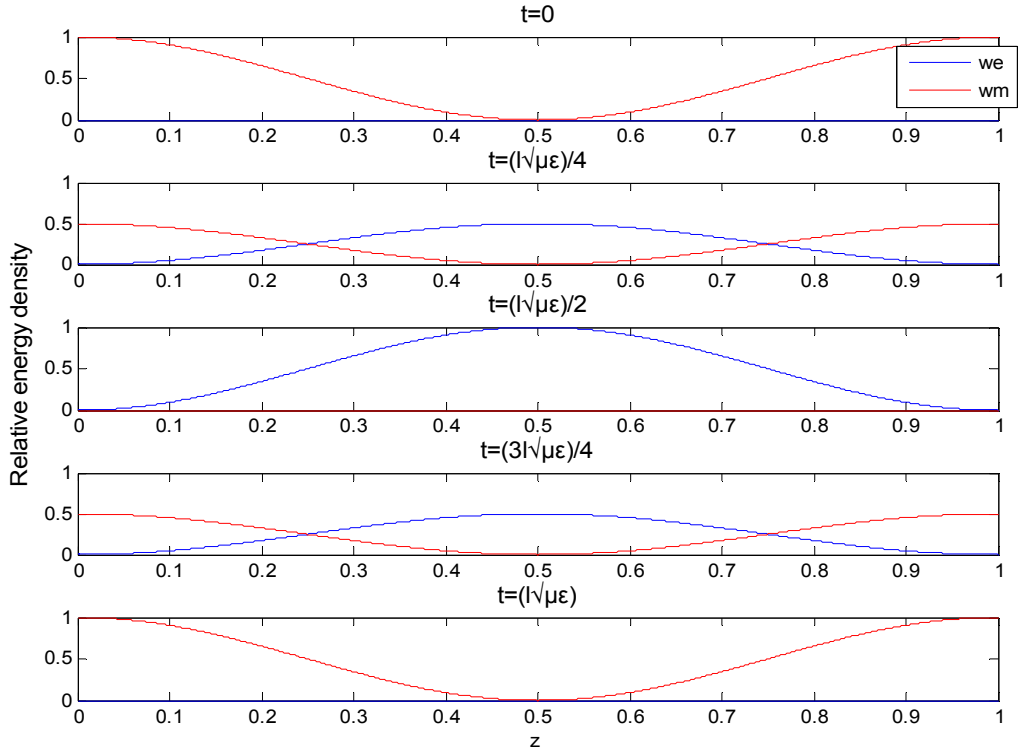


Figure 48: The enegry density at $t = 0, l\sqrt{\mu\epsilon}/4, l\sqrt{\mu\epsilon}/2, 3l\sqrt{\mu\epsilon}/4$ and $l\sqrt{\mu\epsilon}$

Note that the result is independent of n . This process of energy exchange between the plates, from electric to magnetic and vice versa, is the phenomenon of resonance; the structure itself is called a resonator. The frequencies $f_n = n/2l\sqrt{\mu\epsilon}$ are known as the resonant frequencies of the resonator.

7.4 Poynting's vector flow of energy in a lossy material

7.4.1 Introduction

In the previous chapter, electric and magnetic fields were in phase because we assumed a wave propagated in a lossless medium. In fact, the attenuation of air is typically negligible with little polarization or magnetization. Thus, we generally model air as free space with attenuation constant at zero. However, what if the electric field and the magnetic field are not in phase?

The most common case where fields are not in phase is electromagnetic field flows in a lossy dielectric. The fields can be written as

$$\vec{E} = E_0 e^{-\alpha z} \cos(\omega t - kz) \hat{x} \quad (7.28)$$

$$\vec{H} = \frac{E_0}{|\eta|} e^{-\alpha z} \cos(\omega t - kz - \theta) \hat{y} \quad (7.29)$$

and the power density is

$$\vec{P} = \vec{E} \times \vec{H} = \frac{E_0^2}{|\eta|} e^{-2\alpha z} \cos(\omega t - \beta z) \cos(\omega t - \beta z - \theta) \hat{z} \quad (7.30)$$

where α is attenuate constant.

When we apply product to sum formula to the equation,

$$\cos \theta \cos \varphi = \frac{\cos(\theta - \varphi) + \cos(\theta + \varphi)}{2} \quad (7.31)$$

we get

$$\vec{P} = \frac{1}{2} \frac{E_0^2}{|\eta|} e^{-2\alpha z} [\cos(2\omega t - 2\beta z - 2\theta) + \cos(\theta)] \quad (7.32)$$

From the equation above, we find that the Poynting's vector in lossy dielectric

materials has only a dc term and a second-harmonic term. The time period of Poynting's vector is twice that of the fields. After we average the equation over a period, the $\cos(2\omega t - 2\beta z - 2\theta)$ term goes to zero. The time-averaged Poynting's vector is

$$\langle \vec{P} \rangle = \frac{1}{2} \frac{E_0^2}{|\eta|} e^{-2\alpha z} \cos \theta \quad (7.33)$$

As with the plane wave, we can also change the notations to phasor forms:

$$\vec{E} = E_0 e^{-\alpha z} e^{-j\beta z} \hat{x} \quad (7.34)$$

$$\vec{H} = \frac{E_0}{\eta} e^{-\alpha z} e^{-j\beta z} e^{-j\theta} \hat{y} \quad (7.35)$$

$$\vec{P} = \frac{1}{2} \frac{E_0^2}{|\eta|} e^{-2\alpha z} e^{+j\theta} \hat{z} \quad (7.36)$$

Finally, we can observe that once an electromagnetic field enters a lossy material, it starts attenuating as $e^{-\alpha z}$. According to the Poynting's vector, the power transmitting in the material attenuates as $e^{-2\alpha z}$, which is twice as fast as in the electromagnetic field. The rate of attenuation is also relevant to wave frequency because

$$\alpha = \omega \sqrt{\frac{\mu\epsilon}{2} \left[\sqrt{1 + \left(\frac{\sigma}{\omega\epsilon}\right)^2} - 1 \right]} \quad (7.37)$$

From equation (7.37), we know that the power drops faster when the frequency of the wave is higher.

7.4.2 Example

An uniform plane wave in distilled water is excited, and the electric field and magnetic field are determined by

$$\vec{E} = 5 \times 10^{-3} e^{-\alpha z} e^{-j6.8z} \hat{x} \quad (7.38)$$

$$\begin{aligned}\vec{H} &= \frac{E_0}{\eta} e^{-\alpha z} e^{-jkz} e^{-j\theta} \hat{y} = \frac{5 \times 10^{-3}}{377} e^{-\alpha z} e^{-j6.8z} e^{-j\theta} \hat{y} \\ &= 1.33 \times 10^{-5} e^{-\alpha z} e^{-j6.8z} e^{-j\theta} \hat{y}\end{aligned}\quad (7.39)$$

From (7.38) and (7.39), we can calculate the Poynting's vector:

$$\begin{aligned}\langle \vec{P} \rangle &= \frac{1}{2} \vec{E} \times \vec{H}^* = \frac{1}{2} \times 5 \times 10^{-3} e^{-\alpha z} e^{-j6.8z} \times 1.33 \times 10^{-5} e^{-\alpha z} e^{+j6.8z} e^{+j\theta} \hat{z} \\ &= 3.325 \times 10^{-8} e^{-2\alpha z} e^{+j\theta} \hat{z} \text{ W/m}^2 = 33.25 e^{-\alpha z} e^{+j\theta} \hat{z} \text{ nW/m}^2\end{aligned}\quad (4.31)$$

The attenuation coefficient of distilled water at a frequency of 1 MHz is 0.0037 nep/m and is 43 nep/m for a frequency of 3 GHz. From (4.31) we know that the power dies out faster when transferring in a media with a higher attenuation coefficient. When the signal is excited at a higher frequency, the attenuation coefficient is higher and therefore fades away faster.

7.5 Poynting's vector flow of energy in a good conductor

7.5.1 Introduction

A good conductor has high conductivity σ in the order of 10^7 (for example, the conductivity for copper is $5.69 \times 10^7 \text{ S/m}$), and the displacement current is negligible in comparison to a large conduction current. Since the conduction current presents continuously, it produces ohmic losses; therefore, the power carried by the wave decreases as the wave propagates. This phenomena is referred to as "skin effect."

Now, we rewrite the field equations in terms of the skin depth

$$\delta = \frac{1}{\alpha} = \frac{1}{\beta} = \frac{1}{\sqrt{\pi f \mu \sigma}} \quad (7.40)$$

we have

$$\vec{E} = E_0 e^{-z/\delta} \cos(\omega t - \frac{z}{\delta}) \hat{x} \quad (7.41)$$

and

$$\vec{H} = \frac{\sigma \delta E_0}{\sqrt{2}} e^{-z/\delta} \cos(\omega t - \frac{z}{\delta} - \frac{\pi}{4}) \hat{y} \quad (7.42)$$

The time-average Poynting's vector is

$$\begin{aligned} \langle \vec{P} \rangle &= \frac{1}{2} E_0 e^{-z/\delta} \cos\left(\omega t - \frac{z}{\delta}\right) \times \frac{\sigma \delta E_0}{\sqrt{2}} e^{-z/\delta} \cos\left(\omega t - \frac{z}{\delta} - \frac{\pi}{4}\right) \hat{z} \\ &= \frac{\sigma \delta E_0^2}{2\sqrt{2}} e^{-2z/\delta} \cos\left(\frac{\pi}{4}\right) = \frac{\sigma \delta E_0^2}{4} e^{-2z/\delta} \end{aligned} \quad (7.43)$$

Next, we rewrite equation (7.41) to (7.43) in phasor notation to represent the fields and Poynting's vector:

$$\vec{E} = E_0 e^{-z/\delta} e^{-jz/\delta} \hat{x} \quad (7.44)$$

$$\vec{H} = \frac{E_0}{\bar{\eta}} e^{-z/\delta} e^{-jz/\delta} \hat{y} \quad (7.45)$$

$$\begin{aligned} \langle \vec{P} \rangle &= \frac{1}{2} E_0 e^{-z/\delta} e^{-jz/\delta} \times \left(\frac{\sigma \delta E_0}{\bar{\eta}} e^{-z/\delta} e^{-jz/\delta} \right)^* \hat{x} \times \hat{y} \\ &= \frac{|E_0|^2}{2\bar{\eta}^*} e^{-2z/\delta} \hat{z} = \frac{\sigma \delta |E_0|^2}{4} (1 + j) e^{-2z/\delta} \hat{z} \end{aligned} \quad (7.46)$$

Substituting $\frac{1}{\sigma} J_0$ for E_0 :

$$\langle \vec{P} \rangle = \frac{\delta |J_0|^2}{4\sigma} (1 + j) e^{-2z/\delta} \hat{z} \quad (7.47)$$

The real part of $\langle \vec{P} \rangle$ is the dissipated power because the sinusoidal power dissipated is the time average. At $z = 0$, the power entering the surface is

$$P_{diss,s} = \frac{\delta |J_0|^2}{4\sigma} W/m^2 \quad (7.48)$$

We can plot the power density as a function of z coordinate for copper, which has a skin depth of 66 μm at a frequency of 1 MHz. Figure 49 makes evident that the power crowds to the surface of the conductor with little penetration.

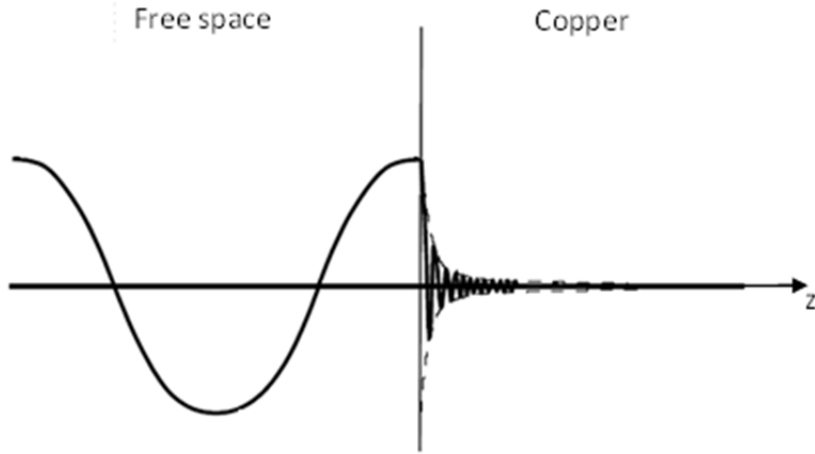


Figure 49: Power density loss when wave enters copper from free space

7.5.2 Example

Consider a 1 m long home copper wiring has a radius of 0.322 mm and is carrying 1 mA of current at 300 MHz. The skin depth for copper at 300 MHz is

$$\delta = \frac{0.066}{\sqrt{f}} = \frac{0.066}{\sqrt{300 \times 10^6}} = 3.81 \times 10^{-6} \quad (7.49)$$

We can approximately compute the AC resistance power as below:

$$\begin{aligned} P_{AC} &= \frac{1}{2} I^2 \left(\frac{l}{\sigma 2\pi\rho\delta} \right) \\ &= \frac{1}{2} (10^{-3})^2 \frac{1}{5.8 \times 10^7 \times 2\pi \times (0.322 \times 10^{-3}) \times (3.81 \times 10^{-6})} \\ &= 1.12 \mu W/m \end{aligned} \quad (7.50)$$

For the DC resistance case, the current would have an average power of

$$\begin{aligned} P_{DC} &= \frac{1}{2} I^2 R = \frac{1}{2} I^2 \left(\frac{l}{\sigma A} \right) = \frac{1}{2} (10^{-3})^2 \frac{1}{5.8 \times 10^7 \times \pi \times (0.322 \times 10^{-3})^2} \\ &= 0.0265 \mu W/m \end{aligned} \quad (7.51)$$

Note that P_{AC} is 42 times higher than P_{DC} for the same current. This is why the cables heat up faster at higher frequencies. Now, we use Poynting's vector to compute the power flowing into the wire. Since copper is a good conductor, the current flows very close to the surface. Thus, the current can be approximated by surface current:

$$\vec{J}_s = \frac{I_z}{2\pi\rho} \hat{z} = \frac{10^{-3}}{2\pi \times 0.322 \times 10^{-3}} \hat{z} = 0.494 \hat{z} A/m \quad (7.52)$$

Since we have assumed that this is a perfect conductor, we can calculate the magnetic field from the boundary condition,

$$\vec{J}_s = \hat{n} \times \vec{H} = \hat{\rho} \times \vec{H} = 0.494 \hat{z} \quad (7.53)$$

$$\vec{H} = 0.494 \hat{\phi} A/m \quad (7.54)$$

Again, we assume the current flows uniformly along depth δ , and the annular ring through which the current flows by a rectangle depth by $2\pi\rho$. The electric field can be derived at the surface:

$$\begin{aligned} \vec{E}(\rho = 0.322 \times 10^{-3}) &= \frac{\vec{J}(\rho = 0.322 \times 10^{-3})}{\sigma} = \frac{I}{\delta 2\pi\rho} \\ &= \frac{10^{-3}}{\frac{3.8 \times 10^{-6} \times 2\pi \times 0.322 \times 10^{-3}}{5.8 \times 10^7}} = 0.00224 \hat{z} V/m \end{aligned} \quad (7.55)$$

Therefore, the Poynting's vector is

$$\langle \vec{P} \rangle = \frac{1}{2} \vec{E} \times \vec{H}^* = \frac{1}{2} \times 0.00224 \hat{z} \times 0.494 \hat{\phi} = 0.554(-\hat{\rho}) mW/m^2 \quad (7.56)$$

The power that flows into the wire surface is then

$$\langle \vec{P} \rangle \cdot A = 0.554(-\hat{\rho}) \cdot (1 \times 2\pi \times 0.322 \times 10^{-3})(-\hat{\rho}) = 1.12 \mu W/m \quad (7.57)$$

The results for Equation (7.57) show the same power as that calculated on the basis of AC resistant loss, as shown in equation (7.50). Therefore, the Poynting's vector entering the wire is dissipated as heat, or say Joule loss.

7.6 Poynting's vector in a transmission line

7.6.1 Introduction

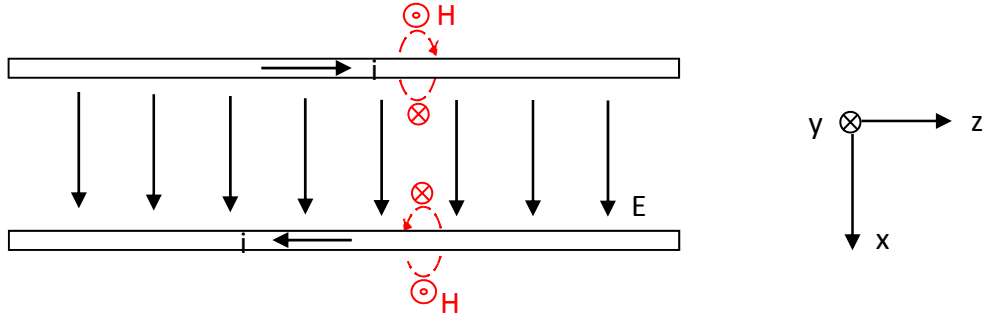


Figure 50: Electromagnetic fields in a transmission line

When a pair of conductors filled with material medium between them, they form a transmission line. A transmission line guides power from one end of the line to the other. As shown in Figure 50, electric field created by the voltage difference between conductors is directed vertically between the two conductors. Since current flows in the z-direction, there is magnetic field surrounds the wires according to the Ampere's circuital law.

Since a transmission line can only support a TEM wave, we use the analogy for TEM mode and the electric field and magnetic field for positive traveling wave component around a two-conductor transmission line are

$$\vec{E} = E_0 e^{-jkz} \hat{x} \quad (7.58)$$

$$\vec{H} = H_0 e^{-jkz} \hat{y} \quad (7.59)$$

and the fields are plotted in Figure 51.

Therefore, the Poynting's vector can be written as

$$\vec{P} = \frac{1}{2} \vec{E} \times \vec{H}^* = E_0 e^{-jkz} H_0^* e^{+jkz} \hat{x} \times \hat{y} = \frac{1}{2} \frac{|E_0|^2}{\eta} \hat{z} = \frac{1}{2} |H_0|^2 \eta \hat{z} \quad (7.60)$$

where η is called wave impedance.

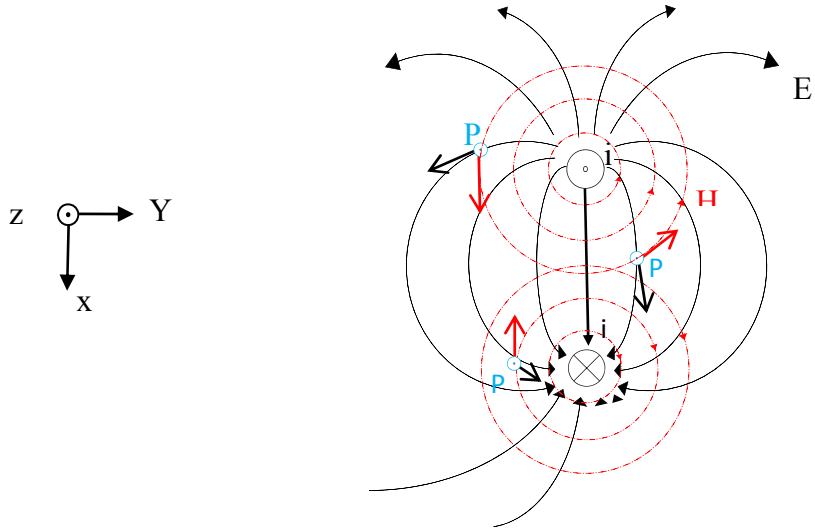


Figure 51: The side view of a transmission line

At any point in the transmission line system, the power is traveling parallel to the line, or in the z direction, through the material between the two conductors. From Figure 51 we discover that the power also radiates out of the transmission line system. From equation (7.60), we know the Poynting's vector is proportional to the square of the electric field E . Also, the phase velocity, u , is $1/\sqrt{\epsilon\mu}$, we can rewrite Poynting's vector as

$$\vec{P} = \frac{1}{2} u \mu |H_0|^2 \hat{z} \quad (7.61)$$

We can interpret the Poynting's vector as the power propagating in the positive direction of the z axis, and with magnitude of the phase velocity multiplied by the average field energy density.

7.6.2 Example

Calculating the Poynting's vector for an infinite two-conductor lossless transmission line, where each conductor is 25.4 mm in diameter with spacing between centers of 76.2 mm and a voltage between the two conductors of 10 V rms. we can

plot the power flow contour plot as shown in Figure 52. (From Electromagnetics, John Daniel Kraus, Keith R. Carver [10].)

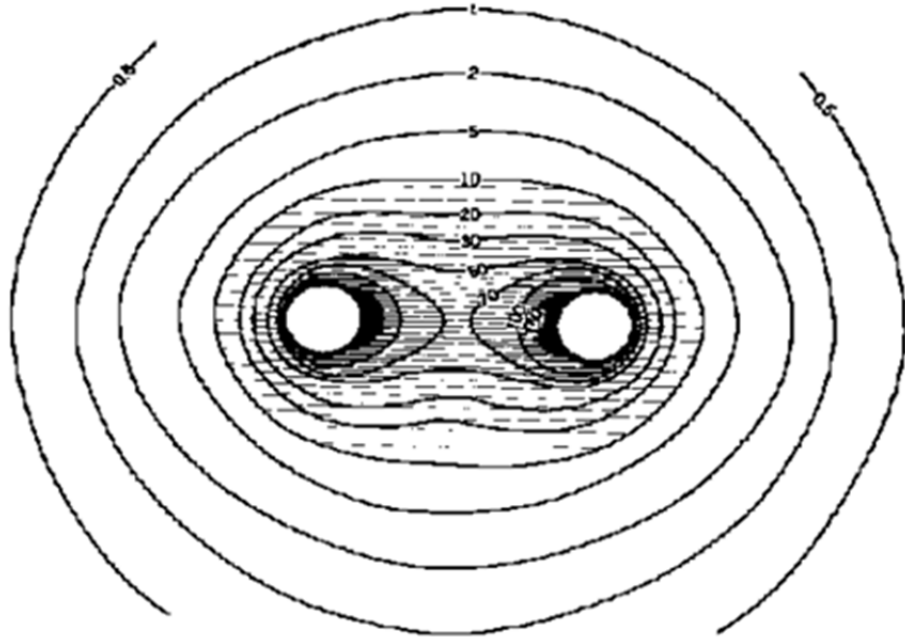


Figure 52: The power flow contour plot of a transmission line

The contours indicate power flow in watts per square meter for this case. Note that the power flow is concentrated between the two conductors and the maximum happens at the outer surface of the two conductors. If we integrate the Poynting's vector over an infinite plane that is perpendicular to the conductors, we have the total power transmitted. In this case, the total power can be obtained from the voltage between the conductors, 10 V rms, and the characteristic impedance $Z_0 = \frac{E}{H} = \sqrt{\frac{\mu_0}{\epsilon_0}} =$

376.7Ω (assume the transmission line is filled with air). Now we have the total power to be

$$P = \frac{V^2}{Z_c} = \frac{10^2}{376.7} = 0.265 = 265 \text{ mW} \quad (7.62)$$

Compare the Poynting's vector to the circuit theory of power, we have the power equations

$$P = \frac{1}{2} \frac{|V|^2}{R} = \frac{1}{2} |I|^2 R \quad (7.63)$$

$$\vec{P} = \frac{1}{2} \frac{|E_0|^2}{\eta} \hat{z} = \frac{1}{2} |H_0|^2 \eta \hat{z} \quad (7.64)$$

We can treat electric field as voltage and magnetic field as current with spatial orientation as well as phasor representation. From another perspective, voltage can be mathematically expressed as the line integral of electric field and current enclosed by a loop is equal to the line integral of magnetic field over the loop.

7.7 Traveling in two conductors system

7.7.1 Parallel Planes (TEM mode)

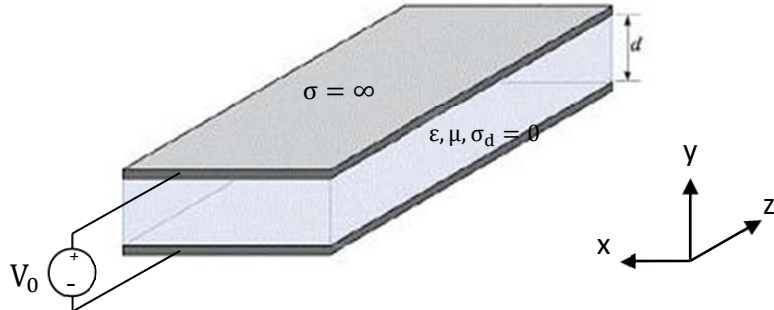


Figure 53: Parrallel plane waveguide

There is a parallel plane waveguide that extends to $\pm\infty$ in x , 0 to d in y and 0 to ∞ in z as shown in Figure 53. The conductors are assumed perfect and the dielectric is assumed lossless. For parallel planes systems, the TEM mode is the most often used mode. In TEM mode, the electric and magnetic fields are transverse to the direction of wave propagation without longitudinal components. Now, a sinusoidal voltage wave with voltage applied between the two conductors creates the electric field and magnetic field:

$$\vec{E} = -\frac{V_0}{d} e^{-jkz} \hat{y} \quad (7.65)$$

$$\vec{H} = \frac{V_0}{\eta d} e^{-jkz} \hat{x} \quad (7.66)$$

and therefore the Poynting's vector is

$$\vec{P} = \frac{1}{2} \frac{V_0^2}{\eta d^2} \hat{z} \quad (7.67)$$

The result of the Poynting's vector for TEM is also a constant, like the Poynting's vector of plane wave. Now, we take a snapshot at a specific time, the distributions of the fields and the Poynting's vector for the TEM mode are plotted in Figure 54.

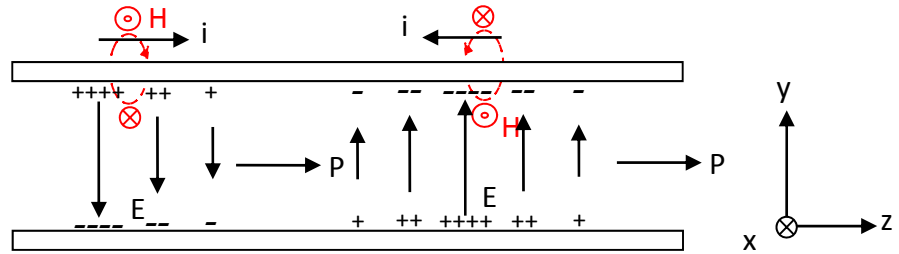


Figure 54: TEM mode in parallel plane waveguide

7.7.2 Parallel Planes (TM mode)

Transverse magnetic modes, also called TM modes, are the modes that the magnetic field is transverse to the direction, or say does not obtain longitudinal magnetic field component. The modes satisfy the boundary conditions for the fields and are the solutions to the wave equation.

We can construct electric and magnetic field by solving wave equation and applying boundary conditions:

$$\begin{aligned}\vec{E}(y, z) = & -j \frac{d}{n\pi} k \sqrt{1 - \left(\frac{k_{c,TM}}{k}\right)^2} B \cos \frac{n\pi}{d} y e^{-j\sqrt{k^2 - \left(\frac{n\pi}{d}\right)^2} z} \hat{y} \\ & + B \sin \frac{n\pi}{d} y e^{-j\sqrt{k^2 - \left(\frac{n\pi}{d}\right)^2} z} \hat{z}, \quad n = 1, 2, 3, \dots\end{aligned}\quad (7.68)$$

$$\vec{H}(y, z) = j \frac{\omega \epsilon d}{n\pi} B \cos \frac{n\pi}{d} y e^{-j\sqrt{k^2 - (n\pi/d)^2} z} \hat{x}, \quad n = 1, 2, 3, \dots \quad (7.69)$$

where $k_{c,TM} = \frac{n\pi}{d}$ and B is a constant that cannot be determined unless the generator amplitude is known.

For each different value of n , we have a certain pattern of electric and magnetic fields. These solutions that can exist in a given conductor geometry for a transmission line or waveguide is so called modes.

The Poynting's vector then can be calculated:

$$\begin{aligned}\vec{P} = & \frac{1}{2} \vec{E} \times \vec{H}^* = \frac{1}{2} \frac{\omega \epsilon d^2}{n^2 \pi^2} k \sqrt{1 - \left(\frac{k_{c,TM}}{k}\right)^2} B^2 \cos^2 \left(\frac{n\pi}{d} y\right) \hat{z} \\ & - j \frac{1}{2} \frac{\omega \epsilon d}{n\pi} B^2 \cos \left(\frac{n\pi}{d} y\right) \sin \left(\frac{n\pi}{d} y\right) \hat{y}, \quad n = 1, 2, 3, \dots\end{aligned}\quad (7.70)$$

And the time average Poynting's vector is

$$\langle \vec{P} \rangle = \frac{1}{2} \operatorname{Re} \{ \vec{E} \times \vec{H}^* \} = \frac{1}{2} \frac{\omega \epsilon d^2}{n^2 \pi^2} k \sqrt{1 - \left(\frac{k_{c,TM}}{k}\right)^2} B^2 \cos^2 \left(\frac{n\pi}{d} y\right) \hat{z} \quad (7.71)$$

The value of the time-average Poynting's vector is independent of x since the phase and amplitude of the propagating wave are independent of x . The power is zero at $y = d/2n$ and reaches maximum at the walls $y = 0$ and $y = d$.

For both TM and TE (will show more detail in the following chapter) modes, equation (7.70) shows that the Poynting's vector does not only have component in the z direction but also in the y direction. The Poynting's vector is imaginary in the y direction and is real in the z direction. Thus, we know that real power flows in the z direction and reactive power component exists in the y direction. This means that the power in bouncing back and forth between the conductors pair as the wave propagate

along the wave guide. An interesting physical interpretation of Poynting's vector is cutoff frequency $k_{c,TM/TE}$. When $\sqrt{1 - \left(\frac{k_{c,TM/TE}}{k}\right)^2} = 0$, the real part of Poynting's vector is zero so the Poynting's vector is pure imaginary. In other word, at or below the cutoff frequency, the power transmitted in the z direction is zero. If so, the power is stored in both in the z and y direction in the wave guide and therefore the wave is being cutoff. This is why the frequency at $k_{c,TM/TE}$ is called cutoff frequency.

7.7.3 Parallel Planes (TE mode)

Transverse electric modes, also called TE modes, are the modes that the electric field is transverse to the direction, or say does not obtain longitudinal electric field component. We can construct electric and magnetic field by solving wave equation and applying boundary conditions:

$$\vec{E}(y, z) = j \frac{\omega \epsilon d}{n\pi} A \sin \frac{n\pi}{d} y e^{-j\sqrt{k^2 - (n\pi/d)^2} z} \hat{x} \quad (7.72)$$

$$\begin{aligned} \vec{H}(y, z) = & j \frac{d}{n\pi} k \sqrt{1 - \left(\frac{k_{c,TE}}{k}\right)^2} A \sin \frac{n\pi}{d} y e^{-j\sqrt{k^2 - \left(\frac{n\pi}{d}\right)^2} z} \hat{y} \\ & + A \cos \frac{n\pi}{d} y e^{-j\sqrt{k^2 - \left(\frac{n\pi}{d}\right)^2} z} \hat{z}, \quad n = 1, 2, 3, \dots \end{aligned} \quad (7.73)$$

where $k_{c,TE} = \frac{n\pi}{d}$ and A is a constant that cannot be determined unless the generator amplitude is known.

The Poynting's vector:

$$\begin{aligned} \vec{P} = & \frac{1}{2} \vec{E} \times \vec{H}^* = \frac{1}{2} \frac{\omega \epsilon d^2}{n^2 \pi^2} k \sqrt{1 - \left(\frac{k_{c,TE}}{k}\right)^2} A^2 \sin^2 \left(\frac{n\pi}{d} y\right) \hat{z} \\ & - j \frac{1}{2} \frac{\omega \epsilon d}{n\pi} A^2 \cos \left(\frac{n\pi}{d} y\right) \sin \left(\frac{n\pi}{d} y\right) \hat{y}, \quad n = 1, 2, 3, \dots \end{aligned} \quad (7.74)$$

The time-average Poynting's vector:

$$\langle \vec{P} \rangle = \frac{1}{2} \frac{\omega \epsilon d^2}{n^2 \pi^2} k \sqrt{1 - \left(\frac{k_{c,TE}}{k} \right)^2} A^2 \sin^2 \left(\frac{n\pi}{d} y \right) \hat{z} \quad (7.75)$$

The value of the time-average Poynting's vector for the TE mode is also independent of x since the phase and amplitude of the propagating wave are also independent of x . The power is zero at the walls $y = 0$ and $y = d$ and reaches maximum at $y = d/2n$.

In Figure 55, we plot the configurations of time average Poynting's vector for both the first three TM modes and TE modes on x-y plane. As we can see in Figure 55, the

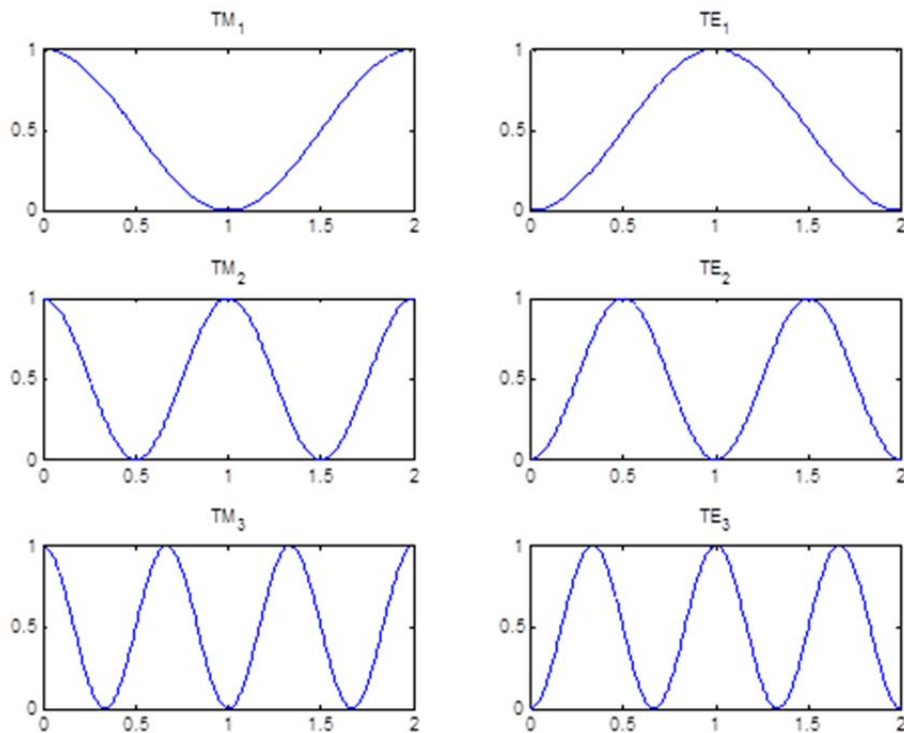


Figure 55: The first three TM and TE modes of time-average Poynting vector

power contains more nodes when it comes to higher mode. For TM modes, the n th mode contains n node/nodes only between the two ends in the x direction. For TE modes, the n th mode contains $n + 1$ nodes on and between the two ends in the x direction. From the other prospective, the power oscillates faster for higher modes.

This idea is actually intuitive because higher modes require higher operating frequency, which oscillate faster. As for the total power transmitting in the parallel planes, it is equal to the sum of all the power components associated with each mode that exist inside the system. Thus, higher operating frequency excites more modes and contains higher power flow.

Chapter 8: Other Applications

8.1 RLC circuit

For the Poynting's vector in the battery-wires-load set example, we know that the power flow is essentially external to the wires. Now, we replace the battery with a slowly time-varying voltage $V(t)$ and assign a series RLC circuit to be the load, as shown in Figure 56. We know the complex power from the circuit theory,

$$\begin{aligned}\bar{S} &= \frac{1}{2} \bar{V} \bar{I}^* = \frac{1}{2} (\bar{Z} \bar{I}) \bar{I}^* = \frac{1}{2} \left(R + j\omega L - j \frac{1}{\omega C} \right) \bar{I} \bar{I}^* \\ &= \frac{1}{2} R \bar{I} \bar{I}^* + j2\omega \left(\frac{L \bar{I}^*}{4} - \frac{\bar{I}^*}{4\omega^2 C} \right) = P + j2\omega(W_L - W_c)\end{aligned}\quad (8.1)$$

For ϵ and μ are both real and independent of time,

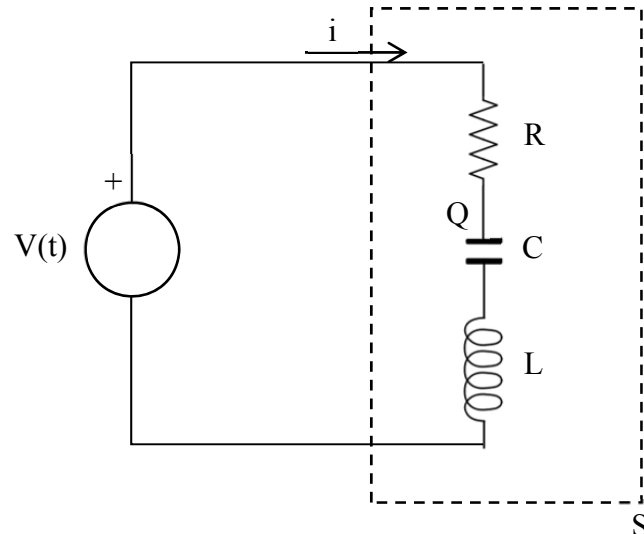


Figure 56: A series RLC circuit

Applying Poynting's theorem to the surface S , for the time-rate change of the total energy in the capacitor, we get

$$\begin{aligned}\frac{\partial}{\partial t} \int_{\text{vol}} \frac{\epsilon E^2}{2} d\nu &= \frac{\partial}{\partial t} \int_{\text{vol}} \frac{\epsilon}{2} \left(\frac{V}{d} \right)^2 d\nu = \frac{\partial}{\partial t} \int_{\text{vol}} \frac{\epsilon}{2} \left(\frac{Q}{Cd} \right)^2 d\nu \\ &= \frac{1}{dA} \frac{\partial}{\partial t} \int_{\text{vol}} \frac{1}{2} \frac{Q^2}{C} d\nu = \frac{d}{dt} \frac{Q^2}{2C}\end{aligned}\quad (8.2)$$

When we apply the same theorem on the inductor and resistor, we get

$$\frac{\partial}{\partial t} \int_{\text{vol}} \frac{\mu H^2}{2} dv = \frac{d}{dt} \frac{1}{2} L i^2 \quad (8.3)$$

for the inductor and

$$\int_{\text{vol}} \frac{J^2}{\sigma} dv = R i^2 \quad (8.4)$$

for the resistor. We can rewrite Poynting's theorem in another form to show the connection between circuit theory and field theory:

$$-\oint_S (E \times H) \cdot dS = R i^2 + \frac{d}{dt} \left(\frac{Q^2}{2C} + \frac{1}{2} L i^2 \right) \quad (8.5)$$

From the previous battery-wires-load example, we know that

$$-\oint_S (E \times H) \cdot dS = Vi \quad (8.6)$$

Therefore,

$$Vi = R i^2 + \frac{d}{dt} \left(\frac{Q^2}{2C} + \frac{1}{2} L i^2 \right) \quad (8.7)$$

Equation (8.7) shows how the voltage generator distributes instantaneous power to the RLC circuit. Moreover, the equation is specific about how much power is transformed into heat in the resistor, the time-rate of change of stored electric power in the capacitor, and magnetic power in the inductor.

To prove Poynting's theorem for the RLC circuit, the equation can be rewritten as

$$Vi = R i^2 + L i \frac{di}{dt} + \frac{Q}{C} \frac{dQ}{dt} \quad (8.8)$$

To yield the loop equation for the RLC circuit, we divide both sides by i ($i = dQ/dt$):

$$V = Ri + L \frac{di}{dt} + \frac{Q}{C} \quad (8.9)$$

8.2 A solenoidal coil

Consider a long solenoid filled with air carrying a time-harmonic current $i = I_0 \cos \omega t$ in its winding, as indicated in Figure 57. The magnetic field inside the

solenoid is

$$\vec{H} = N'i(t)\hat{z}, \quad \text{for } r < a \quad (8.10)$$

where N' is the number of wire turns per unit solenoid length, and a is the circular cross section radius of the solenoid.

We can find the induced electric field inside the solenoid in Figure 58 from

$$\phi = B\pi r^2 = \mu H\pi r^2 = \mu N'i(t)\pi r^2 \quad (8.11)$$

$$\vec{E}_{ind} 2\pi r = -\frac{d\phi}{dt} = -\frac{d}{dt}(\mu N'i(t)\pi r^2) = -\mu N'\pi r^2 \frac{di}{dt} \quad (8.12)$$

$$\vec{E}_{ind} = -\frac{\mu N' r}{2} \frac{di}{dt} \quad (8.13)$$

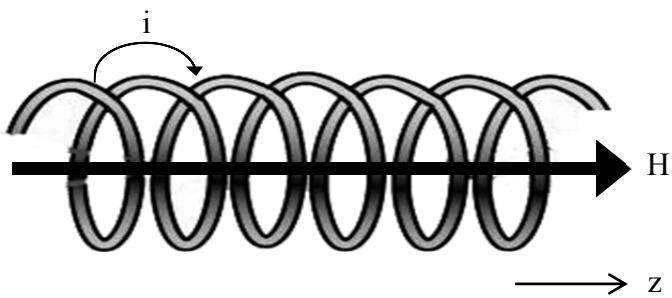


Figure 57: The magnetic field inside a solenoid

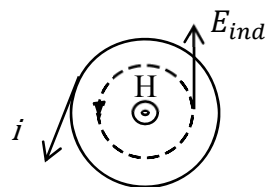


Figure 58: The induced electric field inside a solenoid

Thus, the instantaneous Poynting's vector inside the solenoid is

$$\begin{aligned}
\vec{P}(r, t) &= \vec{E}_{ind} \times \vec{H} = -\frac{\mu N'^2}{2} r i \frac{di}{dt} \hat{\phi} \times \hat{z} = \frac{\mu N'^2}{2} r I_0 \cos(\omega t) I_0 \omega \sin(\omega t) \hat{r} \\
&= \frac{\mu N'^2 \omega I_0^2}{4} r \sin(2\omega t) \hat{r}, \text{ for } r < a
\end{aligned} \tag{8.14}$$

The distribution of Poynting's vector can be plotted as Figure 59. At the center of the solenoid ($r = 0$), the power flow is zero. As the radius increases, the power flow also increases. Note that the power flow points at the \hat{r} direction. This indicates that the power is being stored in the solenoid, and that there is no power transferred along the solenoid. This explains why an inductor is a passive component that stores power. As for the Poynting's vector, outside the solenoid it is equal to zero because there is no magnetic field outside the solenoid.

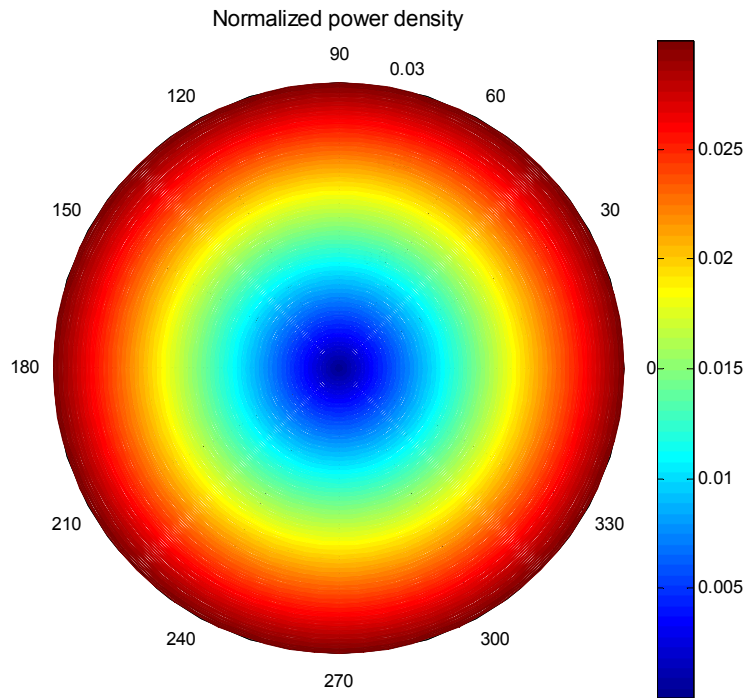


Figure 59: The power density inside a solenoid

8.3 Poynting's vector around a Hertzian dipole

The Hertzian dipole is a theoretical dipole that consists of an infinitesimally small

oscillating current source. Although a Hertzian dipole does not exist in the real world, it can be approximated by a very short dipole with a length is significantly smaller than the wavelength:

$$l < \frac{\lambda}{50}$$

This idea is most often applied for antennas. The first dipole antenna was developed by a German physicist, Heinrich Rudolph Hertz, around 1886. This kind of antenna can be made easily from a simple wire with excitation in the center of the element. The excitation creates a current which can transmit or receive power.

Consider a Hertzian dipole located at the origin, and orient it along the z axis, as shown in Figure 60. It consists of two equal and opposite time-varying charges that

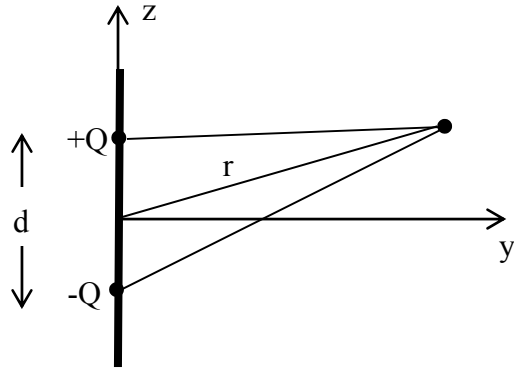


Figure 60: A Hertzian dipole

are separated by an infinitesimal distance. The electric and magnetic fields can be derived from Maxwell's equations, and vector potential \vec{A} , with reasonable approximations. We do not list all the calculation here, as the goal here is to obtain Poynting's vector. Therefore, we simply start from the fields in phasor form:

$$\begin{aligned} E_r &= -\frac{2\beta^2\eta I_0 dl \cos \theta}{4\pi} \left[\frac{1}{(j\beta r)^3} + \frac{1}{(j\beta r)^2} \right] e^{-j\beta r} \\ &= \frac{2I_0 dl \cos \theta}{4\pi\epsilon} \left[-\frac{j}{\omega r^3} + \frac{1}{\nu r^2} \right] e^{-j\omega r/\nu} \end{aligned} \quad (8.15)$$

$$\begin{aligned}
E_\theta &= -\frac{\beta^2 \eta I_0 dl \sin \theta}{4\pi} \left[\frac{1}{(j\beta r)^3} + \frac{1}{(j\beta r)^2} + \frac{1}{j\beta r} \right] e^{-j\beta r} \\
&= -\frac{I_0 dl \sin \theta}{4\pi \epsilon} \left[-\frac{j}{\omega r^3} + \frac{1}{vr^2} + \frac{j\omega}{v^2 R} \right] e^{-j\omega r/v}
\end{aligned} \tag{8.16}$$

$$H_\phi = -\frac{\beta^2 I_0 dl \sin \theta}{4\pi} \left[\frac{1}{(j\beta r)^2} + \frac{1}{j\beta r} \right] e^{-j\beta r} = \frac{I_0 dl \sin \theta}{4\pi} \left[\frac{1}{r^2} + \frac{j\omega}{vr} \right] e^{-j\omega r/v} \tag{8.17}$$

where $\beta = \omega/v$, $\eta = \sqrt{\mu/\epsilon}$, and I_0 is the peak value for the current on the dipole.

If we only consider far fields, also called radiation fields, the $1/r$ terms dominate $1/r^3$ and $1/r^2$ terms. Thus, for a distance of a few wavelengths from the dipole, we can neglect the $1/r^3$ and $1/r^2$ terms in comparison with the $1/r$ terms. The fields then reduce to

$$E_r = 0 \tag{8.18}$$

$$E_\theta = \frac{j\beta \eta I_0 dl \sin \theta}{4\pi r} e^{-j\beta r} \tag{8.19}$$

$$H_\phi = \frac{j\beta I_0 dl \sin \theta}{4\pi r} e^{-j\beta r} \tag{8.20}$$

We note that the ratio of E_θ to H_ϕ for the radiation fields is equal to η , which is the same as the case of fields associated with a uniform plane wave. As in that case, we can consider the $\sin \theta$ as constant because of the large radius. Each small area becomes approximately a plane surface, and thus, the fields are almost like uniform plane waves.

Now, we obtain the complex Poynting's vector from equation (8.15) to (8.17) as

$$\begin{aligned}
\vec{P} &= \frac{1}{2} \vec{E} \times \vec{H}^* = \frac{1}{2} (E_\theta H_\phi^* \hat{r} - E_r H_\phi^* \hat{\theta}) \\
&= \frac{|I_0|^2 (dl)^2 \sin^2 \theta}{32\pi^2 \epsilon} \left[-\frac{j}{\omega r^3} + \frac{1}{vr^2} + \frac{j\omega}{v^2 R} \right] \left[\frac{1}{r^2} - \frac{j\omega}{vr} \right] \hat{r} \\
&\quad - \frac{|I_0|^2 (dl)^2 \sin 2\theta}{32\pi^2 \epsilon} \left[-\frac{j}{\omega r^3} + \frac{1}{vr^2} \right] \left[\frac{1}{r^2} - \frac{j\omega}{vr} \right] \hat{\theta} \\
&= \frac{|I_0|^2 (dl)^2 \sin^2 \theta}{32\pi^2 \epsilon} \left[\frac{\omega^2}{v^3 r^2} - \frac{j}{\omega r^5} \right] \hat{r} + j \frac{|I_0|^2 (dl)^2 \sin 2\theta}{32\pi^2 \epsilon} \left[-\frac{\omega}{v^2 r^3} + \frac{1}{\omega r^5} \right] \hat{\theta}
\end{aligned} \tag{8.21}$$

The time-average Poynting's vector is

$$\langle \vec{P} \rangle = \text{Re}\{\vec{P}\} = \frac{|I_0|^2 (dl)^2 \sin^2 \theta}{32\pi^2 \epsilon} \left[\frac{\omega^2}{v^3 r^2} \right] \hat{r} \quad (8.22)$$

Equation (8.22) indicates that the dipole antenna is radiating electromagnetic waves and power away from itself. Note that the time-average power density is decays as $1/r^2$. This is exactly the same as the time-average Poynting's vector if we derive it from equation (8.18) to (8.20). Therefore, we know that the $1/r^3$ and $1/r^2$ terms do not contribute to the time-average power flow in the near fields. Those terms only contribute to the reactive power. The normalized time-average Poynting's vector can be plotted as shown in Figure 61. This figure indicates that power density is zero at the center of the dipole and for $\theta = 0$ and $\theta = 180^\circ$. Maximum power density is reached at $\theta = 90^\circ$. In other words, the dipole radiates most of the power on the broadside to the dipole and does not transmit energy along the dipole.

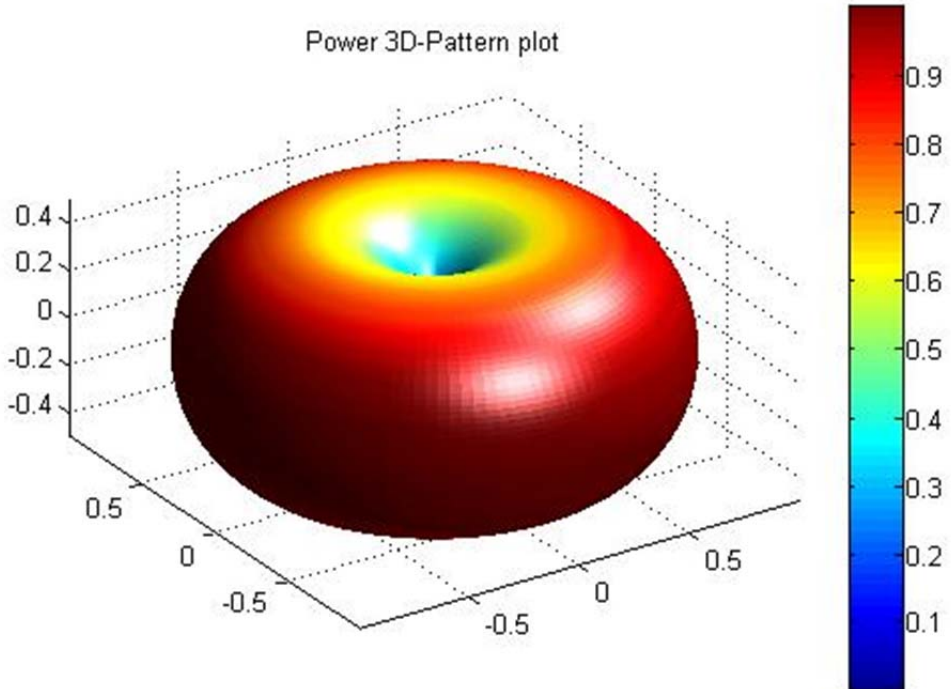


Figure 61: The 3-D power pattern of a Hertzian dipole

The time-average power radiated by the dipole can be calculated by integrating the

time-average Poynting's vector in (8.22) over a surface of radius r centered at the dipole:

$$\begin{aligned}
 \langle P_{rad} \rangle &= \int_{\theta=0}^{\pi} \int_{\phi=0}^{2\pi} \langle \vec{P} \rangle \cdot r^2 \sin \theta d\theta d\phi \hat{r} \\
 &= \int_{\theta=0}^{\pi} \int_{\phi=0}^{2\pi} \frac{\omega^2 |I_0|^2 (dl)^2}{32\pi^2 \epsilon v^3} \sin^3 \theta d\theta d\phi \\
 &= \frac{\omega^2 |I_0|^2 (dl)^2}{32\pi^2 \epsilon v^3} \frac{8\pi}{3} = \frac{\omega^2 |I_0|^2 (dl)^2}{12\pi \epsilon v^3} = \frac{\eta \beta^2 |I_0|^2 (dl)^2}{12\pi} = \frac{\pi \eta |I_0|^2}{3} \left(\frac{dl}{\lambda} \right)^2
 \end{aligned} \tag{8.23}$$

Equation (8.23) tells us why the near fields cannot contribute to the time-average power flow. The power flow through a spherical area of one radius should be equal to the power flow through any another radius. This means that the power must be independent of r , as we can see in (8.23). Because the surface area is a function of r^2 , when the electric and magnetic fields only depend on $1/r$, this cancels out the r^2 term and makes the power flow independent of radius.

8.4 Half-wave Antenna

A half-wave antenna is composed from a straight conductor with length of half a free-space wavelength as shown in Figure 62. It is commonly used for radiating

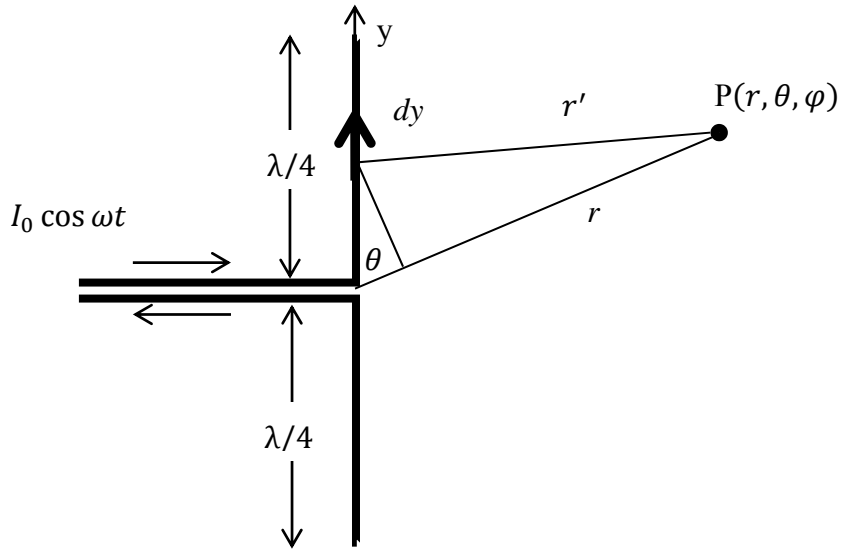


Figure 62: A half-wave antenna

electromagnetic waves into space to transfer signal. When we feed the antenna a current $I_0 \cos \omega t$ at the center, a standing wave is created along the antenna and the current I at y is

$$\begin{aligned} I &= I_0 \cos \frac{y}{\lambda} \cos \omega t \\ &= \frac{I_0}{2} \operatorname{Re} \left\{ e^{j(\omega t - \frac{y}{\lambda})} + e^{j(\omega t + \frac{y}{\lambda})} \right\} \end{aligned} \quad (8.24)$$

If we cut the antenna into small pieces, we can treat each element of it radiates an electromagnetic wave as a Hertzian dipole. Thus, the field at any interested point in space is the sum of all these fields. The electric field intensity $d\vec{E}$ from the element dl is then

$$d\vec{E} = -\frac{I_0}{j8\pi c \epsilon_0 \lambda r'} \left\{ e^{j(\omega t - \frac{y}{\lambda} - \frac{r'}{\lambda})} + e^{j(\omega t + \frac{y}{\lambda} - \frac{r'}{\lambda})} \right\} \sin \theta dy \hat{\theta} \quad (8.25)$$

where r' is the distance between the given point (r, θ, φ) , as shown in Figure 62. We can approximate r' as

$$r' \approx r - l \cos \theta$$

Also we assume that $r \gg \lambda$ so that the electric field intensities can be treated as

parallel for a interested point and can be assumed to have the same magnitude with different phases. Next, we integrate equation (8.25), we get

$$\begin{aligned}
\vec{E} &= -\frac{I_0 e^{j\omega t}}{j8\pi c \epsilon_0 \lambda r} \sin \theta \left\{ e^{j\frac{1}{\lambda}(\cos \theta - 1)} + e^{j\frac{1}{\lambda}(\cos \theta + 1)} \right\} dy \hat{\theta} \\
&= \frac{jI_0 e^{j\omega t}}{4\pi c \epsilon_0} \sin \theta \left(\frac{\sin \left\{ \frac{\pi}{2} (\cos \theta - 1) \right\}}{\cos \theta - 1} + \frac{\sin \left\{ \frac{\pi}{2} (\cos \theta + 1) \right\}}{\cos \theta + 1} \right) \hat{\theta} \\
&= \frac{jI_0 e^{j\omega t}}{2\pi c \epsilon_0} \frac{\cos \left(\frac{\pi}{2} \cos \theta \right)}{\sin \theta} \hat{\theta}
\end{aligned} \tag{8.26}$$

After we have electric field, it is a simple matter to find the magnetic field:

$$\vec{H} = \frac{jI_0 e^{j\omega t}}{2\pi r} \frac{\cos \left(\frac{\pi}{2} \cos \theta \right)}{\sin \theta} \hat{\phi} \tag{8.27}$$

The time-average Poynting's vector is

$$\begin{aligned}
\vec{P} &= \frac{1}{2} \vec{E} \times \vec{H}^* = \frac{1}{2} \frac{jI_0 e^{j\omega t}}{2\pi c \epsilon_0} \frac{\cos \left(\frac{\pi}{2} \cos \theta \right)}{\sin \theta} \hat{\theta} \times \frac{-jI_0 e^{-j\omega t}}{2\pi r} \frac{\cos \left(\frac{\pi}{2} \cos \theta \right)}{\sin \theta} \hat{\phi} \\
&= \frac{I_0^2}{8\pi^2 c \epsilon_0 r^2} \frac{\cos^2 \left(\frac{\pi}{2} \cos \theta \right)}{\sin^2 \theta} \hat{r}
\end{aligned} \tag{8.28}$$

Poynting's vector indicates that the power radiates radially outward and varies as $1/r^2$. Therefore, the power delays along the radial axis, which ensures conservation of energy. The 3D power density plot is very similar to the pattern of a Hertzian dipole, as shown in Figure 61.

Chapter 9: Conclusion

In the classical electromagnetics we express the energy of an electromagnetic field using a formalism in which volume integrals are employed. We have the possibility of interpreting such expressions as showing that the energy of the electromagnetic field is localized in space with a definite volume density.

The assumptions in derivation of the formulae are:

- The changes are reversible;
- The building-up of the electric and magnetic fields is assumed to be so slow that it can be represented as a succession of stationary states (we are not sure that the energy density expressions are valid for very rapid variation of the fields).
- If all the above assumptions are met then the change in electromagnetic energy densities can be associated with the flow of energy from or toward the source.

This work offers an enumeration and a short catalog of applications of Poynting's vector and Poynting's theorem. Citing "Stratton" [13], "The classical interpretation of Poynting's theorem appears to rest to a considerable degree on hypothesis. The hypothesis of an energy density in the electromagnetic field and a flow of energy (actually the specific rate of flow) $\vec{P} = \vec{E} \times \vec{H}$ has proved extraordinarily fruitful. A theory is not an absolute truth but a self-consistent analytical formulation of the relations governing a group of natural phenomena."

Bibliography

- [1] Gayle F. Miner, 1996. Lines and Electromagnetic Fields for Engineers, New York Oxford, Oxford University Press.
- [2] Constantine A. Balanis, 1989. Advanced Engineering, New York : Wiley.
- [3] M. Ibanescu, Y. Fink, S. Fan, E. L. Thomas, J. D. Joannopoulos, 2000, An All-Dielectric Coaxial Waveguide, Science, Volume 289, 21 July 2000.
- [4] Paul Lorrain, Dale R. Corson, 1970. Electromagnetic Fields and Waves, 2nd edition, San Francisco, W.H. Freeman.
- [5] Edwin M. Anderson, 1985. Electric Transmission Line Fundamentals, Reston, Va. : Reston Pub. Co..
- [6] Slavko Majcen, Ryan K. Haaland, Scott C. Dudley, 2000. The Poynting's Vector and Power in a Simple Circuit, Am. J. Phys. 68 (9), September 2000.
- [7] Richard K. Moore, 1960. Traveling-Wave Engineering, New York, McGraw-Hill.
- [8] Branislav M. Notaros, 2010. Electromagnetics, Pearson Education Canada.
- [9] Stephen Stanley Attwood, 1967. Electric and Magnetic Fields, Dover Publications.
- [10] John Daniel Kraus, Keith R. Carver, 1973. Electromagnetics, McGraw-Hill.
- [11] Matthew N. O. Sadiku, 2010. Elements of Electromagnetics, New York Oxford, Oxford University Press.
- [12] William H. Hayt, Jr., John A. Buck, 2001. Engineering Electromagnetics, McGraw-Hill.
- [13] J. A. Stratton, 2007. Electromagnetic Theory, pp. 131-137, McGraw Hill.

Vita

Hsin I Hsu was born in Taichung, Taiwan on September 25th, 1985, the daughter of Yeougeng Hsu and Chiahsien Yen. She attended National Experimental High School in Hsinchu, Taiwan. After completing her high school education in 2004, Hsin I enrolled in National Taiwan University to pursue an education in Engineering Science and Ocean Engineering and received her Bachelor's of Science and Program for Photonics Technologies in June, 2008. For the next year, she worked at National Taiwan University as a full time teaching assistant. In the fall of 2009, Hsin I entered the Electrical Engineering and Computer Engineering department at the University of Texas at Austin in pursuit of a master's degree. As a graduate student, Hsin I had the opportunity to work as a consultant at Bracewell & Giuliani LLP in the summer of 2010. Under the supervision of Dr. Mircea Driga, Hsin I graduated with a Master's of Science in Engineering in May 2011.

Email: hsinihsu@utexas.edu

This thesis was typed by Hsin I Hsu.